

**Photooxidative and Photoreductive Degradation of Chlorinated  
Hydrocarbons on Aqueous Titanium Dioxide Colloids**

Thesis by  
Wonyong Choi

In Partial Fulfillment of the Requirements  
for the Degree of  
Doctor of Philosophy

California Institute of Technology

Pasadena, California

1996

(Submitted February 22, 1996)

c 1996

Wonyong Choi

All Rights Reserved

## Acknowledgments

I would like to express my sincere gratitude to Caltech and numerous people who have given me lots of support during my years of graduate studies. Caltech provided me with a most wonderful environment for my graduate study and life. It would be hard to forget the most productive and enjoyable days in my life spent in Pasadena.

I was really lucky to meet Prof. Michael Hoffmann when I came to Caltech four and a half years ago. Since then, he has been my advisor and given me generous support (mental and material), encouragement, and guidance. Being a member of his research group led me into a field of *environmental science research*, which was totally new to me at that time and I found very interesting. I am very grateful to him for all of these.

A number of students and research fellows taught me numerous experimental techniques, provided valuable scientific insight and ideas, and offered generous help. They include Beth Carraway, Dean Willberg, Peter Green, Ralf Hoechemer, Amy Hoffmann, Inez Hua, Axel Kratel, Patrick Lang, John Lewis, Sooyeol Lim, Tom Lloyd, Simo Pehkonen, Robert Rossi, Ron Siefert, Linda Weavers, and Jay Winkler. I would like to give special thanks to Andreas Termin for his cooperative efforts and laborious synthetic work in metal-ion doping study, to Scot Martin for the companionship and cooperative research efforts throughout the last four years, and to Nicole Peill and Janet Kesselman for various help and cooperation in the TiO<sub>2</sub> research.

Joe Fontana, Carol Garland, Rayma Harrison, Linda Scott, and Hai Vu deserve special thanks for their excellent technical support.

I deeply appreciate constant and unlimited love and support from my parents in Korea. I completely owe them what I am today. Thanks, Mom and Dad!! Care and support from my parents-in-law in Korea are also deeply acknowledged. I also want to acknowledge the support from my grandparents, my aunt and uncle who live in the Los Angeles area.

Lastly, I would like to mention a very special person. My wife and best friend, Hee Jung. I do not know how to say how grateful I am for the enduring love and support she has shown me. She and my seventeen-month-old son, Won-Joon have been a constant source of encouragement, rest, joy and laughter. I just want to say "Thank you" to them for being in my life.

## Abstract

Studies on photocatalytic degradation reactions of chlorinated hydrocarbons on  $\text{TiO}_2$  colloids are presented in this thesis. Photoreactivities of metal-ion doped quantum-sized  $\text{TiO}_2$  colloids and photochemical mechanisms of  $\text{CHCl}_3$  and  $\text{CCl}_4$  degradation are investigated in detail.

A systematic study of 21 metal-ion doped quantum-sized (2-4 nm)  $\text{TiO}_2$  colloids is performed by measuring their photoreactivities and the transient charge-carrier recombination dynamics. Doping with  $\text{Fe}^{3+}$ ,  $\text{Mo}^{5+}$ ,  $\text{Ru}^{3+}$ ,  $\text{Os}^{3+}$ ,  $\text{Re}^{5+}$ ,  $\text{V}^{4+}$ , and  $\text{Rh}^{3+}$  at 0.1-0.5 atom% significantly increases the photoreactivity for both  $\text{CHCl}_3$  oxidation and  $\text{CCl}_4$  reduction while  $\text{Co}^{3+}$  and  $\text{Al}^{3+}$  doping decreases the photoreactivity. The quantum yields obtained during CW photolyses are quantitatively correlated with the measured transient absorption signals of the charge-carriers.

The photoreductive degradation of  $\text{CCl}_4$  in  $\text{TiO}_2$  particulate suspensions in the presence of a variety of organic electron donors (alcohols, carboxylic acids, and benzene derivatives) has been examined. The rate of  $\text{CCl}_4$  dechlorination can be enhanced significantly when alcohols and organic acids are used as electron donors. It is demonstrated that  $\text{CCl}_4$  can be fully degraded under both oxic and anoxic conditions. A photodegradation mechanism of  $\text{CCl}_4$  that includes both one-electron and two-electron transfer is proposed.

The mechanism of photoreduction of  $\text{CCl}_4$  on illuminated  $\text{TiO}_2$  surfaces is investigated by selectively trapping transient free radical intermediates. Dichlorocarbene and trichloromethyl radical are trapped with 2,3-dimethyl-2-butene during the photocatalytic degradation of  $\text{CCl}_4$ . The rate of formation of trapped  $:\text{CCl}_2$  and  $\cdot\text{CCl}_3$  is found to be a function of  $[\text{H}_2\text{O}]$ , pH,  $[\text{CCl}_4]$ , the nature

of the dissolved gas, and light intensity. A two-electron photoreductive pathway (via dichlorocarbene formation) is suggested to be the dominant mechanism leading to the full degradation of  $\text{CCl}_4$ .

The photocatalytic degradation reactions of  $\text{CHCl}_3$ ,  $\text{CHBr}_3$ ,  $\text{CCl}_4$ , and  $\text{CCl}_3\text{CO}_2^-$  are investigated in aqueous  $\text{TiO}_2$  suspensions.  $\text{CHCl}_3$  and  $\text{CHBr}_3$  are degraded into carbon monoxide and halide ion in the absence of dissolved oxygen. The anoxic degradation proceeds through a dihalocarbene intermediate which is produced by sequential reactions of the haloform molecule with a valence band hole and a conduction band electron. Degradation of haloform is enhanced dramatically at  $\text{pH} > 11$ . This enhancement is ascribed to "*photoenhanced hydrolysis*".

## Table of Contents

<i>Acknowledgments</i>	iii
<i>Abstract</i>	v
<b>Chapter 1</b>	
<b>Introduction</b>	1
References	7
<b>Chapter 2</b>	
<b>The Role of Metal Ion Dopants in Quantum-Sized TiO<sub>2</sub>: Correlation between Photoreactivity and Charge Carrier Recombination Dynamics</b>	11
Abstract	12
Introduction	13
Experimental Section	14
Results	19
Discussion	24
Conclusions	35
Acknowledgments	35
References	36
<b>Chapter 3</b>	
<b>Photoreductive Mechanism of CCl<sub>4</sub> Degradation on TiO<sub>2</sub> Particles and Effects of Electron Donors</b>	54
Abstract	55
Introduction	56
Experimental Section	57

Results and Discussion	60
Acknowledgments	74
References	75

## **Chapter 4**

### **Kinetics and Mechanism of CCl<sub>4</sub> Photoreductive Degradation on TiO<sub>2</sub>: The Role of Trichloromethyl Radical and**

<b>Dichlorocarbene</b>	89
Abstract	90
Introduction	91
Experimental Section	93
Results	95
Discussion	104
Conclusions	110
Acknowledgments	111
References	112

## **Chapter 5**

### **Novel Photocatalytic Mechanism of CHCl<sub>3</sub> and CHBr<sub>3</sub> Degradation and Fate of Photogenerated Trihalomethyl Radical**

<b>on TiO<sub>2</sub></b>	126
Abstract	127
Introduction	128
Experimental Section	130
Results	133
Discussion	137
Acknowledgments	144
References	145

**Chapter 6**

**Summary and Conclusions**

158

References

164

## List of Tables

### Chapter 2

**Table I.** Summary of the Chloroform Degradation Quantum Yields ( $\Phi_{\text{CHCl}_3}$ , %) for Several Doped  $\text{TiO}_2$  Colloids at Various Dopant Concentrations,  $[\text{CHCl}_3]_0 = 3.15 \text{ mM}$ . 40

**Table II.** Effects of Heat Treatment at Various Temperatures on the Photoreactivities of the Undoped and Doped  $\text{TiO}_2$  Measured in Term of the Chloroform Degradation Rate,  $v_{\text{CHCl}_3}$  ( $\mu\text{M min}^{-1}$ ). Suspension Concentrations Are Given in Brackets. 41

**Table III.** Comparison of the Fitting Parameters (Eq 5) from the Transient Absorption Decays with the Photocatalytic Quantum Yields (%) from Figure 2 for Various Doped Q-sized  $\text{TiO}_2$ . 42

### Chapter 3

**Table I.**  $\text{CCl}_4$  Dechlorination Rates with Various Alcohols Serving as Electron Donors. 78

**Table II.** Kinetic Isotope Effects on Rate of Photocatalytic  $\text{CCl}_4$  Dechlorination with Methanol and 2-Propanol. 79

**Table III.**  $\text{CCl}_4$  Dechlorination Rates with Various Organic Acids as Electron Donors. 80

**Chapter 4**

**Table I.** Elementary Reaction Steps of  $\text{CCl}_4$  Photolysis in UV-Irradiated  $\text{TiO}_2$ . 115

**Table II.** Kinetic Rate Equations of  $\text{TCCl}_2$  Production for Three Different Cases of Electron Transfers to  $\text{CCl}_4$ . 116

**Chapter 5**

**Table I.** Chloride Production ( $\mu\text{M}$ ) after 1-hr of Photolysis of 6 mM Trichloroacetate Solution on  $\text{TiO}_2$  as a Function of pH. 148

**Table II.** Concentrations of  $\text{Cl}^-$ ,  $\text{C}_2\text{Cl}_6$ , and  $\text{C}_2\text{Cl}_4$  Produced after 1-hr Photolysis of 1 mM  $\text{CCl}_4$  in Air-Equilibrated  $\text{TiO}_2$  Suspensions in the Presence of *tert*-Butanol (t-BuOH), 2-Propanol (2-PrOH), and Methanol as Electron Donors. 149

**Table III.**  $\text{CO}_2$ , CO, and  $\text{Cl}^-$  Generation after 2-hr of Photolysis of  $\text{CHCl}_3$  on  $\text{TiO}_2$ . 150

**Table IV.**  $\text{CO}_2$ , CO, and  $\text{Cl}^-$  Generation after 2-hr of Photolysis of  $\text{CCl}_4$  on  $\text{TiO}_2$  with *tert*-Butanol (t-BuOH) or 2-Propanol (2-PrOH) Present as Electron Donors. 151

## List of Figures

### Chapter 1

**Figure 1.** (a) Photooxidative degradation of organic compound (RH) in the presence of dissolved oxygen and (b) photoreductive degradation of chlorinated hydrocarbons (RCl) in the presence of electron donor (DH) on illuminated TiO<sub>2</sub> particle.

10

### Chapter 2

**Figure 1.** Absorption spectra of (a) Fe<sup>3+</sup>-doped Q-sized TiO<sub>2</sub> (1.34 g/L) at 0.0, 1.0, 2.0, 5.0, 10.0 % Fe<sup>3+</sup> concentrations (from left to right), (b) Ru<sup>3+</sup>-doped Q-sized TiO<sub>2</sub> (0.5 g/L) at 0.0, 0.5, 1.0, 2.0, and 3.0 % Ru<sup>3+</sup> concentrations (from bottom to up), and (c) undoped, Rh<sup>3+</sup> 3.0 %, V<sup>4+</sup> 3.0 %, and Mn<sup>3+</sup> 3.0 % Q-sized TiO<sub>2</sub> at 0.5 g/L (from left to right).

43

**Figure 2.** Periodic chart of the photocatalytic effects of various metal ion dopants in TiO<sub>2</sub>. The upper bold-faced numbers are the quantum yields (%) for the oxidative chloroform degradation,  $\Phi_{\text{CHCl}_3}$  and the lower numbers are the quantum yields (%) for Cl<sup>-</sup> production from the reductive dechlorination of carbon tetrachloride,  $\Phi_{\text{CCl}_4/\text{Cl}^-}$ . The numbers in the parentheses are the ionic radii (Å) for a coordination number of 6. All the oxidation states represent those of the precursor metal ions. All dopant concentrations are 0.5 atom% except Mo<sup>5+</sup> (0.1 atom%). Ti<sup>4+\*</sup> refers to the undoped TiO<sub>2</sub> (see Experimental Section for details).

44

**Figure 3.** Correlation plot between the oxidation quantum yield ( $\Phi_{\text{CHCl}_3}$ ) and the reduction quantum yield ( $\Phi_{\text{CCl}_4/\text{Cl}^-}$ ) from the data of Figure 2. Some dopants, which show little effect on the photoreactivity, are omitted for clarity of the figure. The straight lines are drawn only as a visual guide. 45

**Figure 4.** Light intensity ( $I$ ) dependence of the photodegradation rate of chloroform ( $v_{\text{ox}}$ ) for the undoped and  $\text{Fe}^{3+}$ -doped (0.5 %) Q-sized  $\text{TiO}_2$  under the condition of  $[\text{CHCl}_3]_0 = 3.15 \text{ mM}$  and pH 11. 46

**Figure 5.** Ratio of relative chloride production from  $\text{CCl}_4$  dechlorination as a function of added methanol concentration for the undoped and the  $\text{Fe}^{3+}$ -doped (0.5%) Q-sized  $\text{TiO}_2$ . 47

**Figure 6.** TEM pictures of (a) Q-sized  $\text{TiO}_2$  particles and (b) an aggregate of small particles ( $\text{Fe}^{3+}$  0.5%) resulting from heating at  $400 \text{ }^\circ\text{C}/4\text{h}$ . Several Q-sized particles are outlined for clarity. 48

**Figure 7.** Transient absorption decays observed at 600 nm in the  $\mu\text{s}$ -time scale for (a) undoped,  $\text{Fe}^{3+}$  0.5%, and  $\text{Co}^{3+}$  0.5%, and (b) undoped,  $\text{V}^{4+}$  0.5%, and  $\text{Al}^{3+}$  0.5% doped Q-sized colloids. 49

**Figure 8.** Transient absorption decays observed at 600 nm in the ms-time scale for  $\text{Fe}^{3+}$  0.5%,  $\text{V}^{4+}$  0.5%,  $\text{Ru}^{3+}$  0.5% doped and undoped Q-sized colloids. 50

**Figure 9.** Transient absorption decays observed at 600 nm for  $\text{Fe}^{3+}$ -doped colloids at 0.1, 0.5, and 3.0 %  $\text{Fe}^{3+}$  concentration in the (a)  $\mu\text{s}$ -time scale and (b) ms-time scale. 51

**Figure 10.** Correlation plot between the quantum yields [(a)  $\Phi_{\text{avg}}$ , (b)  $\Phi_{\text{red}}$ , and (c)  $\Phi_{\text{ox}}$ ] and  $A_{\infty}$  from Table III. 52

**Figure 11.** Energy levels of impurity ions in rutile proposed by Mizushima et al. and Triggs (\*). 53

### Chapter 3

**Figure 1.**  $\text{CCl}_4$  dechlorination rates as a function of added methanol concentration where  $[\text{CCl}_4]_0 = 5.1 \text{ mM}$ ,  $\text{pH} = 2.8 \pm 0.1$ ,  $[\text{TiO}_2] = 0.5 \text{ g/L}$ ,  $I = 2.1 \times 10^{-4} \text{ einstein L}^{-1} \text{ min}^{-1}$  (at  $\lambda = 320 \text{ nm}$ , FWHM 15 nm), and  $[\text{O}_2]_{\text{diss}} \sim 0.2 \text{ mM}$  (air-equilibrated). 81

**Figure 2.**  $\text{CCl}_4$  dechlorination rates as a function of added acetate concentration at an initial pH of 2.8 ( $\bullet$ ) and 6.0 (o). Other conditions are the same with those of Fig. 1. 82

**Figure 3.**  $\text{CCl}_4$  dechlorination rates as a function of pH in the presence of 1 mM of sodium acetate. Other conditions are the same with those of Fig.1. 83

**Figure 4.** Rates of acid generation (corrected by eq. 6) from  $\text{CCl}_4$  degradation as a function of pH with 0.1 M of *tert*-butanol ( $\Delta$ ), methanol ( $\bullet$ ), and 2-propanol (o). The pH was maintained constant within  $\pm 0.05$  during each separate photolysis. Other conditions are the same with those of Fig. 1. 84

**Figure 5.** Plot of the rates of  $\text{CCl}_4$  dechlorination with aliphatic carboxylic acids against the  $k_{\text{OH}}$  from Table III. The corresponding numbers refer to 1, trifluoroacetate; 2, oxalate; 3, acetate; 4,

malonate; 5, monofluoroacetate; 6, propionate; 7, isobutyrate; 8, trimethylacetate; 9, butyrate; 10, formate. 85

**Figure 6.** CCl<sub>4</sub> degradation at pH 2.7 and the production of Cl<sup>-</sup> and intermediates in the presence of 2-propanol (0.1 M) in (a) an oxygenated and (b) a deoxygenated suspension. [TiO<sub>2</sub>] = 0.5 g/L, and I = 1.46 x 10<sup>-3</sup> einstein L<sup>-1</sup> min<sup>-1</sup> (310 - 400 nm). 86

**Figure 7.** CCl<sub>4</sub> degradation at pH 12.4 and the production of Cl<sup>-</sup> and intermediates in the presence of 2-propanol (0.1 M) in (a) an oxygenated and (b) a deoxygenated suspension under the same condition of Fig.6. 87

**Figure 8.** CCl<sub>4</sub> degradation with *tert*-butanol (0.1 M) in the oxygenated and deoxygenated suspensions at both pH 2.7 and pH 12.4. The other conditions are the same with those of Fig. 6. 88

#### Chapter 4

**Figure 1.** Mass spectra (extracted from a GC total ion chromatogram) of (a) TCCl<sub>2</sub> and (b) TCCl<sub>3</sub> which were generated during the CCl<sub>4</sub> photolysis in the presence of TiO<sub>2</sub> and traps. The mass signal intensities were normalized. 117

**Figure 2.** The time-dependent production of TCCl<sub>2</sub> during the photolysis with varying amount of water (0, 0.2, 1, and 10 M). The experimental conditions were: [CCl<sub>4</sub>]<sub>0</sub> = 5 mM, [TiO<sub>2</sub>] = 0.5 g L<sup>-1</sup>, I = 1.43 x 10<sup>-3</sup> einstein L<sup>-1</sup> min<sup>-1</sup> ( 310 < λ < 400 nm), [Trap] = 0.1 M, air-equilibration, and no pH adjustment. 118

**Figure 3.** The comparison of the production of TCCl<sub>2</sub>, TCCl<sub>3</sub>, and chloride after 30 min irradiation as a function of water concentration in TiO<sub>2</sub> suspension. Other experimental conditions were the same to those of Fig. 2. The concentration of TCCl<sub>3</sub> was not determined. 119

**Figure 4.** The productions of (a) TCCl<sub>2</sub> and (b) TCCl<sub>3</sub> as a function of irradiation time in TiO<sub>2</sub> suspensions saturated with N<sub>2</sub>, air, and O<sub>2</sub> gases before irradiation. Water concentration was 10 molar and other experimental conditions were the same to those of Fig. 2. 120

**Figure 5.** The production of (a) TCCl<sub>2</sub> and (b) TCCl<sub>3</sub> as a function of initial CCl<sub>4</sub> concentration. The concentration dependences are compared at two different light intensities (1.4 mE L<sup>-1</sup> min<sup>-1</sup> vs. 61 μE L<sup>-1</sup> min<sup>-1</sup>). Water concentration was 10 molar and other experimental conditions were the same to those of Fig. 2. 121

**Figure 6.** Light intensity dependence of TCCl<sub>2</sub> production rate under the same experimental conditions of Fig. 2. Water concentration was 10 molar. The solid lines represent the light-intensity dependence of I<sup>2.0</sup>, I<sup>1.0</sup>, and I<sup>0.5</sup>, respectively. 122

**Figure 7.** The pH (relative scale) dependence of the production rate of TCCl<sub>2</sub>, TCCl<sub>3</sub>, and chloride in the TiO<sub>2</sub> suspension having the same condition of Fig. 2. Water concentration was 10 molar. The production rate of TCCl<sub>3</sub> is relative. 123

**Figure 8.** The pH dependence of CCl<sub>4</sub> degradation, which were measured by monitoring the acid generation rate, in an aqueous

TiO<sub>2</sub> suspension where [CCl<sub>4</sub>]<sub>0</sub> = 5.1 mM, [TiO<sub>2</sub>] = 0.5 g L<sup>-1</sup>, I = 2.1 x 10<sup>-4</sup> einstein L<sup>-1</sup> min<sup>-1</sup> (λ = 320 ± 10 nm), [CH<sub>3</sub>OH] = 0.1 M, and air-equilibration.

124

**Figure 9.** The degradation of CCl<sub>4</sub> and the production of intermediates and chloride in an aqueous TiO<sub>2</sub> suspension at (a) pH 2.7 and (b) pH 12.4. Other experimental conditions were [TiO<sub>2</sub>] = 0.5 g L<sup>-1</sup>, I = 1.46 x 10<sup>-3</sup> einstein L<sup>-1</sup> min<sup>-1</sup> (310 < λ < 400 nm), [(CH<sub>3</sub>)<sub>2</sub>CHOH] = 0.1 M, and N<sub>2</sub> saturation prior to light illumination.

125

## Chapter 5

**Figure 1.** The production of halide ions from the photocatalytic decomposition of (a) 6 mM CHCl<sub>3</sub> and (b) 6 mM CHBr<sub>3</sub> solutions, which were saturated with N<sub>2</sub> prior to the photolysis, in a sealed reactor at the initial pH 5 and 12 as a function of irradiation time. The halide generations from dark hydrolysis of the same substrates at pH 12 are shown as well. There was no hydrolysis at pH 5.

152

**Figure 2.** Chloride generation from the photolysis of 6 mM CHCl<sub>3</sub> solutions (pH<sub>i</sub> 4.5) which were saturated with O<sub>2</sub>, air, and N<sub>2</sub>, respectively prior to irradiation. The dotted line represents the chloride level corresponding to the stoichiometric consumption of dissolved oxygen (0.25 mM) in an air-saturated solution.

153

**Figure 3.** Dependence of the photocatalytic chloride generation rates in 6 mM CHCl<sub>3</sub> solution on the dissolved oxygen concentration. The dechlorination rates were measured over an initial 1-hr photolysis period. The concentration of dissolved oxygen

was varied by changing the ratio of the flow rates of  $O_2$  and  $N_2$  bubbling gases and calculated by assuming that the dissolved oxygen concentration in an  $O_2$ -saturated solution was 1.27 mM.

The solid line is a fit to eq 12.

154

**Figure 4.** Effect of the initial pH of  $TiO_2$  suspension on the photocatalytic production of (a) chloride and (b)  $C_2Cl_4$  and  $C_2Cl_6$  in 6 mM  $CHCl_3$  solutions, which were saturated with  $O_2$  or  $N_2$  prior to irradiation. Concentrations were measured after 1 hr irradiation.

The dotted line in (a) represents calculated pH-dependent chloride production after 1 hr dark hydrolysis.

155

**Figure 5.** Production of dimerized halogenated intermediates ( $C_2Cl_4$  and  $C_2Cl_6$  from 6 mM  $CHCl_3$  solution and  $C_2Br_4$  from 6 mM  $CHBr_3$  solution) as a function of irradiation time. The concentration of  $C_2Br_4$  could not be quantified since its authentic sample was not available. The data were obtained from the same photolysis run of Figure 1. The  $TiO_2$  suspension was initially saturated with  $N_2$  and set to pH 12 before irradiation.

156

**Figure 6.** Three proposed photocatalytic mechanisms of  $CHX_3$  ( $X = Cl$  or  $Br$ ) degradation on  $TiO_2$  and a dark hydrolysis reaction are illustratively compared.

157

## **Chapter 1**

### Introduction

Since Fujishima and Honda<sup>1</sup> reported the light-induced water splitting reaction to produce hydrogen gas on TiO<sub>2</sub> electrode in 1972, there have been tremendous amount of research efforts driven into the field of "semiconductor photoelectrochemistry", which is often related to energy resource issues.<sup>2</sup> The photoelectrochemical reactions on semiconductor are often classified into "photocatalysis" and "photosensitization" respectively, depending on whether the overall reaction is thermodynamically spontaneous or not. While most of photoelectrochemical oxidation reactions fall into the first category, water splitting reaction and the fixation of nitrogen and carbon dioxide,<sup>2</sup> which are central reactions to solar energy storage, are in the second category. Since this thesis work is related to the photodegradation of chlorinated compounds which is thermodynamically spontaneous, the term "photocatalysis" is used throughout the text.

The photocatalytic reactions which are initiated by a band-gap excitation of an electron-hole pair occur not only on semiconductor electrodes but also on colloidal semiconductor particles.<sup>3,4</sup> There are several unique advantages in the colloidal semiconductor system: (1) It has large surface area and high light absorption efficiency, which leads to the maximum light energy utilization; (2) Both conduction band (CB) electrons ( $e_{cb}^-$ ) and valence band (VB) holes ( $h_{vb}^+$ ) in the same particle can be used in the chemical redox process; (3) Due to the small dimension of the particle, the charge-carrier diffusion to the interface is rapid, competing effectively with electron-hole recombination; (4) The surface and bulk properties of the semiconductor particle can be easily modified by various methods such as metal ion doping,<sup>5</sup> noble metal deposition,<sup>6</sup> surface complexation,<sup>7</sup> semiconductor coupling,<sup>8</sup> and dye sensitization<sup>9</sup> in order to enhance the quantum efficiency. In particular, when the particle size is getting

small (less than 10 nm) enough to perturb the semiconductor band structure, the semiconductor particles show substantially different photophysical properties from those of bulk materials, which is commonly referred to as “quantum-size effect”.<sup>3,10</sup>

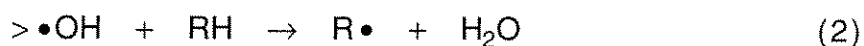
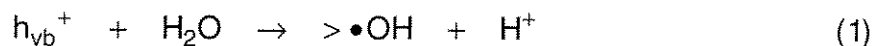
While the research of photoelectrochemistry was making its progress toward the goal of new energy resource, other applications of semiconductor photocatalysis to a variety of chemical reactions have been recognized very useful. They include chemical synthesis,<sup>11</sup> the total mineralization of organic compounds in water and air,<sup>12</sup> the destruction of microorganism such as bacteria and viruses,<sup>13</sup> the inactivation of cancer cells,<sup>14</sup> indoor odor control,<sup>15</sup> coating for self-cleaning materials,<sup>16</sup> the removal of toxic metals from aqueous solution,<sup>17</sup> and the clean-up of oil spills.<sup>18</sup> More than 1200 works have been published in these fields of research between 1970 and 1995.<sup>19</sup> In particular, the application to the environmental remediation<sup>12</sup> of polluted water and air has been one of the most active research areas since Pruden and Ollis<sup>20</sup> demonstrated the photocatalytic degradation of chloroform and trichloroethylene in 1983.

Among a wide range of semiconductor materials tested,  $\text{TiO}_2$  has proven itself to be suitable for various photocatalytic applications due to its outstanding photochemical stability, availability, and non-toxicity.<sup>21</sup>  $\text{TiO}_2$  photocatalysis has shown to be successful for the total destruction for a wide range of organic compounds owing to its strong oxidation potential (VB hole, 2.7 V vs NHE).<sup>22</sup> In general other semiconductor materials have been found to be less active than titanium dioxide. However,  $\text{TiO}_2$  has a wide band gap (3.2 eV for anatase and 3.0 eV for rutile), which prevents the utilization of visible light that accounts for most of solar energy. In order to improve the overlap of the absorption spectrum

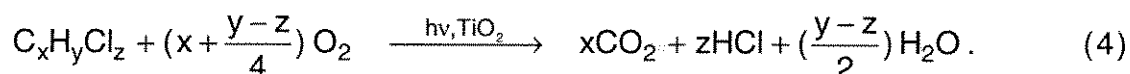
of  $\text{TiO}_2$  with the solar spectrum, a great deal of work has been done on modifying  $\text{TiO}_2$  by using the methods listed in the second paragraph.

Besides their photophysical process in the lattice,  $\text{TiO}_2$  particles take charge on surface in the aqueous solution due to the amphoteric property of surface hydroxyl groups ( $\text{pH}_{\text{zpc}} 6.2$ ) and surround themselves with an oppositely charged "electrical double layer".<sup>23</sup> The electrostatic interaction between surface and substrates sometimes critically affects the photocatalytic reaction.<sup>24</sup> In addition to the purely electrostatic interaction, many organic and inorganic substrates undergo inner-sphere ligand substitution reactions with the surface functionality of  $\text{TiO}_2$ . Such direct chemical bond formation at the surface makes the charge transfer to substrates more favorable,<sup>25</sup> which leads to more efficient photodegradation. Therefore, understanding the heterogeneous surface chemistry of  $\text{TiO}_2$  as well as the photochemistry is valuable for improving the efficiency of photocatalytic reactions.

Figure 1a shows primary photooxidation steps on  $\text{TiO}_2$  particle. Once electron-hole pairs are generated through photoexcitation, most of them recombine generating heat. Only a small fraction successfully transfers to the interface to initiate redox reactions. Typical quantum yields of photocatalytic reactions range from a fraction of a percent to a few percent at best.<sup>26</sup> The process of chemical destruction is initiated at the surface of the photocatalyst through an interfacial charge-transfer. The oxidation of substrates (RH) on  $\text{TiO}_2$  is thought to proceed through a surface adsorbed hydroxyl radical (reactions 1,2) in most cases and through a direct VB hole transfer (reaction 3) in some cases.<sup>27-29</sup>



Subsequent chemical reactions, which lead to full degradation, generally involve radical species.<sup>22</sup> Dissolved oxygen is usually necessary for complete mineralization of organic compounds.<sup>24</sup> It serves not only as a CB electron acceptor to reduce recombination but also as a reactant. A typical reaction of O<sub>2</sub> is its addition to a carbon-centered radical, which occurs very rapidly with a rate constant of diffusion limit, producing a peroxy radical.<sup>30</sup> The chemistry of peroxy radical is well understood from homogeneous radiolysis studies.<sup>31</sup> When oxygen is absent, most of the organic compounds have shown negligible photodegradation rates.<sup>32,33</sup> Various oxygen-containing radical species such as  $\cdot\text{OH}$  ( $\text{O}\cdot$ ) and  $\cdot\text{O}_2\text{H}$  ( $\cdot\text{O}_2^-$ ) are formed from O<sub>2</sub> on the illuminated TiO<sub>2</sub> surface and they may oxidize substrates directly.<sup>22</sup> A general stoichiometry for the photocatalytic oxidation of chlorinated hydrocarbons to complete mineralization can be written as follows:



Photoreductive degradation of chlorinated hydrocarbons can be initiated through a similar process (Figure 1b). In this case, organic substrates are CB electron acceptors instead of dioxygen molecules and the presence of electron donors to scavenge VB holes is required for efficient photoreduction.<sup>34</sup> Upon receiving a CB electron, a chloride ion is dissociatively detached from a chlorinated compound with generation of a carbon-centered radical. Following reactions are similar to those of photooxidation. However, photoreduction

reactions on  $\text{TiO}_2$  are largely limited due to the weak reduction potential of CB electrons (-0.5 V vs NHE at pH 7).

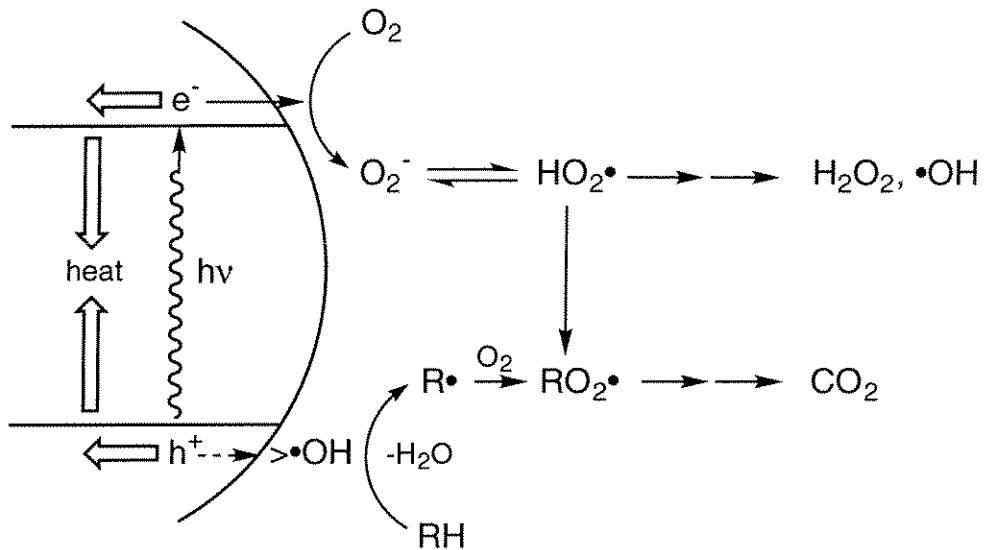
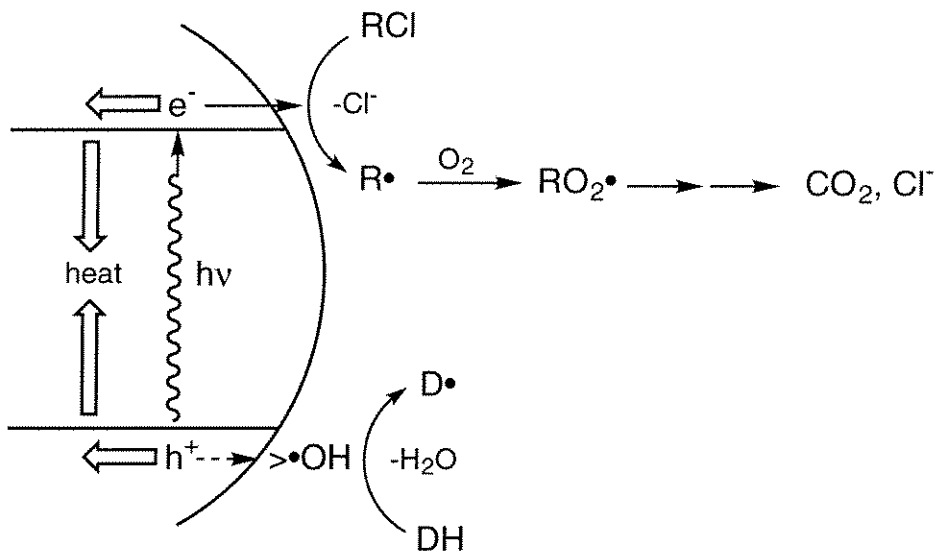
This thesis consists of six chapters. Chapter 1 (this chapter) describes a general background of photocatalysis. Chapter 2 through 5 are research works on  $\text{TiO}_2$  photocatalysis, each of which can be read independently. In Chapter 2, a systematic study of 21 metal-ion doped quantum-sized  $\text{TiO}_2$  colloids is described. The photoelectronic properties of semiconductor is greatly influenced by the presence of dopants. In this study we offer a general explanation for the role of metal ion dopants in  $\text{TiO}_2$  photocatalysis on the basis of both photochemical and photophysical measurements. Chapter 3 examines the photoreductive degradation reaction of  $\text{CCl}_4$  (Figure 1b type) in illuminated  $\text{TiO}_2$  suspension. Effects of various electron donors on the photoreduction are investigated in detail and a mechanism for  $\text{CCl}_4$  photodegradation is proposed. The photocatalytic mechanism of  $\text{CCl}_4$  degradation proposed in Chapter 3 is verified in the study of Chapter 4 where the transient free radical intermediates of trichloromethyl radical and dichlorocarbene are chemically trapped during the photolysis. A detailed kinetic analysis for their reaction is also presented. Inspired by the studies of  $\text{CCl}_4$  reaction in Chapters 3 and 4, the photooxidation of  $\text{CHCl}_3$  is reinvestigated in Chapter 5. The study reveals a new photocatalytic mechanism of  $\text{CHCl}_3$  degradation in addition to a known mechanism. Chapter 6 summarizes the results, discusses the implication of this thesis work, and suggests future research.

## References

- (1) Fujishima, A.; Honda, K. *Nature* **1972**, *37*, 238.
- (2) *Energy Resources through Photochemistry and Catalysis*; Grätzel, M., Ed.; Academic Press: New York, 1983.
- (3) Henglein, A. *Chem. Rev.* **1989**, *89*, 1861.
- (4) Kamat, P.V. *Chem. Rev.* **1993**, *93*, 267.
- (5) Chapter 2 in this thesis and references therein.
- (6) (a) Hermann, J.-M.; Disdier, J.; Pichat, P. *J. Phys. Chem.* **1986**, *90*, 6028. (b) Pichat, P.; Mozzanega, M.-N.; Courbon, H. *J. Chem. Soc. Faraday Trans. 1* **1987**, *83*, 697.
- (7) (a) Vrachnon, E.; Grätzel, M.; McEvoy, A.J. *J. Electroanal. Chem.* **1989**, *258*, 193. (b) Moser, J.; Punchedewa, S.; Infelta, P.P.; Grätzel, M. *Langmuir* **1991**, *7*, 3012.
- (8) (a) Gopidas, K.R.; Bohorquez, M.; Kamat, P.V. *J. Phys. Chem.* **1990**, *94*, 6435. (b) Vinodgopal, K.; Kamat, P.V. *Environ. Sci. Technol.* **1995**, *29*, 841.
- (9) Vinodgopal, K.; Hua, X.; Dahlgren, R.L.; Lappin, A.G.; Patterson, L.K.; Kamat, P.V. *J. Phys. Chem.* **1995**, *99*, 10883.
- (10) Brus, L. *J. Phys. Chem.* **1986**, *90*, 2555.
- (11) Fox, M.A.; Dulay, M.T. *Chem. Rev.* **1993**, *93*, 341.
- (12) Ollis, D.F., Al-Ekabi, H., Eds, *Photocatalytic Purification and Treatment of Water and Air*; Elsevier: Amsterdam, 1993.
- (13) (a) Ireland, J.C.; Klostermann, P.; Rice, E.W.; Clark, R.M. *Appl. Environ. Microbiol.* **1993**, *59*, 1668. (b) Sjogren, J.C.; Sierka, R.A. *Appl. Environ. Microbiol.* **1994**, *60*, 344.

- (14) (a) Cai, R.X.; Kubota, Y.; Shuin, T.; Sakai, H.; Hashimoto, K.; Fujishima, A. *Cancer Res.* **1992**, *52*, 2346. (b) Cai, R.X.; Hashimoto, K.; Kubota, Y.; Fujishima, A. *Chem. Lett.* **1992**, 427.
- (15) Suzuki, K. In *Photocatalytic Purification and Treatment of Water and Air*; Ollis, D.F., Al-Ekabi, H., Eds.; Elsevier: Amsterdam, 1993.
- (16) Kojima, E.; Watanabe, T.; Kimura, T.; Mizukane, M. In *Abstracts of the First International Conference on Advanced Oxidation Technologies for Water and Air Remediation*; London, Ontario, 1994.
- (17) Borgarello, E.; Serpone, N.; Emo, G.; Harris, R.; Pelizzetti, E.; Minero, C. *Inorg. Chem.* **1986**, *25*, 4499.
- (18) Nair, M.; Luo, Z.H.; Heller, A. *Ind. Eng. Chem. Res.* **1993**, *32*, 2318.
- (19) Blake, D.M., Ed., *Bibliography of Work on the Heterogeneous Photocatalytic Removal of Hazardous Compounds from Water and Air: Update Number 1 To June, 1995*; NREL/TP-473-20300; NREL: Golden, CO, 1995.
- (20) (a) Pruden, A.L.; Ollis, D.F. *Environ. Sci. Technol.* **1983**, *17*, 628. (b) Pruden, A.L.; Ollis, D.F. *J. Catal.* **1983**, *82*, 404.
- (21) Schiavello, M., Ed. *Photocatalysis and Environment: Trends and Applications*; Kluwer Academica Publishers: Dordrecht, 1988.
- (22) Hoffmann, M.R.; Martin, S.T.; Choi, W.; Bahnemann, D.W. *Chem. Rev.* **1995**, *95*, 69.
- (23) Stumm, W.; Morgan, J.J. *Aquatic Chemistry*, 2nd ed.; Wiley-Interscience: New York 1981.
- (24) Kormann, C.; Bahnemann, D.W.; Hoffmann, M.R. *Environ. Sci. Technol.* **1991**, *25*, 494.
- (25) (a) Tunesi, S.; Anderson, M. *J. Phys. Chem.* **1991**, *95*, 3399. (b) Frei, H.; Fitzmaurice, D.F.; Grätzel, M. *Langmuir* **1990**, *6*, 198.
- (26) Chapters 2 and 3 in this thesis.

- (27) Mao, Y.; Schöneich, C.; Asmus, K.-D. *J. Phys. Chem.* **1991**, *95*, 10080.
- (28) Cunningham, J.; Srijaranai, S. *J. Photochem. Photobiol. A: Chem.* **1988**, *43*, 329.
- (29) Stafford, U.; Gray, K.A.; Kamat, P.V. *J. Phys. Chem.* **1994**, *98*, 6343.
- (30) Lal, M.; Schöneich, C.; Mönig, J.; Asmus, K.-D. *Int. J. Radiat. Biol.* **1988**, *54*, 773.
- (31) (a) Köster, R.; Asmus, K.-D. *Z. Naturforsch.* **1971**, *26b*, 1108. (b) Mönig, J.; Bahnemann, D.; Asmus, K.-D. *Chem.-Biol. Interactions* **1983**, *45*, 15. (c) Mönig, J.; Asmus, K.-D. *J. Chem. Soc. Perkin Trans. II* **1984**, 2057.
- (32) Hsiao, C.-Y.; Lee, C.-L.; Ollis, D.F. *J. Catal.* **1983**, *82*, 418.
- (33) Hidaka, H.; Nohara, K.; Zhao, J.; Serpone, N.; Pelizzetti, E. *J. Photochem. Photobiol. A: Chem.* **1992**, *64*, 247.
- (34) Chapter 3 in this thesis.

**(a) Photooxidation****(b) Photoreduction**

**Figure 1.** (a) Photooxidative degradation of organic compound (RH) in the presence of dissolved oxygen and (b) photoreductive degradation of chlorinated hydrocarbons (RCl) in the presence of electron donor (DH) on illuminated  $\text{TiO}_2$  particle.

## Chapter 2

### The Role of Metal-Ion Dopants in Quantum-Sized TiO<sub>2</sub>: Correlation between Photoreactivity and Charge-Carrier Recombination Dynamics

[ The text of this chapter appears in: W. Choi, A. Termin, and M.R. Hoffmann  
*Journal of Physical Chemistry* **1994**, *98*, 13669 - 13679.]

## Abstract

A systematic study of metal-ion doping in quantum (Q-) sized (2-4 nm) TiO<sub>2</sub> colloids is performed by measuring their photoreactivities and the transient charge-carrier recombination dynamics. The presence of metal-ion dopants in the TiO<sub>2</sub> crystalline matrix significantly influences photoreactivity, charge-carrier recombination rates and interfacial electron-transfer rates. The photoreactivities of 21 metal-ion doped colloids are quantified in terms of both the conduction band electron reduction of an electron acceptor (CCl<sub>4</sub> dechlorination) and the valence band hole oxidation of an electron donor (CHCl<sub>3</sub> degradation). Doping with Fe<sup>3+</sup>, Mo<sup>5+</sup>, Ru<sup>3+</sup>, Os<sup>3+</sup>, Re<sup>5+</sup>, V<sup>4+</sup>, and Rh<sup>3+</sup> at 0.1-0.5 atom% significantly increases the photoreactivity for both oxidation and reduction while Co<sup>3+</sup> and Al<sup>3+</sup> doping decreases the photoreactivity. The transient absorption signals upon laser flash photolysis ( $\lambda_{\text{ex}} = 355 \text{ nm}$ ) at  $\lambda = 600 \text{ nm}$  are extended up to 50 msec for Fe<sup>3+</sup>, V<sup>4+</sup>, Mo<sup>5+</sup>, and Ru<sup>3+</sup>-doped TiO<sub>2</sub> while the undoped Q-sized TiO<sub>2</sub> shows a complete "blue electron" signal decay within 200  $\mu\text{sec}$ . Co<sup>3+</sup> and Al<sup>3+</sup>-doped TiO<sub>2</sub> are characterized by rapid signal decays with a complete loss of absorption signals within 5  $\mu\text{sec}$ . The quantum yields obtained during CW photolyses are quantitatively correlated with the measured transient absorption signals of the charge-carriers. Photoreactivities are shown to increase with the relative concentration of trapped charge carriers. The photoreactivity of doped TiO<sub>2</sub> appears to be a complex function of the dopant concentration, the energy level of dopants within the TiO<sub>2</sub> lattice, their d-electronic configuration, the distribution of dopants, the electron donor concentration, and the light intensity.

## Introduction

TiO<sub>2</sub> photocatalysis has been the focus of numerous investigations in recent years,<sup>1</sup> particularly because its application for the quantitative destruction of undesirable chemical contaminants appears to be a promising process for water- and air-pollution control.<sup>2</sup> Complete mineralization of a wide variety of organic compounds to CO<sub>2</sub>, H<sub>2</sub>O and inorganic constituents has been reported.<sup>1a</sup> Photocatalytic efficiency of TiO<sub>2</sub> depends, in part, upon the relative degree of branching of the reactive electron/hole pairs into interfacial charge-transfer reactions. In order to enhance interfacial charge-transfer reactions, the properties of TiO<sub>2</sub> colloids and electrodes have been modified by selective surface treatments such as surface chelation,<sup>3</sup> surface derivatization,<sup>4</sup> and platinization<sup>5</sup> and by selective metal-ion doping<sup>6-20</sup> of the crystalline TiO<sub>2</sub> matrix.

Several transition metal-ion dopants in TiO<sub>2</sub> have been investigated previously. Fe<sup>3+</sup> was shown to increase the efficiency of photoreduction of N<sub>2</sub><sup>8,10</sup> and methyl viologen<sup>6</sup> and to inhibit electron/hole pair recombination in TiO<sub>2</sub>.<sup>7b</sup> In the case of the photodegradation of phenol, Fe<sup>3+</sup>-doping of TiO<sub>2</sub> had little effect on relative photoreactivity.<sup>10</sup> Enhanced photoreactivity for water cleavage<sup>18</sup> and N<sub>2</sub> reduction<sup>10b</sup> with Cr<sup>3+</sup>-doped TiO<sub>2</sub> has been reported while other researchers have shown that Cr<sup>3+</sup> was detrimental to the photocatalytic activity.<sup>13c,15</sup> TiO<sub>2</sub> doped with Mo and V exhibited significantly reduced photoactivity<sup>14</sup> although Grätzel and Howe<sup>7a</sup> suggested an inhibition of electron/hole pair recombination with these dopants based on EPR data. Mu et al.<sup>15</sup> reported that doping with trivalent or pentavalent metal ions were detrimental to the photocatalytic reactivity while Karakitsou and Verykios<sup>16</sup> showed that doping with cations of valency higher than that of Ti<sup>4+</sup> enhanced photoreactivity.

Even though metal-ion doping effects on the reactivity of  $\text{TiO}_2$  have been a frequent topic of investigation, direct comparisons and unifying conclusions are difficult to make since widely-varying experimental conditions for sample preparation and for the determination of photoreactivity have been employed. Furthermore, there appears to be no direct correlation between the photophysical measurements<sup>7</sup> and photochemical reactivity.<sup>10,15</sup>

In this paper, we present a systematic study of metal-ion doping of quantum- (Q-) sized  $\text{TiO}_2$  for 21 metal ions. Based on both photochemical and photophysical measurements, we offer a general explanation for the role of metal-ion dopants in  $\text{TiO}_2$  photocatalysis. The photoreactivities of doped Q-sized  $\text{TiO}_2$  colloids (transparent particle suspensions) are quantified in terms of both the conduction band (CB) electron reduction of  $\text{CCl}_4$  and the valence band (VB) hole oxidation of  $\text{CHCl}_3$ .<sup>21</sup> Measured photoreactivities for the doped  $\text{TiO}_2$  colloids are compared with their photoexcited transient absorption spectra in order to probe the relationship between photoreactivity and charge-pair recombination.

## Experimental Section

**Colloid Synthesis and Characterization.** Q-sized  $\text{TiO}_2$  colloids were prepared from the controlled hydrolysis of titanium tetraisopropoxide.<sup>22</sup> 1.25 mL of  $\text{Ti}(\text{OCH}(\text{CH}_3)_2)_4$  (Aldrich 97%) dissolved in 25 mL absolute ethanol was added dropwise under vigorous stirring to 250 mL distilled water (4 °C) adjusted to pH 1.5 with nitric acid. The resulting transparent colloidal suspension (1.34 g/L) was stirred overnight. The colloidal suspension can be stored in a cold room (4 °C) for over one year without coagulation. To obtain a powder sample, the above colloidal solution was evaporated (35 °C) using a rotavapor and dried under

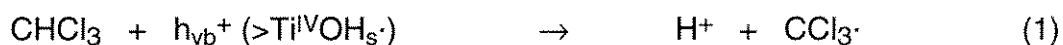
vacuum. The powdered sample contained ~30 wt% of HNO<sub>3</sub>. Redissolving the powder in distilled water with 0.5 gTiO<sub>2</sub>/L resulted in a transparent suspension of pH 2.8 ± 0.1. The presence of nitrate in the TiO<sub>2</sub> samples may induce secondary photochemical effects because the direct photolysis of nitrate can result in the formation of hydroxyl radicals which directly initiate degradation reactions of organic substrates.<sup>23</sup> In order to assess this side effect from nitrate, a TiO<sub>2</sub> sample was prepared using perchloric acid instead of nitric acid under otherwise same conditions. No difference in the photocatalytic reactivity was found between the two TiO<sub>2</sub> samples.

Doped Q-sized TiO<sub>2</sub> was prepared according to the above procedure in the presence of added metal salts to give a doping level from 0.1 to 3.0 atom%. All the dopant concentrations mentioned in this work are the nominal atomic concentration which is based upon the assumption of quantitative incorporation of the dopant. All the available dopant metal ions which have an ionic radius similar to that of Ti<sup>4+</sup> (0.75 Å) were chosen for substitution into the lattice. Metal salts used as precursors for dopant ions are listed as follows: LiOH, Mg(ClO<sub>4</sub>)<sub>2</sub>, AlCl<sub>3</sub>, VCl<sub>3</sub>, VOSO<sub>4</sub>·3H<sub>2</sub>O, VOCl<sub>3</sub>, Cr(NO<sub>3</sub>)<sub>3</sub>, MnF<sub>3</sub>, Fe(NO<sub>3</sub>)<sub>3</sub>·9H<sub>2</sub>O, CoF<sub>3</sub>, NiCl<sub>2</sub>, Zn(ClO<sub>4</sub>)<sub>2</sub>, Ga(NO<sub>3</sub>)<sub>3</sub>, Zr(OCH(CH<sub>3</sub>)<sub>2</sub>)<sub>4</sub>, NbCl<sub>5</sub>, MoCl<sub>5</sub>, RuCl<sub>3</sub>, Rh(NO<sub>3</sub>)<sub>3</sub>·2H<sub>2</sub>O, SnCl<sub>4</sub>, SbCl<sub>5</sub>, TaCl<sub>5</sub>, ReCl<sub>5</sub>, and OsCl<sub>3</sub>. Precursors of Zr(OCH(CH<sub>3</sub>)<sub>2</sub>)<sub>4</sub>, NbCl<sub>5</sub>, SbCl<sub>5</sub> and TaCl<sub>5</sub> were dissolved in ethanol along with titanium tetraisopropoxide while the others were added to the acidic water. Doped TiO<sub>2</sub> powder samples displayed various colors depending on the kind of metal ions and their concentrations: V<sup>3+</sup>, V<sup>4+</sup>, V<sup>5+</sup>, Fe<sup>3+</sup>, Rh<sup>3+</sup>, and Re<sup>5+</sup> -doped samples were yellowish, Cr<sup>3+</sup>-doped greenish, Co<sup>3+</sup>-doped pink, Ni<sup>2+</sup>-doped bright blue, Ru<sup>3+</sup>-doped dark brown, and Mn<sup>3+</sup> and Os<sup>3+</sup>-doped greenish to brownish grey. Inductively Coupled Plasma - Mass Spectrometry (ICP-MS)

analysis of the supernatant from coagulated doped colloids showed no significant amount of dissolved metal ions.

The particle sizes were determined by a Philips EM 430 transmission electron microscope (TEM) at 300 kV. TEM samples were prepared on a copper mesh substrate covered with an amorphous carbon film. The particle sizes were 2 - 4 nm. A particle of 3 nm-diameter consists of 410 TiO<sub>2</sub> monomers. Analysis of lattice fringes in an individual small particle showed the lattice spacing of 3.6 ± 0.1 Å, which is in good agreement with the anatase (101) lattice spacing of 3.51 Å. X-ray diffraction (XRD) and Raman spectroscopy analysis showed the presence only of the anatase as well. The line broadening in the diffractogram of Q-sized TiO<sub>2</sub> was analyzed by the Scherrer equation to give the particle sizes of 3 - 4 nm, which well matched the TEM analysis. UV-Visible absorption spectra of various doped TiO<sub>2</sub> colloidal suspensions were recorded on a HP8451A diode array spectrophotometer.

**Photoreactivity measurements.** The photoreactivity of each doped TiO<sub>2</sub> system was quantified in terms of CHCl<sub>3</sub> oxidation by VB holes (or trapped holes):<sup>24</sup>

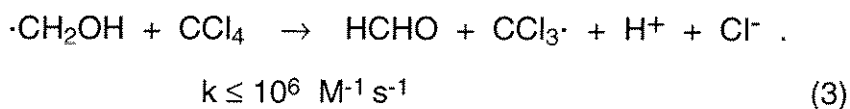


and CCl<sub>4</sub> reduction by CB electrons (or trapped electrons):<sup>25,28</sup>



where  $h_{\text{vb}}^+$  refers to a valence band hole, a trapped hole or a surface-bound ·OH radical and  $e_{\text{cb}}^-$  refers to a conduction-band electron or a trapped electron. Reaction 2 was performed in the presence of added methanol (0.1 M) as a hole scavenger.

One complexity may arise in the CCl<sub>4</sub>/CH<sub>3</sub>OH system because methanol forms  $\alpha$ -hydroxymethyl radicals upon the hole-initiated hydrogen-atom abstraction which are strong one-electron reductants ( $E_{1/2}(\cdot\text{CH}_2\text{OH}/\text{HCHO}) = -0.74 \text{ V vs. NHE}$ ).<sup>26</sup> As a result, the  $\alpha$ -hydroxymethyl radicals can directly reduce CCl<sub>4</sub> as follows:<sup>27</sup>



The above reaction enables CCl<sub>4</sub> to be reduced by the hole-initiated pathway, which makes the assessment of photoreduction by CB electrons difficult. However, under the air-saturation condition of the present study, reaction 3 competes with the addition of molecular oxygen to the  $\cdot\text{CH}_2\text{OH}$  radical. Using the experimental conditions employed in this paper (vide infra) and the literature rate constants ( $k(\cdot\text{CH}_2\text{OH} + \text{O}_2) = 4.9 \times 10^9 \text{ M}^{-1} \text{ s}^{-1}$ )<sup>27</sup>, we calculate that only 0.5 % of the  $\cdot\text{CH}_2\text{OH}$  radicals proceed via reaction 3. In the recent study of CCl<sub>4</sub> photoreduction in TiO<sub>2</sub> suspensions,<sup>28</sup> we compared the efficiency of methanol as a hole scavenger with that of *tert*-butanol which does not form  $\alpha$ -hydroxyalkyl radicals; the dechlorination rate was only slightly higher in the CCl<sub>4</sub>/methanol system than in the CCl<sub>4</sub>/*tert*-butanol system under the same experimental conditions to this work.

Irradiation was performed with a 1000-W Xe arc lamp (Spindler and Hoyer). Light was filtered by a 10-cm IR water filter and a UV interference filter (Oriel) which transmits light only at  $320 \pm 7 \text{ nm}$ , and subsequently focused onto a reactor cell. The light intensity measurement was performed by chemical actinometry using (E)- $\alpha$ -(2,5-dimethyl-3-furylethylidene) (isopropylidene) succinic anhydride (Aberchrome 540).<sup>29</sup> Light intensity was varied using neutral density

filters. In our experiments, the intrinsic quantum yield for each reaction was measured precisely since transparent colloidal suspensions, which exhibit negligible light-scattering, were used. Both reaction 1 and 2 were followed by measuring the  $\text{Cl}^-$  production after 1 hr of UV-irradiation with an Orion chloride ion-selective electrode. Chloride production was linear over this time period (1 hr). Chloride adsorption on the colloidal particles was found to be negligible under our experimental condition. Solutions of desired organic substrate concentrations were prepared by dilution of the saturated stock solutions ( $\text{CHCl}_3$  63 mM and  $\text{CCl}_4$  5.1 mM). In a typical experiment, a glass reactor cell (35 mL) with a quartz irradiation window was filled to capacity, sealed tightly from the atmosphere, and irradiated with constant magnetic stirring. Reaction 1 was performed at  $\text{pH } 11.0 \pm 0.2$  with  $[\text{CHCl}_3]_0 = 3.15 \text{ mM}$ . Colloidal suspensions at this basic pH were prepared without coagulation by fast addition of 1.0 N NaOH solution to a vigorously stirred acidic suspension. Reaction 2 was performed at  $\text{pH } 2.8 \pm 0.1$  with  $[\text{CCl}_4]_0 = 5.1 \text{ mM}$  and  $[\text{CH}_3\text{OH}]_0 = 0.1 \text{ M}$ . In both cases  $[\text{TiO}_2] = 0.5 \text{ g L}^{-1}$ ,  $[\text{O}_2]_{\text{diss}} \approx 0.2 \text{ mM}$  (air-equilibration),  $I = 1.28 \times 10^{-4} \text{ einstein L}^{-1} \text{ min}^{-1}$  (at 320 nm, full width at half maximum 15 nm).

**Transient Absorption Experiments.**  $\text{TiO}_2$  samples for the laser flash-photolysis experiments were prepared using hydrochloric acid instead of nitric acid for a pH control in order to avoid the interference from the conduction band electron transfer to nitrate ions. Colloidal solutions of Q-sized  $\text{TiO}_2/\text{HCl}$  ( $1 \text{ g L}^{-1}$ ,  $\text{pH } 2.3 \pm 0.2$ ) were transferred into a vacuum cell having an 1.0-cm optical cuvette side arm. The samples were degassed under vacuum and purged with Ar on a vacuum/argon line. At least 5 vacuum/fill cycles were done to deoxygenate samples. The deoxygenated samples were excited with pulses from a Q-switched frequency-tripled Nd-YAG laser (355 nm, 10 ns fwhm).

Excitation pulse energies were  $\sim 1.5$  mJ/pulse ( $2.7 \times 10^{15}$  photons/pulse). Single wavelength transient absorption kinetics were observed using a 75 W Xe arc lamp (pulsed-lamp mode) as a probe source. All the decay kinetics were monitored by following the trapped charge-carrier absorption at 600 nm. A detailed description of the experimental setup has been provided previously.<sup>30</sup>

## Results

**Absorption Spectra of Colloids.** The band-gap of the undoped Q-sized  $\text{TiO}_2$  particles was determined to be 3.37 eV (369 nm) according to the spectral analysis described by Kormann et al.<sup>22b</sup> This corresponds to 0.17 eV blue shift from the bulk-phase band gap for anatase (3.2 eV). According to a theoretical prediction proposed by Brus:<sup>38</sup>

$$\Delta E_g = \frac{h^2}{8R^2\mu} - \frac{1.8e^2}{\epsilon R} \quad (4)$$

(R, radius of the particle;  $\mu$ , reduced mass of the exciton =  $1.63m_e$  for  $\text{TiO}_2$ <sup>22b</sup>;  $\epsilon$ , dielectric constant of the semiconductor = 184 for  $\text{TiO}_2$ <sup>22b</sup>)

the band-gap shift of 0.17 eV in  $\text{TiO}_2$  corresponds to a particle size of 2.2 nm, which well matches the particle size determined by TEM. Figure 1 shows the absorption spectra of some doped colloids. The spectra of  $\text{Fe}^{3+}$ -doped colloids show a red-shift in the band-gap transition with an increase in dopant concentration. This shift is consistent with the incorporation of the doping metal ions into the  $\text{TiO}_2$  nanoparticles.  $\text{V}^{4+}$ ,  $\text{Rh}^{3+}$  and  $\text{Mn}^{3+}$  show similar band-gap shifts. Red shifts of this type can be attributed to the charge-transfer transitions between the metal ion d-electrons and the  $\text{TiO}_2$  conduction or valence band.<sup>7b,18</sup> In the case of  $\text{Ru}^{3+}$ , which was incorporated into the  $\text{TiO}_2$  lattice, a strong absorption band centered at 437 nm was observed. This band is not present in

the spectrum of hexaquo  $\text{Ru}^{3+}$  ions in solution. In addition, free hexaquo  $\text{Ru}^{3+}$  ions have a fluorescence peak centered at 361 nm ( $\lambda_{\text{ex}} = 320$  nm) while the  $\text{Ru}^{3+}$ -doped  $\text{TiO}_2$  colloids do not exhibit fluorescence. This result is consistent with the incorporation of  $\text{Ru}^{3+}$  ions into the  $\text{TiO}_2$  lattice. However, the  $\text{Ru}^{3+}$ -doped colloid exhibited no photoactivity for either oxidation or reduction with  $\lambda > 390$  nm.

**Photoreactivities of Doped Q-sized  $\text{TiO}_2$ .** The photoreactivities of doped Q-sized  $\text{TiO}_2$  depend on the dopants and their concentrations. Table I lists the chloroform degradation quantum yields (%) for several doped colloids as a function of dopant level. All dopants show an optimum concentration above which the observed quantum yields for  $\text{CHCl}_3$  degradation decrease. The highest quantum yields are generally seen at 0.5 %. The number of dopant ions per individual  $\text{TiO}_2$  particle at the dopant concentration of 0.5 atom% is between one to five.  $\text{Co}^{3+}$ -doped  $\text{TiO}_2$  shows a steady decrease in the  $\Phi_{\text{CHCl}_3}$  with increasing the dopant concentration.

The measured photoreactivities of 21 doped Q-sized  $\text{TiO}_2$  colloids are summarized in Figure 2 in terms of the observed quantum yield for  $\text{CHCl}_3$  oxidation ( $\Phi_{\text{CHCl}_3} = 1/3\{(d[\text{Cl}^-]/dt)/I_a\}$ ) and for  $\text{CCl}_4$  reduction ( $\Phi_{\text{CCl}_4/\text{Cl}^-} = (d[\text{Cl}^-]/dt)/I_a$ ). Several dopants increase the photoreactivity significantly compared to the undoped Q-sized  $\text{TiO}_2$ . In order of decreasing reactivity they are:  $\text{Fe}^{3+}$  (15-fold),  $\text{Mo}^{5+}$  (11-fold),  $\text{Ru}^{3+}$  (11-fold),  $\text{Os}^{3+}$  (10-fold),  $\text{Re}^{5+}$  (7.5-fold),  $\text{V}^{4+}$  (7-fold), and  $\text{Rh}^{3+}$  (5-fold) in terms of the chloroform oxidation. On the other hand,  $\text{Co}^{3+}$  and  $\text{Al}^{3+}$ -doped  $\text{TiO}_2$  exhibited reduced photoreactivities. The data presented in Figure 2 are plotted in Figure 3 to show a direct linear correlation between  $\Phi_{\text{CHCl}_3}$  and  $\Phi_{\text{CCl}_4/\text{Cl}^-}$ .

The observed photodegradation rates for  $\text{CHCl}_3$  ( $v_{\text{ox}}$ ) were found to depend on the incident light intensity for both the undoped and  $\text{Fe}^{3+}$ -doped (0.5 %) Q-sized  $\text{TiO}_2$  (Figure 4). In the case of undoped Q-sized  $\text{TiO}_2$   $v_{\text{ox}} \propto I^{0.77}$  while for  $\text{Fe}^{3+}$ -doped Q-sized  $\text{TiO}_2$  two distinct regimes of  $v_{\text{ox}} \propto I^{1.03}$  ( $I_0 < 5.5 \times 10^{-4}$  einstein  $\text{L}^{-1} \text{min}^{-1}$ ) and  $v_{\text{ox}} \propto I^{0.34}$  ( $I_0 > 5.5 \times 10^{-4}$  einstein  $\text{L}^{-1} \text{min}^{-1}$ ) were observed. The photon flux into a single particle at  $I_0 = 5.5 \times 10^{-4}$  einstein  $\text{L}^{-1} \text{min}^{-1}$  corresponds to a flux of  $\sim 1$  photon/particle-sec.

Since the steady-state photolyses ( $\lambda_{\text{ex}} = 320 \text{ nm}$ ) and the laser flash-photolyses ( $\lambda_{\text{ex}} = 355 \text{ nm}$ ) were performed at different wavelengths, photoreactivities of undoped Q-sized  $\text{TiO}_2$  and  $\text{Fe}^{3+}$ -doped (0.5 %) Q-sized  $\text{TiO}_2$  were measured at the two different wavelength regions in order to ensure that the photochemical processes were wavelength-independent. Two UV-band pass filters were used. One transmits light in the range of 300 - 340 nm (centered at 320 nm,  $I = 1.39 \times 10^{-4}$  einstein  $\text{L}^{-1} \text{min}^{-1}$ ) and the other transmits light in the range of 310 - 400 nm (centered at 360 nm,  $I = 1.89 \times 10^{-4}$  einstein  $\text{L}^{-1} \text{min}^{-1}$ ). In both cases, the ratio of  $\Phi_{\text{CHCl}_3}(\text{Fe}^{3+}\text{-doped TiO}_2)$  to  $\Phi_{\text{CHCl}_3}(\text{undoped TiO}_2)$  was 12.

The photoreductive dechlorination of  $\text{CCl}_4$  was investigated as a function of the hole scavenger ( $\text{CH}_3\text{OH}$ ) concentration. In Figure 5, the ratios of the chloride production rates with methanol to those without methanol are plotted as a function of the added methanol concentration for the undoped and  $\text{Fe}^{3+}$ -doped (0.5 %) Q-sized  $\text{TiO}_2$ . The relative rates for the undoped Q-sized  $\text{TiO}_2$  are enhanced up to 13-fold with added methanol while the  $\text{Fe}^{3+}$ -doped Q-sized  $\text{TiO}_2$  shows little change.

**Photoreactivity Study of Heat-Treated Samples.** Undoped and several doped Q-sized TiO<sub>2</sub> samples were heat-treated under temperatures of 100 °C, 200 °C, and 400 °C for 4 hours each in order to investigate the effect of particle agglomeration and sintering on the photoreactivity. All suspensions of heat-treated TiO<sub>2</sub> samples were turbid due to the agglomeration. A 305-nm cutoff long-pass filter was used for irradiation instead of a 320-nm UV interference filter due to the low reactivity of the heated samples. Table II summarizes the photoreactivities of heat-treated undoped and doped samples. All the doped TiO<sub>2</sub> samples lose their photoreactivity gradually as the sintering temperature is increased. Doped TiO<sub>2</sub> samples heated above 200 °C show lower reactivities than the undoped TiO<sub>2</sub>. The particle size data obtained from TEM and SEM analysis of the heat-treated samples shows that both the primary particle size (up to ~ 40 nm) and the aggregate size (up to ~ 5 μm) of the particles increase as the heating temperature increases up to 400 °C. Figure 6 shows the TEM pictures of Q-sized TiO<sub>2</sub> (unheated) particles and an agglomerated TiO<sub>2</sub> (400 °C/ 4h) particle which consists of fused nanocrystals of doped (Fe<sup>3+</sup> 0.5%) TiO<sub>2</sub>. The loss of photoactivity of doped heat-treated samples can not be ascribed to a simple decrease in reactive surface area due to agglomeration because the photoreactivity of the undoped sample remains constant up to 200 °C.

**Transient Absorption Spectra of Doped Q-sized TiO<sub>2</sub>** The transient absorption decays of the undoped Q-sized TiO<sub>2</sub> were monitored over the wavelength range of 450 nm to 750 nm. The absorption spectrum showed a broad characteristic peak attributed to trapped electrons with  $\lambda_{\text{max}} \approx 600 \text{ nm}$ .<sup>31</sup> The decay kinetics were found to be independent of  $\lambda$ . The transient absorption decays monitored at 600 nm for several doped Q-sized TiO<sub>2</sub> are shown in Figures 7, 8 , and 9. In Figure 7, the transient absorption decays of Fe<sup>3+</sup>, Co<sup>3+</sup>,

V<sup>4+</sup>, and Al<sup>3+</sup>-doped (all at 0.5 %) TiO<sub>2</sub> are compared to an undoped sample in  $\mu$ s-time region. The transient decays of Mo<sup>5+</sup>(0.1 %)- and Ru<sup>3+</sup>(0.5%)-doped TiO<sub>2</sub> were similar to that of V<sup>4+</sup>-doped sample over the same time scale. The absorption signals were developed within the laser pulse duration and decay rapidly until a plateau was reached. Further decay occurred on a longer time scale. In general, doped Q-sized TiO<sub>2</sub> samples that were shown to increase (or decrease) photoreactivity have higher (or lower) absorption signal intensities than the others in the plateau region. The average number of e<sup>-</sup>/h<sup>+</sup> pairs present initially in one undoped-TiO<sub>2</sub> particle (Fig. 7a) is 0.66 based on an extinction coefficient of 1200 M<sup>-1</sup> cm<sup>-1</sup> for the electron absorption at 600 nm.<sup>31</sup> This corresponds roughly to 10 % of the absorbed photons. All excited-state decays in the  $\mu$ s-time region were fitted to the following double exponential equation:

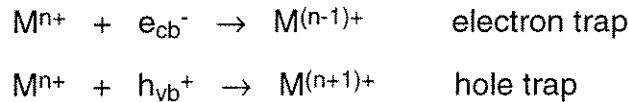
$$A(t) = A_{\infty} + C_1 \exp(-k_1 t) + C_2 \exp(-k_2 t) \quad (5)$$

In Table III, the fitting parameters for the doped TiO<sub>2</sub> samples are listed along with their corresponding quantum yields,  $\Phi_{\text{CHCl}_3}$  and  $\Phi_{\text{CCl}_4/\text{Cl}^-}$ . No correlation was seen between the photoreactivity and either of the decay constants ( $k_1$  and  $k_2$ ). However, the  $A_{\infty}$ , which is determined from the plateau region, appears to correlate well with the photoreactivity. Figure 10 shows a linear correlation between  $A_{\infty}$  and  $\Phi$  (oxidation, reduction, and their average). The correlation is best represented by the plot of  $\Phi_{\text{avg}}$  vs.  $A_{\infty}$ .  $A_{\infty}$  represents the residual absorption by the trapped charge carriers that survive recombination over the ns- to  $\mu$ s-time domain. This trend is clearly shown in Figure 8, in which the absorption decays are followed over the ms-time scale. The absorption signals of Fe<sup>3+</sup>, V<sup>4+</sup>, Ru<sup>3+</sup>-doped TiO<sub>2</sub> show much longer characteristic decay times that extend out to 50 msec while, in contrast, the undoped sample shows a complete decay within 200  $\mu$ sec. These results are consistent with the results obtained by

Grätzel and co-workers<sup>7b</sup> for Fe<sup>3+</sup>-doped TiO<sub>2</sub>. The Ru<sup>3+</sup>-doped TiO<sub>2</sub> shows very slow decay in this time scale compared to the others. Figure 9 shows the absorption decays of Fe<sup>3+</sup>-doped sample at three different dopant concentrations (0.1, 0.5, and 3.0 %). As is shown in Table I, most of the tested dopants have an optimal concentration of 0.5 atom% for enhanced photoreactivity. The observed enhancements are consistent with the transient absorption measurements. The A<sub>∞</sub> shows a maximum at 0.5 %-dopant concentration in both ms- and μs-region, while it is reduced at both lower and higher dopant concentrations.

## Discussion

**Energetics of Charge Trapping/Detrapping and Photoreactivity in Doped TiO<sub>2</sub>.** Metal-ion dopants influence the photoreactivity of TiO<sub>2</sub> by acting as electron (or hole) traps and by altering the e<sup>-</sup>/h<sup>+</sup> pair recombination rate through the following process:<sup>7,8b,14,15</sup>



where the energy level for M<sup>n+</sup>/M<sup>(n-1)+</sup> lies below the conduction band edge (E<sub>cb</sub>) and the energy level for M<sup>n+</sup>/M<sup>(n+1)+</sup> above the valence band edge (E<sub>vb</sub>). Available energy levels of metal-ion impurities in rutile TiO<sub>2</sub><sup>32,33</sup> are shown in Figure 11. Introduction of such energy levels in the band gap induces the red shift in the band-gap transition and the visible-light absorption (Figure 1) through a charge transfer between a dopant and CB (or VB) or a d-d transition in the crystal field. The band-gap shift of 0.12 eV in Fe<sup>3+</sup>-doped (2%) TiO<sub>2</sub> can be assigned to the charge-transfer transition from the d-orbital of Fe<sup>3+</sup> to CB according to the energy level diagram in Figure 11. The tailing of the absorption band into the visible region for V<sup>4+</sup> and Mn<sup>3+</sup>-doped TiO<sub>2</sub> (Figure 1c) can be also

assigned to a similar charge-transfer band. The separate absorption band centered at 437 nm (2.8 eV) of Ru<sup>3+</sup>-doped TiO<sub>2</sub> can be assigned to the donor transition of Ru<sup>3+</sup> into CB:<sup>33</sup>



From the onset (520 nm) of this band we suggest the redox level of Ru<sup>3+</sup>/Ru<sup>4+</sup> in anatase Q-sized TiO<sub>2</sub> is located 2.4 eV below E<sub>cb</sub>, which might be slightly different from the redox level in the bulk anatase. The Ru<sup>2+</sup>/Ru<sup>3+</sup> redox level in Figure 11 suggests a possible acceptor transition in rutile:



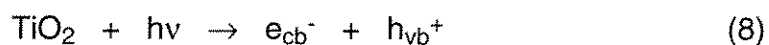
This transition is suggestive from the absorption around 360 ~ 380 nm in Figure 1b which cannot be accounted for by an overlap of the band-gap transition and the 437-nm band. The absence of photoactivity of Ru<sup>3+</sup>-doped colloid with  $\lambda > 390$  nm indicates the ineffectiveness of the sole electron excitation (eq 4) for the interfacial charge transfer. Herrmann et al.<sup>13c</sup> also reported that the photoconductance spectrum of Cr<sup>3+</sup>-doped TiO<sub>2</sub> did not parallel the absorption curve in the visible region.

According to the energy level diagram of Figure 11, V<sup>4+</sup>, Mn<sup>3+</sup>, Co<sup>3+</sup>, and Ru<sup>3+</sup> can act as both hole and electron traps, while Fe<sup>3+</sup>, Cr<sup>3+</sup>, and Ni<sup>2+</sup> can serve only as hole traps. We note that the energy levels in the Q-sized anatase (E<sub>g</sub> = 3.37 eV) may not be identical with those of the single-crystal rutile (E<sub>g</sub> = 3.0 eV). For example, it has been suggested that Fe<sup>3+</sup> can be an electron trap as well in anatase.<sup>8b</sup> In order to continue our analysis we will assume that the energy levels in Figure 11 are applicable to Q-sized TiO<sub>2</sub>. The apparent energy

levels, however, do not seem to provide a unifying explanation that is consistent with our observations.

Even though  $\text{Fe}^{3+}$  and  $\text{Cr}^{3+}$  have similar energy levels in the  $\text{TiO}_2$  lattice (0.1-0.3 eV above  $E_{vb}$ ), similar ionic radii (0.79 vs. 0.76 Å), and identical oxidation states, their efficiencies as dopants with respect to photoreactivity are substantially different. Differences in photoactivity of  $\text{Fe}^{3+}$ - and  $\text{Cr}^{3+}$ -doped  $\text{TiO}_2$  electrodes have been ascribed to differences in the diffusion lengths of the minority carriers (2  $\mu\text{m}$  for  $\text{Fe}^{3+}$  vs. 0.2  $\mu\text{m}$  for  $\text{Cr}^{3+}$ ).<sup>20a</sup> However, this explanation is not appropriate to very small particles whose dimension is much smaller than the characteristic diffusion length. Moser et al.<sup>7b</sup> attributed the inhibition of  $e^-/h^+$  recombination in  $\text{Fe}^{3+}$ -doped  $\text{TiO}_2$  colloids to the local separation of trapped charge carriers. Even though it is widely accepted that the photoreactivities of doped  $\text{TiO}_2$  are related to the dopant trap site, it is often neglected that the trapped charges should be transferred to the interface to initiate the photoreactions. In this context, the energetics of the charge release and migration in the lattice is equally important as well as the charge-trapping energetics. A general photochemical charge-trapping, recombination, detrapping and migration mechanism in the presence of metal-ion dopants can be proposed as follows:

*charge-pair generation:*

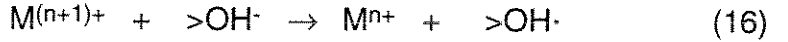


*charge trapping:*

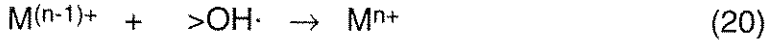
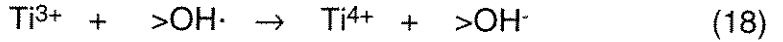




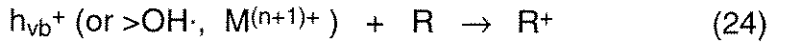
*charge release and migration:*



*recombination:*



*interfacial charge transfer:*



where  $M^{n+}$  is a metal-ion dopant, O is an electron acceptor (oxidant), and R is an electron donor (reductant). The origin of the different photoreactivities between  $Fe^{3+}$  and  $Cr^{3+}$  can be explained based on the above mechanism and the energy level diagram in Figure 11.

The hole trapping by both  $Fe^{3+}$  and  $Cr^{3+}$  (eq 13) after the photoexcitation is equally favorable while the electron trapping is probable only for  $Fe^{3+}$  (eq 12). The trapped holes in  $Fe^{4+}$  and  $Cr^{4+}$  either migrate to the surface (eq 16) or recombine (eqs 21-22). Photoexcited electron in the presence of  $Cr^{3+}$ , which can

not trap an electron, quickly recombines with a trapped hole (eq 21). The trapped hole embodied in  $\text{Fe}^{4+}$  has longer life time due to the immobilized electron in  $\text{Fe}^{2+}$ . According to crystal field theory,  $\text{Fe}^{2+}$  is relatively unstable due to the loss of exchange energy on going from  $d^5$  (half-filled high-spin) to  $d^6$  and tends to return to  $\text{Fe}^{3+}(d^5)$ . However, the  $\text{Fe}^{2+}/\text{Fe}^{3+}$  energy level lies close to  $\text{Ti}^{3+}/\text{Ti}^{4+}$  level. As a consequence of this proximity, the trapped electron in  $\text{Fe}^{2+}$  can be easily transferred to a neighboring surficial  $\text{Ti}^{4+}$  (eq 15) which then leads to interfacial electron transfer (eq 23).

The effect of the energy levels of the dopants on photoreactivity can be generalized based upon the above arguments. First of all, dopants should act as both electron traps and hole traps to be photoactive. Trapping either an electron or a hole alone is ineffective because the immobilized charge species quickly recombines with its mobile counterpart. ESR studies<sup>7a,34</sup> have shown that  $\text{Mo}^{6+}$  and  $\text{Mo}^{5+}$  coexisted in the  $\text{TiO}_2$  lattice where they act an electron trap and a hole trap, respectively. This explanation is in accord with the high photoactivity of  $\text{Mo}^{5+}$  as a dopant. Judging from the fact that  $\text{V}^{3+}$  is readily oxidized to  $\text{V}^{4+}$  under ambient conditions,<sup>35</sup> the  $\text{V}^{3+}$  listed in Figure 2 may actually be present in the  $\text{TiO}_2$  lattice as  $\text{V}^{4+}$ , which can act both an electron trap and a hole trap. Thus, the photoreactivities of  $\text{V}^{3+}$  and  $\text{V}^{4+}$  are very similar. On the other hand, the photoactivity of  $\text{V}^{5+}$  is significantly lower than that of  $\text{V}^{4+}$  since  $\text{V}^{5+}$  can only trap electrons. Even though the energy levels of the other metal ions are not available, some general trends are apparent based on considerations of the electronic configuration of the dopants. All dopants with a closed shell electronic configuration ( $\text{Li}^+$ ,  $\text{Mg}^{2+}$ ,  $\text{Al}^{3+}$ ,  $\text{Zn}^{2+}$ ,  $\text{Ga}^{3+}$ ,  $\text{Zr}^{4+}$ ,  $\text{Nb}^{5+}$ ,  $\text{Sn}^{4+}$ ,  $\text{Sb}^{5+}$ , and  $\text{Ta}^{5+}$ ) have little effect on the observed photoreactivity.

The stability of a closed electronic shell makes electron (or hole) trapping unfavorable. For example, low reactivity of  $\text{Co}^{3+}$ , which is known to have low-spin configuration ( $t_{2g}^6$  in an octahedral field) in many oxides,<sup>36</sup> could be attributed to its stable partly closed electronic configuration. The significant deviation of  $\text{V}^{4+}$  and  $\text{Ru}^{3+}$  from the linear correlation in Figure 3 may arise, in part, from the stable closed shell configuration of  $\text{V}^{5+}$  ( $d^0$ ), a trapped hole and the partly filled low-spin configuration of  $\text{Ru}^{2+}$  ( $t_{2g}^6$ ), a trapped electron. However, this general requirement is not sufficient to predict a good dopant. For example, we did not observe an enhanced photoreactivity with  $\text{Mn}^{3+}$  which can trap both electrons and holes.

The second prerequisite for an effective dopant may involve the possibility of charge detrapping and migration to the surface of previously trapped charges. The importance of trapped charge migration was discussed above for  $\text{Fe}^{3+}$ . The low photoreactivity of  $\text{Mn}^{3+}$ -doped  $\text{TiO}_2$  can be attributed to the low driving force for electron detrapping from  $\text{Mn}^{2+}$  due to the small energy difference between  $\text{Mn}^{2+}$  and  $\text{Mn}^{3+}$ . We extend the caveat that all energetic considerations are valid only for dopants located close to the surface site at which the interfacial charge transfer occurs. Since the diameter of the exciton in Q-sized  $\text{TiO}_2$  is approximately 20 Å, the prerequisites are met within a ns of excitation.

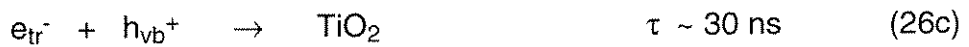
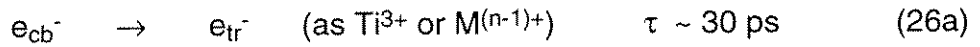
**Recombination, Trapping, Interfacial Transfer of Charge Carriers and Photoreactivity in Doped  $\text{TiO}_2$ .** We should keep in mind that Q-sized particles represent an unusual case with respect to electron transfer at the semiconductor-liquid interface compared to their bulk-phase counterparts. A distinctive feature of Q-sized semiconductors is the lack of appreciable band bending. The total potential drop within a Q-sized particle is given by the equation:<sup>37</sup>

$$\Delta\phi = kT/6e (r_0/L_D)^2 \quad (25)$$

where  $r_0$  is the radius of the particle and  $L_D$  is the Debye length. For a particle of 3-nm diameter with 0.5 atom% of dopants,  $\Delta\phi$  is calculated to be 0.01 V. Considering that the magnitude of the potential drop across the space-charge layer should not be less than 0.1 V for an efficient  $e^-/h^+$  separation,<sup>20e</sup> the small potential drop for Q-sized  $\text{TiO}_2$  (0.01 V) is an insufficient driving force for the charge pair separation within a particle. Moreover, for Q-sized particles the wave function of the charge carrier spreads over the entire semiconductor cluster.<sup>38</sup> As a result, both electrons and holes are readily available at the interface. Oxidation reactions by VB holes and reduction reactions by CB electrons can thus occur concurrently, thereby satisfying the condition of electroneutrality on a semiconductor particle in which an  $e^-$  reacts (eq 23) for each  $h^+$  reacted (eq 24). The correlation between the oxidation and reduction quantum yields in Figure 3 can be explained by the near equal availability of electrons and holes on the surface of Q-sized particles. A direct correlation of oxidation and reduction efficiencies cannot be expected from a semiconductor electrode or large bulk-phase particles ( $\sim\mu\text{m}$ ) in which the space-charge layer is developed near the surface and photogenerated  $e^-/h^+$  pairs are locally separated. The apparent disagreement in the reported photoactivity between this work and previous investigations of the effects of dopants for electrodes<sup>20</sup> or bulk-phase particles<sup>14-16</sup> can be ascribed to the lack of band bending in Q-sized semiconductors.

The photoreactivities of doped  $\text{TiO}_2$  widely vary depending upon the specific dopant as shown in Figure 2. The origin of these different photoreactivities appears to be related to the efficiencies of the dopants in trapping charge carriers and mediating interfacial charge transfer. This idea is

supported by the transient absorption decays of the trapped electron as shown in Figures 7 and 8. The trapped electron in TiO<sub>2</sub> colloids gives rise to a broad absorption band (400 - 1000 nm) with a nominal maximum around 600 nm,<sup>31</sup> while the trapped hole exhibits a broad absorption (400 - 800 nm) band with  $\lambda_{\text{max}} = 475 \text{ nm}$ .<sup>22a</sup> The overlap of absorption bands near 600 nm seems to be negligible over the nanosecond time frame because electron trapping is much faster ( $\tau \sim 30 \text{ ps}$ ) than the hole trapping ( $\tau \sim 250 \text{ ns}$ ).<sup>39</sup> However, this overlap may not be negligible over the  $\mu\text{s}$ -time domain that we are probing. Hole trapping is able to compete effectively with recombination under conditions of our experiment where only 0.66 e<sup>-</sup>/h<sup>+</sup> pair per particle is created by the laser pulse. Furthermore, the presence of metal-ion dopants provides more trap sites for holes in addition to the surface trap sites (>OH<sup>-</sup>).



Considering that the mean life time of a single electron-hole pair in a TiO<sub>2</sub> particle (12-nm diameter) was determined to be 30 ns (eq 26c),<sup>39</sup> the appearance of a plateau in the absorption decay curves ( $\mu\text{s}$ -domain) of the doped TiO<sub>2</sub> colloids (Figure 7) indicates a slow recombination process described by eq 26d. Therefore,  $A_{\infty}$  in eq 5 should be regarded as the relative absorption by both  $e_{\text{tr}}^-$  and  $h_{\text{tr}}^+$  even though their proportions are unknown. The trapped charge carriers have a sufficiently-long life time to reach the surface by detrapping (eqs 15-16)

and electron tunnelling. As a consequence, the higher the  $A_{\infty}$  value, the higher the observed photoreactivity.

The role of a metal-ion dopant as a direct mediator of the interfacial charge transfer is indicated by the data summarized in Table II. Given the size of Q-sized particles the dopants are located within 10 - 20 Å from the surface. Under these conditions, all dopants can be considered as located in the surface region where the charge-transfer to the interface is easily achieved. As the small Q-sized particles agglomerate upon heating, dopants are isolated far from the surface with a much lower chance of transferring trapped charge carriers to the interface. Thus, the data of Table II show steadily decreasing photoreactivities of doped TiO<sub>2</sub> with an increase in sintering temperature. As a result of particle agglomeration, the dopants are more likely to serve as recombination centers than as trap sites for eventual charge transfer at the interface.

The curves shown in Figure 5 can be also interpreted in terms of the integral role of the dopant in mediating interfacial charge transfer. In undoped TiO<sub>2</sub>, the increasing concentration of a hole scavenger (e.g. CH<sub>3</sub>OH) increases the efficiency of interfacial charge transfer (hence the photoreactivity) since effective hole scavenging diverts an increasing fraction of charge carriers toward interfacial transfer. However, in doped colloids, the dopant (i.e., Fe<sup>3+</sup>) functions as an interfacial charge-transfer mediator in the absence of hole scavengers. Thus, in the case of Fe<sup>3+</sup>-doped TiO<sub>2</sub> the relative effect of additional hole scavengers is substantially less.

Several investigations<sup>24,40</sup> have shown that photocatalytic degradation rates undergo a transition from first-order to half-order kinetics with respect to incident light intensity,  $I$  with increasing  $I_0$ . In this study, this predicted transition

was not observed up to  $I = 5.30 \times 10^{-3}$  einstein  $L^{-1} \text{ min}^{-1}$  ( $\sim 7$  photons /particle·sec ) with the undoped Q-sized colloid (Figure 4). However, in a similar study using larger particles (Degussa P25, 0.5 g/L) Martin et al.<sup>41</sup> reported a transition at  $6.87 \times 10^{-5}$  einstein  $L^{-1} \text{ min}^{-1}$  which corresponds approximately to 75 photons/particle·sec assuming an average particle size of 30 nm. These results imply that the Q-sized particles do not reach a saturation  $e^-/h^+$  pair concentration since the number of photons absorbed per particle is much smaller for Q-sized colloids than for their bulk-phase counterparts. On the other hand, a first-order to a fractional-order (0.34) transition is seen for the  $Fe^{3+}$ -doped Q-sized  $TiO_2$ . The higher value of  $dV_{CHCl_3}/dI$  in the doped colloids compared to the undoped colloids (1.03 vs. 0.77) at lower light intensities ( $< \sim 1$  photon/particle·sec) suggests that the trap sites provided by the dopants are more effectively transferring charge carriers than the intrinsic trap sites (e.g.,  $Ti^{3+}$ ). Above the transitional light intensity ( $> \sim 1$  photon/particle·sec),  $dV_{CHCl_3}/dI$  decreases to 0.34, which suggests that recombination dominates over charge transfer. The fact that such a transition occurs at the light flux of  $\sim 1$  photon/particle·sec implies that the charge transfer of trapped charge-carriers to redox couples at the interface is a very slow process which might be extended up to a second. The slow transient absorption decays observed over the ms-time frame region (Fig. 8) may reflect the nature of this slow interfacial charge transfer. The observed low efficiencies at higher light intensities indicate that the dopants are efficient recombination centers (eq 19-22) as well as good trapping sites. Thus, we conclude that the metal-ion dopants are acting as effective trapping sites under low light intensities (i.e., with not all the dopant sites populated as traps). However, when the available trapping sites are fully occupied under conditions of high light intensities, the metal-ion dopants become efficient recombination centers.

**Dopant Concentration and Photoreactivity.** For all of the dopants tested in Table I, there appears to be an optimal dopant concentration above which the observed photoreactivity decreases. Even though similar results<sup>6,8,10b,16</sup> obtained for bulk-phase materials were interpreted in terms of a change in the space-charge layer thickness, the present results with Q-sized particles represent a different situation. In order to interpret these results we note that recombination through tunnelling between the trapped charge-carriers (eq 26d) depends on the distance  $R$  separating the  $e^-/h^+$  pair according to:<sup>37</sup>

$$k_{\text{recomb}} \propto \exp(-2R/a_0) \quad (27)$$

where  $a_0$  is the radius of the hydrogenic wave function of the trapped carriers. As a consequence, the recombination rate increases exponentially with the dopant concentration because the average distance between trap sites decreases with increasing the number of dopants confined within a particle. Considering that the solubility limit of iron in anatase is about 1 atom%,<sup>42</sup> some surface enrichment of iron should be present at higher dopant concentrations. Such a heterogeneity should decrease photoreactivity. At lower concentrations below the optimal value, photoreactivity increases with an increasing dopant concentration because there are fewer trapping sites available. For example, in a 4 nm-diameter particle there is only one dopant ion per particle at 0.1 %, five at 0.5%, and thirty at 3.0%. Therefore, the appearance of an optimal dopant concentration in Q-sized  $\text{TiO}_2$  can be explained by the balance of an increase in trapping sites leading to efficient trapping and fewer trapped carriers leading to longer life-times for interfacial charge transfer. This general argument is supported by the transient absorption spectra of Figure 9. The absorption intensity is maximized at 0.5 atom%  $\text{Fe}^{3+}$  while it is reduced at both 0.1 % and 3.0 %. This means that the

number of trapped carriers in a particle is the highest in 0.5 % Fe<sup>3+</sup>/TiO<sub>2</sub> for which the highest photoreactivity was observed.

## Conclusions

Quantum yields for the steady-state photolyses of CHCl<sub>3</sub> and CCl<sub>4</sub> on doped Q-sized TiO<sub>2</sub> colloids are quantitatively correlated with the transient recombination dynamics of charge carriers. Photoreactivities are shown to increase with the concentration of trapped charge carriers that remain after an initial fast recombination between free charge carriers. The relative efficiency of a metal-ion dopant depends on whether it serves as a mediator of interfacial charge transfer or as a recombination center. The ability of a dopant to function as an effective trap is related to the dopant concentration, the energy level of dopants within the TiO<sub>2</sub> lattice, their d-electronic configuration, the distribution of dopants within the particles, the electron-donor concentration, and the incident light intensity. Enhanced interfacial charge transfer in the presence of effective dopants appears to be the most important factor in enhancement of photoreactivity of doped TiO<sub>2</sub>.

## Acknowledgments

We are grateful to ARPA and ONR {N0014-92-J-1901} for financial support. We thank the Beckman Institute of Caltech for allowing us to use its laser resource center. Dean Willberg, Jay Winkler, Scot Martin, and Nicole Peill were critical to the success of this project.

## References

- (1) (a) Serpone, N., Pelizzetti, E., Eds. *Photocatalysis - Fundamentals and Applications*; Wiley Interscience: New York, 1989. (b) Fox, M.A.; Dulay, M.T. *Chem. Rev.* **1993**, *93*, 341.
- (2) Ollis, D.F.; Al-Ekabi, H., Eds. *Photocatalytic Purification and Treatment of Water and Air*, Elsevier: Amsterdam, 1993.
- (3) (a) Vrachnou, E.; Grätzel, M.; McEvoy, A.J. *J. Electroanal. Chem.* **1989**, *258*, 193. (b) Moser, J.; Punchedewa, S.; Infelta, P.P.; Grätzel, M. *Langmuir* **1991**, *7*, 3012.
- (4) Hong, A.P.; Bahnemann, D.W.; Hoffmann, M.R. *J. Phys. Chem.* **1987**, *91*, 2109.
- (5) (a) Bahnemann, D.W.; Mönig, J.; Chapman, R. *J. Phys. Chem.* **1987**, *91*, 3782. (b) Disdier, J.; Herrmann, J.-M.; Pichat, P. *J. Chem. Soc. Faraday Trans. I* **1983**, *79*, 651.
- (6) Navio, J.A.; Marchena, F.J.; Roncel, M.; Del la Rosa, M.A. *J. Photochem. Photobiol. A: Chem.* **1991**, *55*, 319.
- (7) (a) Grätzel, M.; Howe, R.F. *J. Phys. Chem.* **1990**, *94*, 2566. (b) Moser, J.; Grätzel, M.; Gallay, R. *Helv. Chim. Acta* **1987**, *70*, 1596.
- (8) (a) Schrauzer, G.N.; Guth, T.D. *J. Am. Chem. Soc.* **1977**, *99*, 7189. (b) Soria, J.; Conesa, J.C.; Augugliaro, V.; Palmisano, L.; Schiavello, M.; Sclafani, A. *J. Phys. Chem.* **1991**, *95*, 274.
- (9) Bickley, R.I.; Lees, J.S.; Tilley, R.J.D.; Palmisano, L.; Schiavello, M. *J. Chem. Soc. Faraday Trans.* **1992**, *88*, 377.
- (10) (a) Sclafani, A.; Palmisano, L.; Schiavello, M. *Res. Chem. Interm.* **1992**, *18*, 211. (b) Palmisano, L.; Augugliaro, V.; Sclafani, A.; Schiavello, M. *J. Phys. Chem.* **1988**, *92*, 6710.

- (11) (a) Kiwi, J.; Grätzel, M. *J. Phys. Chem.* **1986**, *90*, 637. (b) Ileperuma, O.A.; Tennakone, K.; Dissanayake, W.D.D.P. *Appl. Catal.* **1990**, *62*, L1.
- (12) Kiwi, J.; Morrison, C. *J. Phys. Chem.* **1984**, *88*, 6146.
- (13) (a) Highfield, J.G.; Pichat, P. *New J. Chem.* **1989**, *13*, 61. (b) Wong, W.K.; Malati, M.A. *Solar Energy* **1986**, *36*, 163. (c) Herrmann, J.-M.; Disdier, J.; Pichat, P. *Chem. Phys. Letters* **1984**, *108*, 618.
- (14) Luo, Z.; Gao, Q.-H. *J. Photochem. Photobiol. A: Chem.* **1992**, *63*, 367.
- (15) Mu, W.; Herrmann, J.-M.; Pichat, P. *Catal. Letters* **1989**, *3*, 73.
- (16) Karakitsou, K.E.; Verykios, X.E. *J. Phys. Chem.* **1993**, *97*, 1184.
- (17) (a) Sabate, J.; Anderson, M.A.; Kikkawa, H.; Xu, Q.; Cervera-March, S.; Hill, C.G., Jr. *J. Catal.* **1992**, *134*, 36. (b) Kikkawa, H.; O'Regan, B.; Anderson, M.A. *J. Electroanal. Chem.* **1991**, *309*, 91.
- (18) Borgarello, E.; Kiwi, J.; Grätzel, M.; Pelizzetti, E.; Visca, M. *J. Am. Chem. Soc.* **1982**, *104*, 2996.
- (19) Kutty, T.R.N.; Avudaithai, M. *Chem. Phys. Lett.* **1989**, *163*, 93.
- (20) (a) Maruska, H.P.; Ghosh, A.K. *Solar Energy Mater.* **1979**, *1*, 237. (b) Ghosh, A.K.; Maruska, H.P. *J. Electrochem. Soc.: Electrochem. Sci. Tech.* **1977**, *124*, 1516. (c) Salvador, P. *Solar Energy Mater.* **1980**, *2*, 413. (d) Matsumoto, Y.; Kurimoto, J.; Amagasaki, Y.; Sato, E. *J. Electrochem. Soc.: Electrochem. Sci. Tech.* **1980**, *127*, 2148. (e) Gautron, J.; Lemasson, P.; Marucco, J.-F. *Faraday Discuss. Chem. Soc.* **1981**, *70*, 81.
- (21) Choi, W.; Termin, A.; Hoffmann, M.R. *Angew. Chem. Int. Ed. Engl.* **1994**, *33*, 1091.
- (22) (a) Bahnemann, D.; Henglein, A.; Lilie, J.; Spanhel, L. *J. Phys. Chem.* **1984**, *88*, 709. (b) Kormann, C.; Bahnemann, D.W.; Hoffmann, M.R. *ibid.* **1988**, *92*, 5196.
- (23) Zepp, R.G.; Hoigne, J.; Bader, H. *Environ. Sci. Technol.* **1987**, *21*, 443.

(24) (a) Kormann, C.; Bahnemann, D.W.; Hoffmann, M.R. *Environ. Sci. Technol.* **1991**, *25*, 494. (b) The overall reaction stoichiometry is



(25) (a) Bard, A.J.; Lund, H. Eds. *Encyclopedia of Electrochemistry of the Elements - Organic Section Vol. XIV*, M. Dekker: New York, 1973, p. 34. (b)

Mönig, J.; Bahnemann, D.; Asmus, K.-D. *Chem.-Biol. Interactions* **1983**, *47*, 15.

(26) Lilie, V.J.; Beck, G.; Henglein, A. *Ber. Bunsenges. Phys. Chem.* **1971**, *75*, 458.

(27) Ross, A.B.; Neta, P. *Rate Constants for Reactions of Aliphatic Carbon-Centered Radicals in Aqueous Solution*, NSRDS-NBS 70, National Bureau of Standards, 1982.

(28) Choi, W.; Hoffmann, M.R. *Environ. Sci. Technol.* **1995**, *29*, 1646.

(29) Heller, H.G.; Langan, J.R. *J. Chem. Soc. Perkin Trans.* **1981**, *2*, 341.

(30) Stowell, M.H.B.; Larsen, R.W.; Winkler, J.R.; Rees, D.C.; Chan, S.I. *J. Phys. Chem.* **1993**, *97*, 3054.

(31) Kölle, U.; Moser, J.; Grätzel, M. *Inorg. Chem.* **1985**, *24*, 2253.

(32) (a) Mizushima, K.; Tanaka, M.; Iida, S. *J. Phys. Soc. Japan* **1972**, *32*, 1519.

(b) Mizushima, K.; Tanaka, M.; Asai, A.; Iida, S.; Goodenough, J.B. *J. Phys. Chem. Solids* **1979**, *40*, 1129.

(33) Triggs, P. *Helv. Phys. Acta.* **1985**, *58*, 657.

(34) Meriaudeau, P. *Chem. Phys. Lett.* **1980**, *72*, 551.

(35) Bielanski, A.; Dyrek, K.; Serwicka, E. *J. Catal.* **1980**, *66*, 316.

(36) Cox, P.A. *Transition Metal Oxides: An Introduction to their Electronic Structure and Properties*, Clarendon Press: Oxford, 1992, p. 121.

(37) Grätzel, M. *Heterogeneous Photochemical Electron Transfer Reactions*, CRC Press: Boca Raton, Florida, USA, 1987.

(38) Brus, L. *J. Phys. Chem.* **1986**, *90*, 2555.

- (39) Rothenberger, G.; Moser, J.; Grätzel, M.; Serpone, N.; Sharma, D.K. *J. Am. Chem. Soc.* **1985**, *107*, 8054.
- (40) (a) Okamoto, K.; Yamamoto, Y.; Tanaka, H.; Itaya, A. *Bull. Chem. Soc. Jpn.* **1985**, *58*, 2023. (b) Turchi, C.S.; Ollis, D.F. *J. Catal.* **1990**, *122*, 178.
- (41) Martin, S.T.; Herrmann, H.; Choi, W.; Hoffmann, M.R. *J. Chem. Soc. Faraday Trans.* **1994**, *90*, 3315.
- (42) Cordishi, D.; Burriesci, N.; D'Alba, F.; Petrera, M.; Polizzotti, G.; Schiavello, M. *J. Solid State Chem.* **1985**, *56*, 182.
- (43) Huheey, J.E. *Inorganic Chemistry; Principles of Structure and Reactivity*. Harper & Row: New York, 1983, pp 73-76.

**Table 1.** Summary of the Chloroform Degradation Quantum Yields (%) for Several Doped TiO<sub>2</sub> Colloids at Various Dopant Concentrations, [CHCl<sub>3</sub>]<sub>0</sub> = 3.15 mM

$\Phi_{\text{CHCl}_3}$ (%)	Dopant Concentration (atomic %)								pH	Light Intensity (einstein L <sup>-1</sup> min <sup>-1</sup> )
Dopant	0.0	0.1	0.25	0.5	1.0	2.0	3.0	5.0		
Fe <sup>3+</sup>	0.08	0.78		1.19	0.80	0.51		0.10	2.7 ± 0.1	0.75 x 10 <sup>-4</sup>
V <sup>4+</sup>	0.08	0.38		0.49	0.35	0.22	0.08			
V <sup>3+</sup>	0.08	0.31	0.40	0.53	0.36	0.19	0.15			
Re <sup>5+</sup>	0.08	0.27	0.31	0.41	0.32	0.24	0.10			
Mo <sup>5+</sup>	0.08	0.49	0.32	0.31	0.30	0.20	0.12			
Ru <sup>3+</sup>	0.08	0.09	0.31	0.38	0.37	0.18	0.15			
Mn <sup>3+</sup>	0.16	0.20	0.32	0.59	0.57	0.23	0.10		11.1 ± 0.3	1.28 x 10 <sup>-4</sup>
Co <sup>3+</sup>	0.16	0.18	0.10	0.08	0.04	< 0.03	< 0.03			
Rh <sup>3+</sup>	0.16	0.48	0.61	0.87	0.46	0.18	0.04			

**Table II.** Effects of Heat Treatment at Various Temperatures on the Photoreactivities of the Undoped and Doped TiO<sub>2</sub> Measured in Term of the Chloroform Degradation Rate,  $v_{\text{CHCl}_3}$  ( $\mu\text{M min}^{-1}$ ). Suspension Concentrations Are Given in Brackets.

dopant $v_{\text{CHCl}_3}$	unheated [ 0.5 g/L ] ( pH 2.9 - 2.6 )	100 °C/ 4h [ 0.5 g/L ] ( pH 3.1 - 2.8 )	200 °C/ 4h [ 1 g/L ] ( pH 3.6 - 3.3 )	400 °C/ 4h [ 1 g/L ] ( pH 5.5 - 4.6 )
undoped	1.5	1.4	1.5	0.1
Fe <sup>3+</sup> 0.5 %	12.5	7.2	0.7	0.03
V <sup>4+</sup> 0.5 %	8.2	4.6	0.4	0.1
Mo <sup>5+</sup> 0.1 %	7.5	6.1	1.1	0.07
Ru <sup>3+</sup> 0.5 %	4.6	1.0	0.6	0.07
Rh <sup>3+</sup> 0.5 %	2.2	1.2	0.2	0.00

**Table III.** Comparison of the Fitting Parameters (eq 5) from the Transient Absorption Decays with the Photocatalytic Quantum Yields from Figure 1 for Various Doped Q-sized TiO<sub>2</sub>

dopant	$A_{\infty}$ ( $\times 10^{-3}$ )	$k_1$ ( $\times 10^7$ )	$k_2$ ( $\times 10^6$ )	$\Phi_{\text{ox}}$	$\Phi_{\text{red}}$	$\Phi_{\text{avg}}$
				(%)		
undoped	1.31	1.79	1.36	0.16	0.08	0.12
Fe <sup>3+</sup>	6.69	1.23	0.84	2.38	1.74	2.06
V <sup>4+</sup>	4.22	3.02	0.98	1.09	1.60	1.35
Mo <sup>5+</sup>	3.62	2.18	0.99	1.82	1.59	1.71
Ru <sup>3+</sup>	3.45	6.98	1.67	1.72	0.38	1.05
Rh <sup>3+</sup>	1.99	0.86	0.60	0.87	0.44	0.66
Mn <sup>3+</sup>	1.04	2.74	1.47	0.59	0.12	0.34
Nb <sup>5+</sup>	0.95	3.82	1.25	0.23	0.08	0.16
Al <sup>3+</sup>	0.60	4.16	1.60	0.08	0.08	0.08
Cr <sup>3+</sup>	0.55	3.19	1.26	0.21	0.16	0.19
Co <sup>3+</sup>	0.04	2.56	1.35	0.08	0.08	0.08

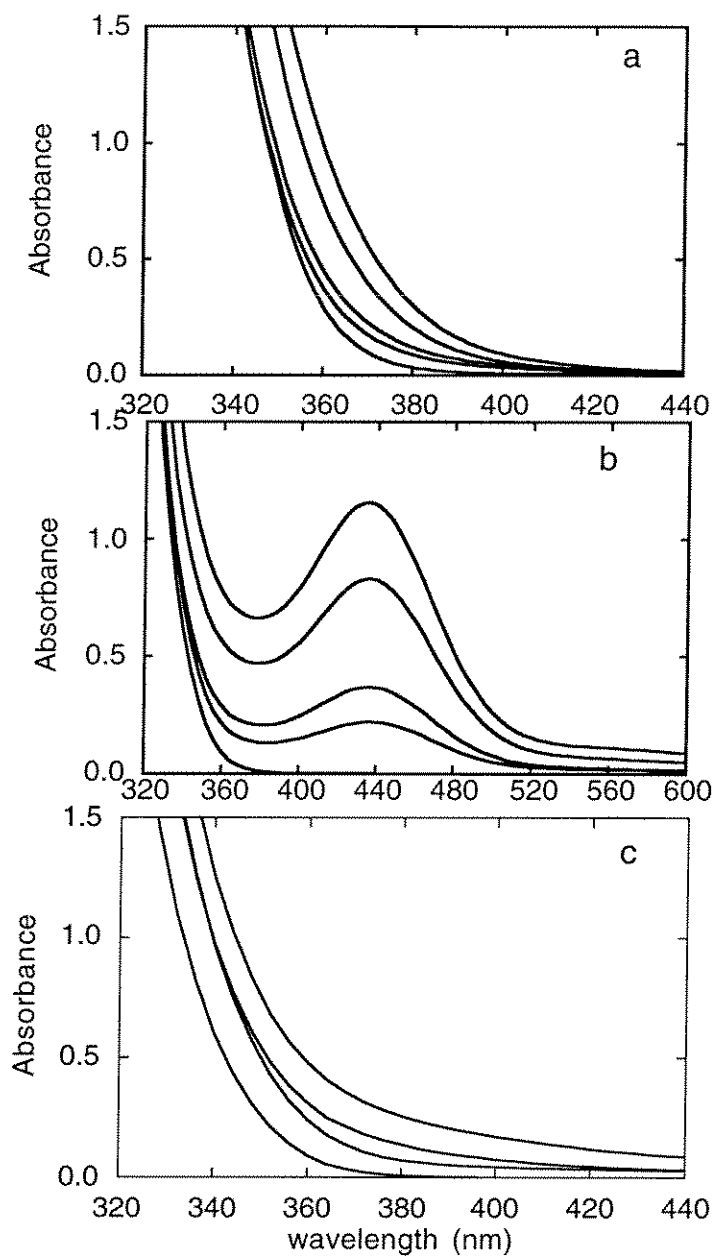


**Figure 1.** Absorption spectra of (a) Fe<sup>3+</sup>-doped Q-sized TiO<sub>2</sub> (1.34 g/L) at 0.0, 1.0, 2.0, 5.0, 10.0 % Fe<sup>3+</sup> concentrations (from left to right), (b) Ru<sup>3+</sup>-doped Q-sized TiO<sub>2</sub> (0.5 g/L) at 0.0, 0.5, 1.0, 2.0, and 3.0 % Ru<sup>3+</sup> concentrations (from bottom to up), and (c) undoped, Rh<sup>3+</sup> 3.0 %, V<sup>4+</sup> 3.0 %, and Mn<sup>3+</sup> 3.0 % Q-sized TiO<sub>2</sub> at 0.5 g/L (from left to right).



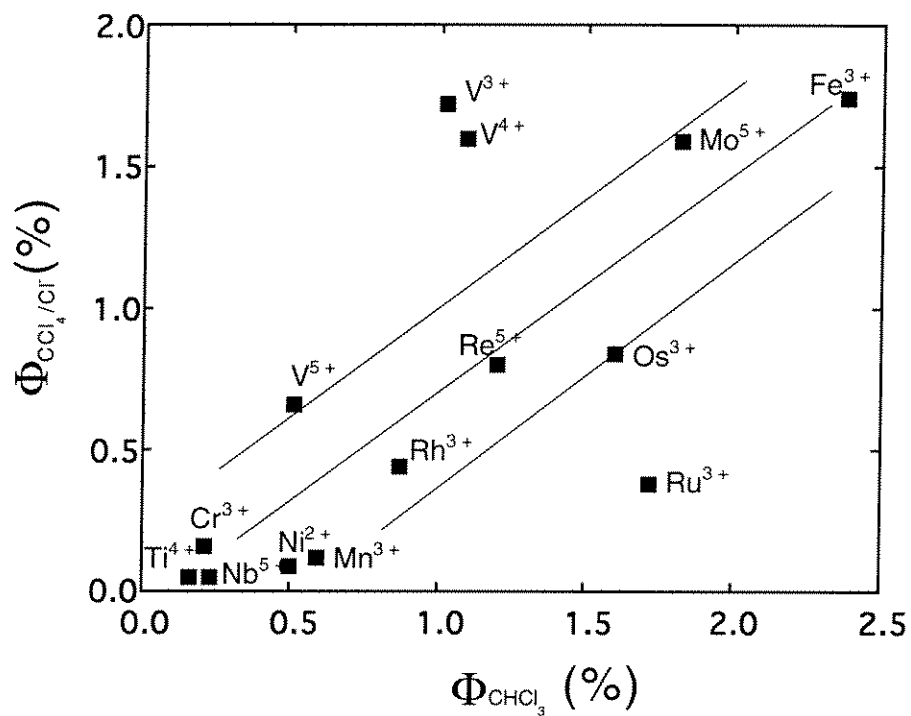


**Figure 3.** Correlation plot between the oxidation quantum yield ( $\Phi_{\text{CHCl}_3}$ ) and the reduction quantum yield ( $\Phi_{\text{CCl}_4/\text{Cl}^-}$ ) from the data of Figure 2. Some dopants, which show little effect on the photoreactivity, are omitted for clarity of the figure. The straight lines are drawn only as a visual guide.

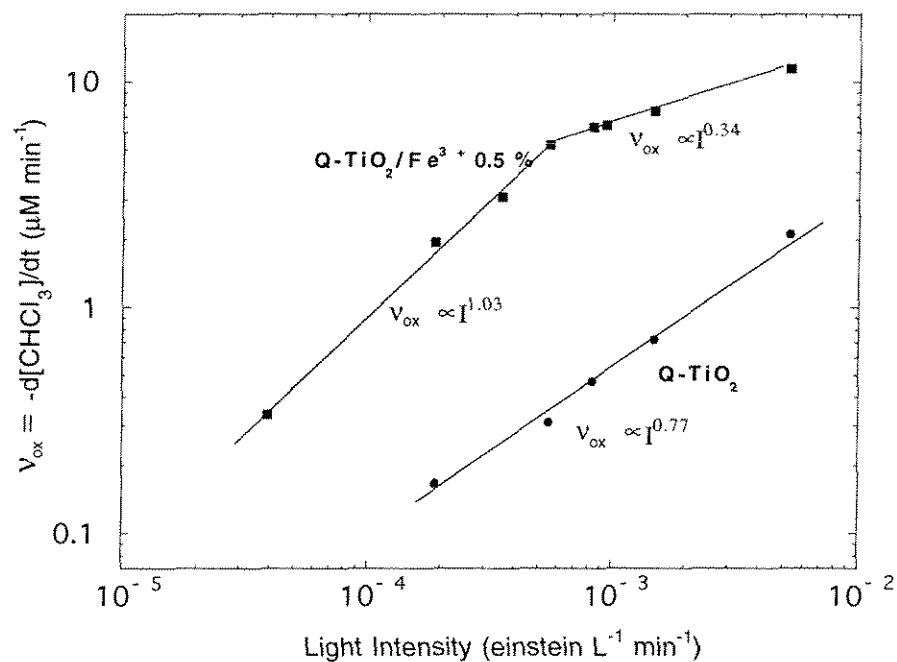


**Figure 4.** Light intensity ( $I$ ) dependence of the photodegradation rate of chloroform ( $V_{ox}$ ) for the undoped and  $Fe^{3+}$ -doped (0.5 %) Q-sized  $TiO_2$  under the condition of  $[CHCl_3]_0 = 3.15 \text{ mM}$  and pH 11.

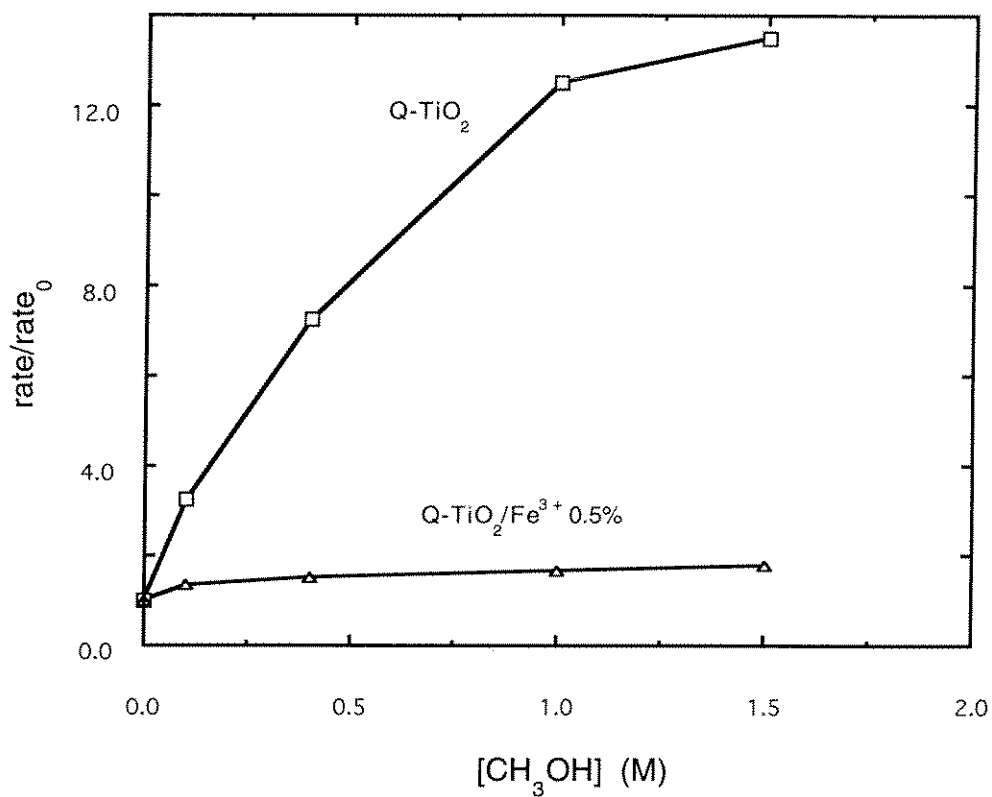


**Figure 5.** Ratio of relative chloride production from  $\text{CCl}_4$  dechlorination as a function of added methanol concentration for the undoped and the  $\text{Fe}^{3+}$ -doped (0.5%) Q-sized  $\text{TiO}_2$ .

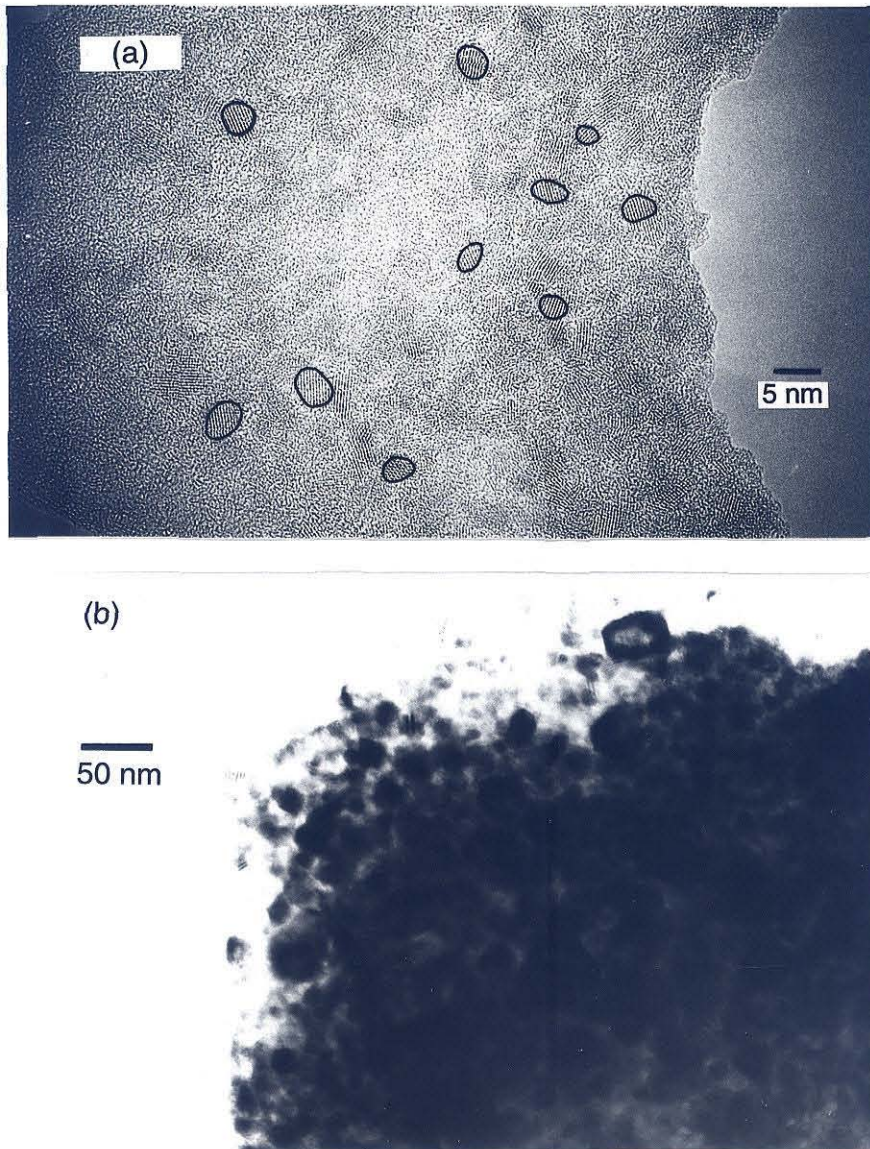


**Figure 6.** TEM pictures of (a) Q-sized  $\text{TiO}_2$  particles and (b) an aggregate of small particles ( $\text{Fe}^{3+}$  0.5%) resulting from heating at 400 °C/4h. Several Q-sized particles are outlined for clarity.

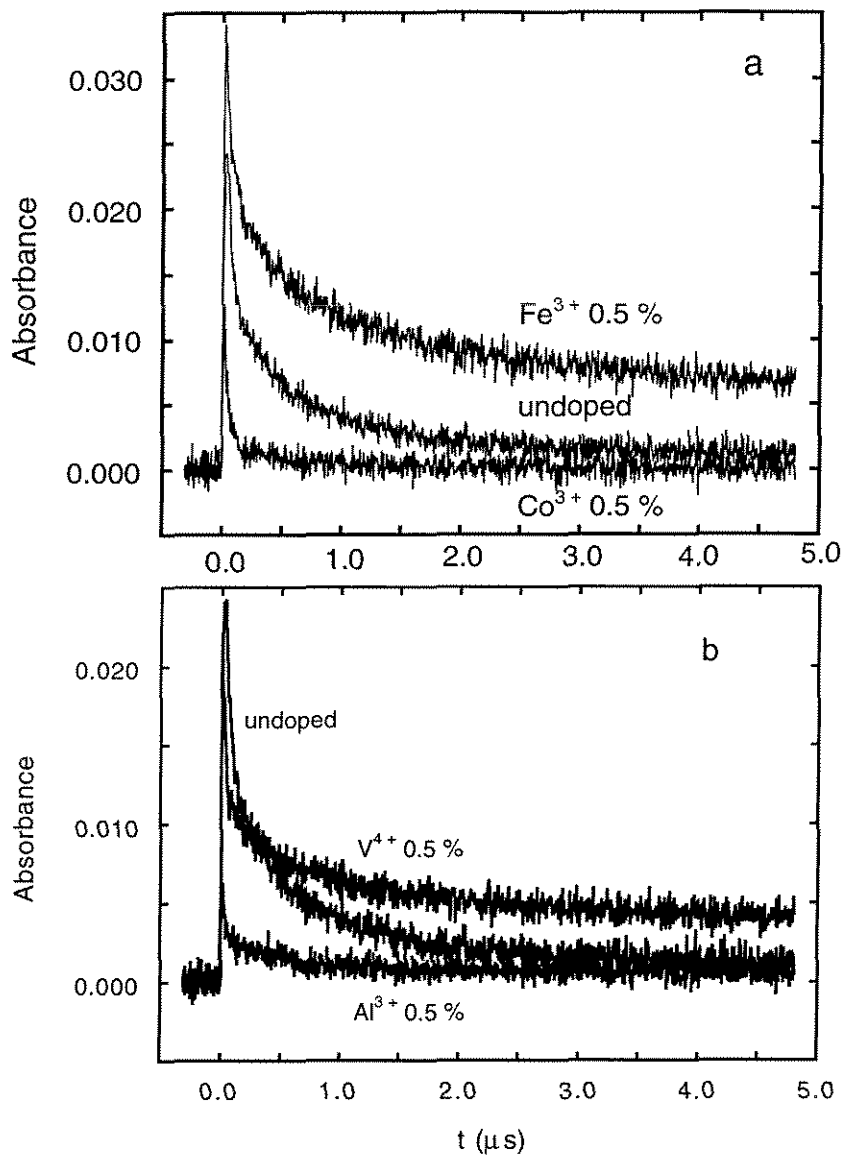


**Figure 7.** Transient absorption decays observed at 600 nm in the  $\mu\text{s}$ -time scale for (a) undoped,  $\text{Fe}^{3+}$  0.5%, and  $\text{Co}^{3+}$  0.5%, and (b) undoped,  $\text{V}^{4+}$  0.5%, and  $\text{Al}^{3+}$  0.5% doped Q-sized colloids.

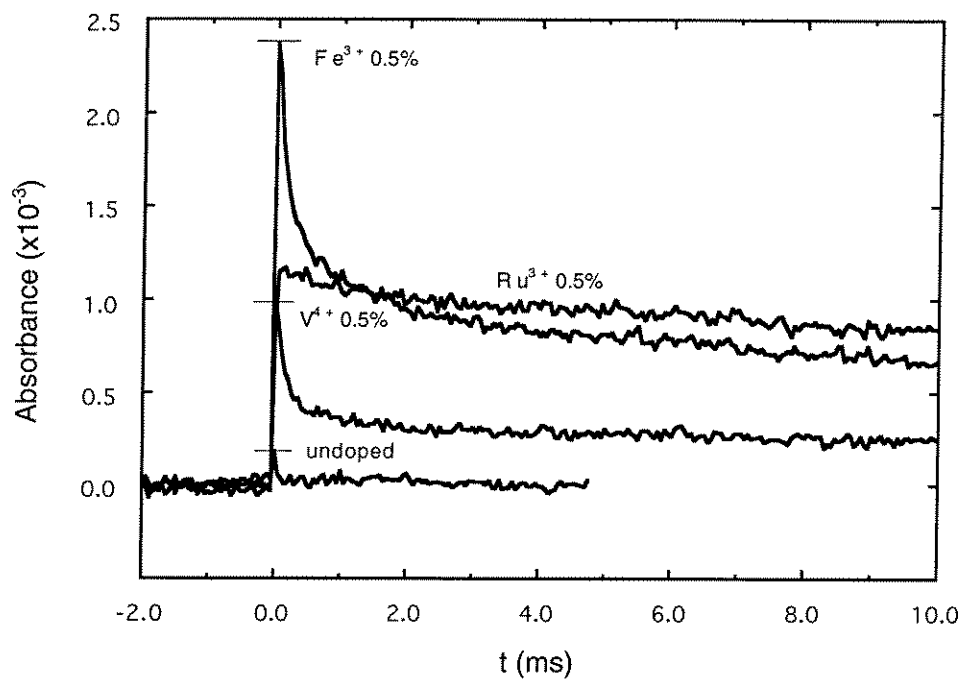


**Figure 8.** Transient absorption decays observed at 600 nm in the ms-time scale for Fe<sup>3+</sup> 0.5%, V<sup>4+</sup> 0.5%, Ru<sup>3+</sup> 0.5% doped and undoped Q-sized colloids.

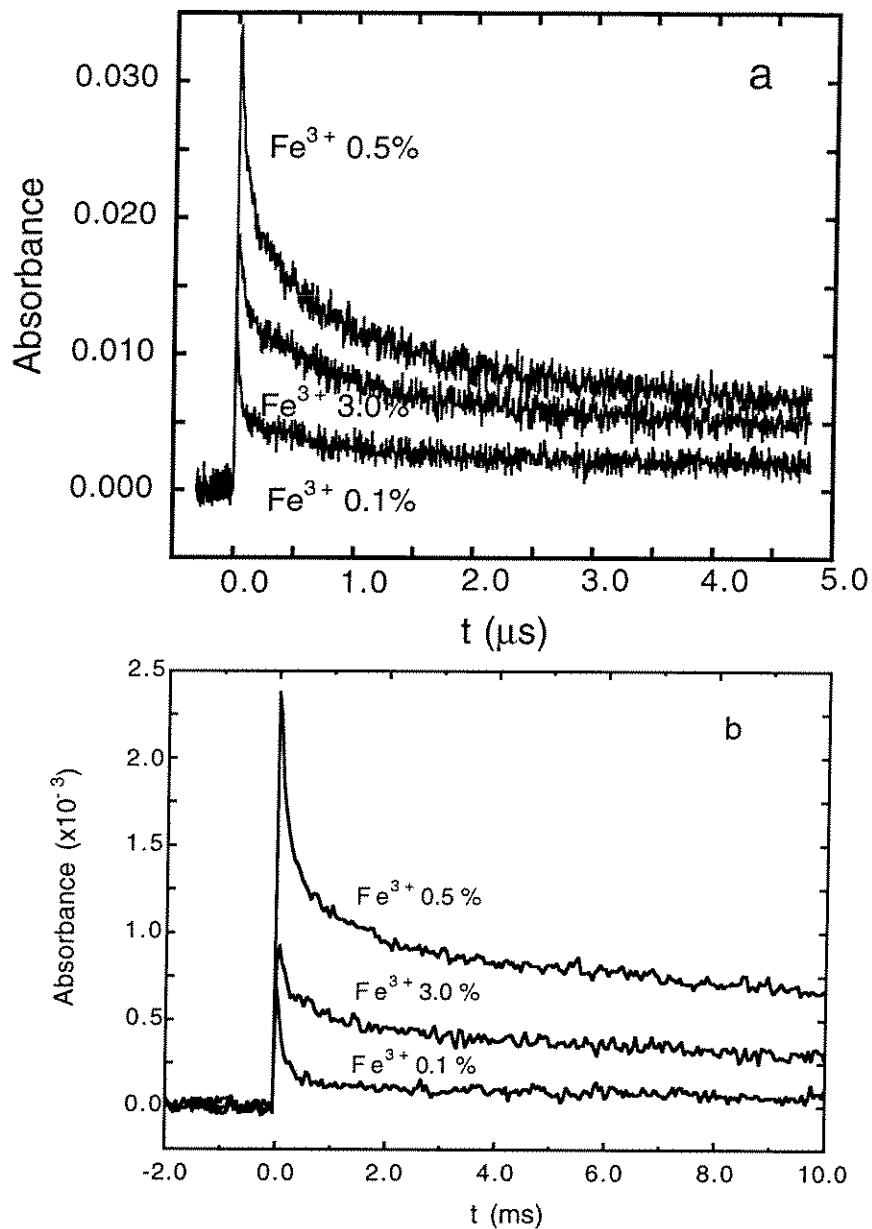


**Figure 9.** Transient absorption decays observed at 600 nm for  $\text{Fe}^{3+}$ -doped colloids at 0.1, 0.5, and 3.0 %  $\text{Fe}^{3+}$  concentration in the (a)  $\mu\text{s}$ -time scale and (b) ms-time scale.

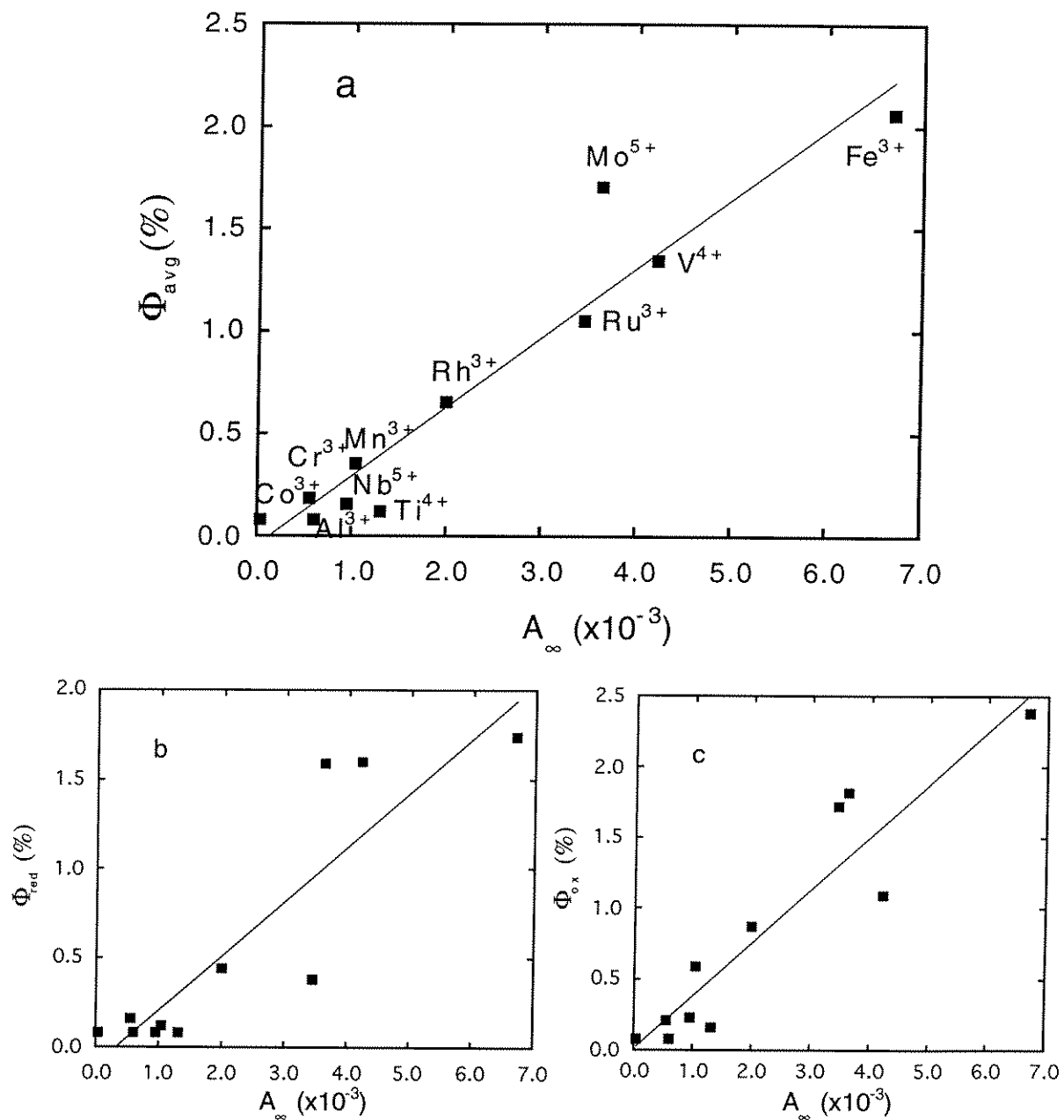


**Figure 10.** Correlation plot between the quantum yields [(a)  $\Phi_{\text{avg}}$ , (b)  $\Phi_{\text{red}}$ , and (c)  $\Phi_{\text{ox}}$ ] and  $A_\infty$  from Table III.

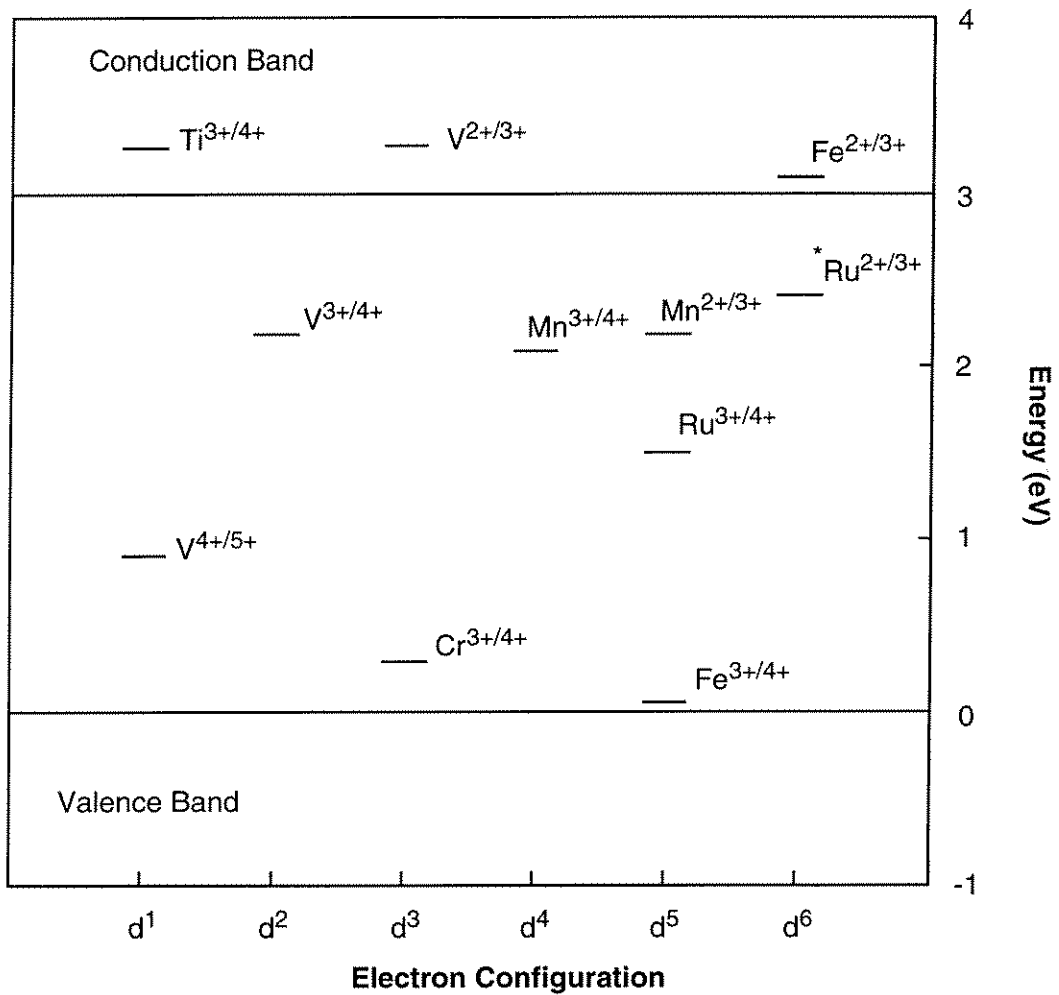


**Figure 11.** Energy levels of impurity ions in rutile proposed by Mizushima et al.<sup>32</sup> and Triggs (\*).<sup>33</sup>

## Chapter 3

### Photoreductive Mechanism of CCl<sub>4</sub> Degradation on TiO<sub>2</sub> Particles and Effects of Electron Donors

[ The text of this chapter appears in: W. Choi and M.R. Hoffmann *Environmental Science & Technology* **1995**, *29*, 1646 - 1654.]

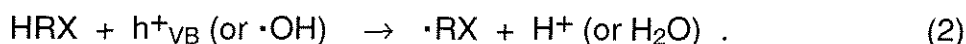
## Abstract

The photoreductive degradation of  $\text{CCl}_4$  in  $\text{TiO}_2$  particulate suspensions in the presence of a variety of organic electron donors (alcohols, carboxylic acids, and benzene derivatives) has been examined. The rate of  $\text{CCl}_4$  dechlorination can be enhanced significantly when alcohols and organic acids are used as electron donors. Alcohols with  $\alpha$ -hydrogens show complex behavior due to the formation of intermediate  $\alpha$ -hydroxyalkyl radicals which directly reduce  $\text{CCl}_4$ . Kinetic isotope effects and structure-reactivity relationships show that hydrogen-abstraction by hydroxyl radicals plays an important role in the hole-scavenging mechanism. The pH of the  $\text{TiO}_2$  suspension influences the rate of  $\text{CCl}_4$  reduction either by altering the electrostatic interactions of electron donors on the  $\text{TiO}_2$  surface or by changing the reduction potential of the conduction band electron in a Nernstian fashion. It is demonstrated that  $\text{CCl}_4$  can be fully degraded under both oxic and anoxic conditions.  $\text{CHCl}_3$ ,  $\text{C}_2\text{Cl}_4$ , and  $\text{C}_2\text{Cl}_6$  are detected as intermediates during photolysis at pH 2.8 while no intermediates are formed at pH 12.4. A photodegradation mechanism of  $\text{CCl}_4$  that includes both one-electron and two-electron transfer processes is proposed. Dichlorocarbene, which is formed through a two-electron reduction of  $\text{CCl}_4$ , is directly trapped during the photolysis.

## Introduction

Photoexcitation of TiO<sub>2</sub> generates strongly oxidative ( $E^{\circ} = +2.7$  V vs. NHE at pH 7) valence band (VB) holes and moderately reductive ( $E^{\circ} = -0.5$  V vs. NHE at pH 7) conduction band (CB) electrons. The  $e_{CB}^{-}/h_{VB}^{+}$  pairs can initiate redox reactions of many halogenated organic compounds which are ultimately degraded into CO<sub>2</sub> and inorganic acids.<sup>1,2</sup>

The decomposition of halogenated hydrocarbons can be initiated by either CB electrons or VB holes when the redox reactions are thermodynamically favorable:

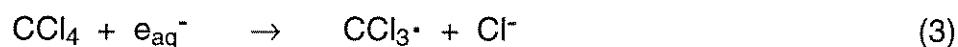


However, under normal conditions the redox potential of  $e_{CB}^{-}$  of TiO<sub>2</sub> is not sufficiently negative to be a versatile reducing agent. As a result, most of the studies on TiO<sub>2</sub> photocatalysis have been focused on hole-initiated oxidations while the CB electron reductions have been largely neglected.<sup>3-10</sup> For perhalogenated hydrocarbons, however, the CB-electron reduction pathway is the only possible pathway for the destruction because they are often inert towards VB holes or hydroxyl radicals.<sup>11</sup> For example, carbon tetrachloride and trichloroacetic acid have been reported to undergo little degradation under the condition of hole-initiated oxidation.<sup>4b,c</sup>

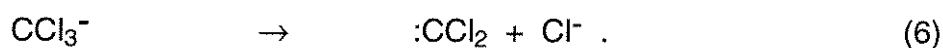
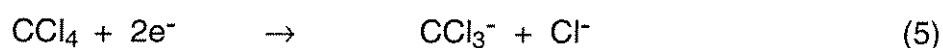
Halothane (2-bromo-2-chloro-1,1,1-trifluoroethane) is reported to be reduced by both one- and two-electron transfers on a platinumized-TiO<sub>2</sub> surface in the presence of suitable hole scavengers.<sup>12</sup> In separate studies, Hilgendorff et al.<sup>13</sup> demonstrated the photoreductive dechlorination of CCl<sub>4</sub> in the presence of

TiO<sub>2</sub> while Choi et al.<sup>14</sup> employed this reaction to assess the relative reactivities of metal-ion doped quantum-sized TiO<sub>2</sub> colloids. A photoreductive mechanism has also been proposed for the photocatalytic decomposition of CFCl<sub>3</sub> and CF<sub>2</sub>Cl<sub>2</sub> on ZnO.<sup>15</sup>

The degradation of carbon tetrachloride has been investigated previously by radiolytic,<sup>16</sup> electrochemical<sup>17,18</sup> and biological methods.<sup>19</sup>  $\gamma$ -radiolysis of CCl<sub>4</sub> in oxygenated aqueous solution leads to the formation of CO<sub>2</sub> and Cl<sup>-</sup> through the one-electron reduction mechanism (eq 3) involving the trichloromethyl radical.<sup>16b</sup>



On the other hand, polarographic<sup>18b</sup> and electrolytic<sup>17</sup> studies have shown that CCl<sub>4</sub> is also reduced through a two-electron process (eq 5) in which dichlorocarbene is formed as a short-lived intermediate as follows:



In this paper, we present a detailed study of photoreductive decomposition of CCl<sub>4</sub> using TiO<sub>2</sub>. Various electron donors (hole scavengers) are tested for their effects on the rate and extent of photoreduction. The complete degradation (i.e., mineralization) of CCl<sub>4</sub> on TiO<sub>2</sub> via a reductive pathway is demonstrated and a detailed reaction mechanism is proposed.

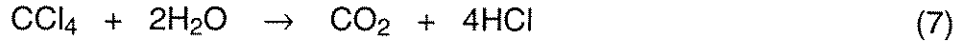
## Experimental Section

Titanium dioxide (Degussa P25), which is a known mixture of 80% anatase and 20% rutile with an average particle size of 30 nm and a reactive

surface area of  $\sim 50 \text{ m}^2/\text{g}$ , was used as a heterogeneous photocatalyst without further treatment.  $\text{TiO}_2$  suspensions were maintained at  $0.5 \text{ g/L}$ . Saturated  $\text{CCl}_4$  solutions ( $5.1 \text{ mM}$ ) were prepared by stirring in an excess of  $\text{CCl}_4$  in water and solutions of a desired concentration were then prepared by dilution. Most of the suspensions used in this work were in air equilibration. In the experiments using oxygenated and deoxygenated suspensions, the suspensions were bubbled with  $\text{O}_2$  and  $\text{N}_2$  gas respectively for an hour before adding electron donors and an aliquot of the saturated  $\text{CCl}_4$  stock solution. The pH of the suspension was adjusted with  $1 \text{ N HClO}_4$  or  $1 \text{ N NaOH}$ .

Steady-state photolyses were performed with a  $1000\text{-W}$  Xe arc lamp (Spindler and Hoyer). Light was filtered through a  $10\text{-cm}$  IR water filter and a UV band pass filter ( $310 - 400 \text{ nm}$ , Corning) or a UV interference filter ( $310 - 330 \text{ nm}$ , Oriel). The filter light was focused onto a  $35 \text{ mL}$  quartz reactor cell filled with the reaction suspension and a minimized head space. Light intensity measurements were performed by chemical actinometry using (E)  $\alpha$ -(2,5-dimethyl-3-furyl)ethyldene) (isopropylidene) succinic anhydride (Aberchrome 540).<sup>20</sup>

The dechlorination of  $\text{CCl}_4$  was followed by measuring the  $\text{Cl}^-$  production after  $20 - 40 \text{ min}$  of UV irradiation with an Orion chloride ion-selective electrode. Chloride production was linear over this time period. Chloride adsorption on the colloidal particles was found to be negligible under our experimental conditions. Since there was a significant pH change during the course of the photodegradation, a pH-stat titration technique<sup>5</sup> instead of the chloride measurement was employed in the investigation of the pH-dependence of  $\text{CCl}_4$  degradation rate (Fig. 4). This technique measured the consumption rate of the standard  $\text{NaOH}$  titrant ( $0.10 \text{ N}$ ) which was added to the reactor to maintain the system pH constant. According to the simple stoichiometry,



the acid generation rate, which is equivalent to the  $\text{OH}^-$  consumption rate, can be used as an indicator of the rate of  $\text{CCl}_4$  degradation. After correcting for the acidity production from carbonates (i.e.,  $\text{CO}_2 \cdot \text{H}_2\text{O}$ ,  $\text{HCO}_3^-$ ,  $\text{CO}_3^{2-}$ ) which originate from both  $\text{CCl}_4$  and electron donors, we obtained

$$\left( \frac{d[\text{H}^+]}{dt} \right)_{\text{HCl}} = \frac{1}{n} \left[ \left( \frac{d[\text{H}^+]}{dt} \right)_{\text{CCl}_4 / \text{ED}} - \left( \frac{d[\text{H}^+]}{dt} \right)_{\text{ED}} \right]$$

$$n = 1 + \frac{1}{4} \left( \frac{1}{1 + 10^{6.3 - \text{pH}} + 10^{\text{pH} - 10.3}} + \frac{2}{1 + 10^{16.6 - 2\text{pH}} + 10^{10.3 - \text{pH}}} \right) \quad (8)$$

where  $(d[\text{H}^+]/dt)_{\text{HCl}}$  is the rate of HCl production,  $(d[\text{H}^+]/dt)_{\text{CCl}_4/\text{ED}}$  is the rate of total acid production in the  $\text{CCl}_4$ -electron donor system, and  $(d[\text{H}^+]/dt)_{\text{ED}}$  is the rate of total acid production in the electron-donor only system. The corrected acid generation rate reasonably matched the chloride production rate for each case.

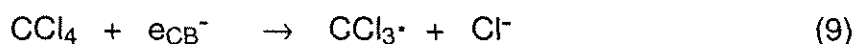
$\text{CCl}_4$  degradation was monitored by gas chromatography (GC). Reaction solutions were sampled by a 1 mL-syringe, filtered through a 0.45  $\mu\text{m}$ -nylon filter, and injected into a 2.5 mL glass vial with PTFE/silicone septum-lined screw-top cap. For extraction, 0.5 mL of pentane was added immediately and the vial was shaken for 20 sec. The vials were stored at 4 °C in the dark up to 48 hrs before GC analysis. Hewlett-Packard 5880A Gas Chromatograph equipped with a  $^{63}\text{Ni}$  electron capture detector and a HP5 column (crosslinked 50% PhMe silicone, 25m x 0.32 mm x 1.05  $\mu\text{m}$ ) was used. Nitrogen was used as the carrier gas. The GC was calibrated daily with external standards and duplicate

measurements were made for each sample with an injection volume of 0.5  $\mu\text{L}$ . All measurements agreed within 10%.

The bottom aqueous phase in the vial was analyzed by ion-exchange chromatography (IC) for chloride and other ionic products. The IC system was a Dionex Bio-LC system equipped with a conductivity detector and a Dionex OmniPac PAX-500 column (8  $\mu\text{m}$  x 5 mm x 250 mm).

## Results and Discussion

**Effects of Electron Donor Concentration and pH.** The reduction of  $\text{CCl}_4$  by CB electrons on  $\text{TiO}_2$  surfaces is strongly dependent on the presence of electron donors, D, which reduce the undesired recombination of photoexcited electron-hole pairs. Therefore, the following reactions should proceed concurrently on the  $\text{TiO}_2$  surface to maximize the photoreduction efficiency.



The effects of increasing concentrations of methanol and acetic acid as added electron donors on the rate of  $\text{CCl}_4$  dechlorination are shown in Figs. 1 and 2. At pH 2.8 both methanol and acetic acid ( $\text{pK}_a = 4.75$ ) are present as neutral molecules; under these conditions the reduction rates increase with increasing concentrations of electron donors until an optimal concentration is obtained. Further increases in concentration then decrease the reduction rate. However, the optimal concentration for methanol (0.1 M) is 100 times higher than that of acetic acid (1 mM). This result indicates that the surficial concentration of acetic acid is saturated at much lower bulk-solution concentrations. Acetic acid undergoes inner-sphere complexation at surface  $>\text{TiOH}$  sites<sup>21</sup> while  $\text{CH}_3\text{OH}$

interacts via weaker hydrogen-bonding interactions. The decrease of the dechlorination rates beyond the optimal concentration can be interpreted in terms of the competition for the reactive surface sites between  $\text{CCl}_4$  and the electron donor molecules. However, at pH 6.0 where acetic acid (acetate) is almost completely dissociated, the concentration dependence is substantially different (Fig. 2). Increasing acetate concentrations up to 8 mM do not result in a decreased dechlorination rate. One possible explanation for this behavior is that the ionic electron donor (acetate) and the neutral electron acceptor ( $\text{CCl}_4$ ) do not compete for the same surface sites. For example, the following site-specific interactions may be involved.

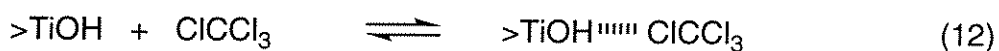
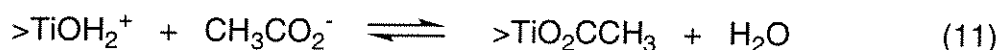


Fig. 3 shows the initial dechlorination rate of  $\text{CCl}_4$  as a function of pH in the presence of 1 mM acetate as an electron donor. The reduction rate steadily increases with pH up to 6.2 above which it quickly decreases to reach a plateau region around pH 8. This can be also explained in terms of the electrostatic interactions of electron donor molecules at the surface. Below pH 6, the  $\text{TiO}_2$  surface ( $\text{pH}_{\text{zpc}} \sim 6$ ) is positively charged and increasing pH results in increasing the concentration of acetate anions, which means more electron donor molecules are attracted to the surface for hole scavenging. Above pH 6, the surface charge is reversed and the acetate anions are repelled from the surface. As a result, the efficiency of hole scavenging is greatly reduced with a corresponding decrease in the  $\text{CCl}_4$  reduction rate. It was previously shown by Kormann et al.<sup>5</sup> that the photocatalytic degradation (oxidation) rates of ionic electron donors are strongly influenced by their electrostatic interactions at the  $\text{TiO}_2$  surface. They<sup>5</sup> showed

that higher surface concentrations of electron donors led to the higher photooxidation rates. In addition, the above results show that the rate of CB-electron transfer to a neutral molecule ( $\text{CCl}_4$ ) is not affected by the surface charge state of the  $\text{TiO}_2$  and is directly related to the surface concentration of electron donors. This clearly demonstrates how the CB-electron and VB-hole transfer are closely related on  $\text{TiO}_2$  particle surface. In a recent study<sup>14</sup> of metal-ion doped  $\text{TiO}_2$  colloids, we reported that the reactivities of CB electrons and VB holes were directly correlated; this observation is in accord with our present results.

The pH-dependence of  $\text{CCl}_4$  reduction was also examined with non-ionic electron donors (*tert*-butanol, methanol and 2-propanol) (see Fig. 4). The reduction rates, which were measured in terms of the acid generation rate (eq. 6), show constant values over a broad pH range. The slight decrease in rates above pH 5 is ascribed to the reduction of the net surface area of the  $\text{TiO}_2$  colloids. Near the  $\text{pH}_{\text{zpc}}$  the  $\text{TiO}_2$  particles undergo a moderately rapid rate of coagulation. The overall pH-independence reflects the absence of electrostatic interactions between the surface and the substrates. However, the reduction rates start to increase dramatically above pH 11 to 12. This latter effect cannot be explained in terms of the surficial electrostatic interactions.

The reduction potential of  $\text{CCl}_4$  is -0.51 V vs. NHE and independent of  $\text{pH}^{18c}$ , while the CB-electron reduction potential is known to follow standard Nernstian behavior:<sup>22</sup>

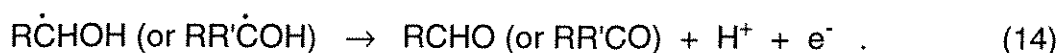
$$E_{\text{CB}} (\text{V vs. NHE}) = -0.1 - 0.059 \text{ pH} . \quad (13)$$

As a result, the driving force of CB electron transfer increases linearly with pH. Thus, the increase in driving force appears to account for the increase of the

reduction rates at high pH. The fact that the rates start to increase above pH 10.5 for methanol and pH 11.5 for 2-propanol and *t*-butanol shows that an overpotential of 0.2 - 0.3 V is required for an efficient CB electron transfer. Prairie et al.<sup>23</sup> have suggested that dissolved metal ion reduction by CB electrons of TiO<sub>2</sub> requires an overpotential of about 0.8 V. The magnitude of an overpotential for an efficient CB electron transfer seems to depend on the nature of the electron acceptor.

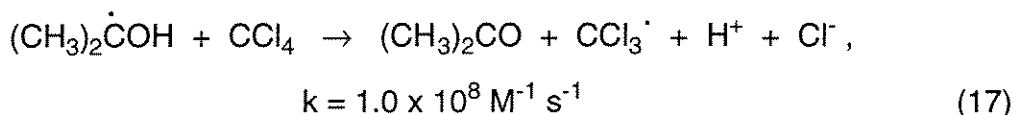
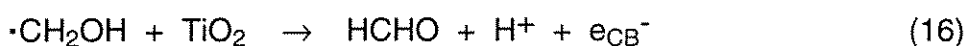
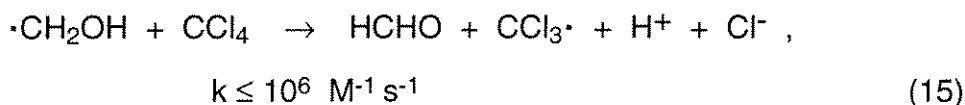
**Electron Donors and CCl<sub>4</sub> Reduction Efficiency.** A summary of results for initial CCl<sub>4</sub> dechlorination rates with various alcohols as electron donors is given in Table 1. Reduction rates are enhanced by factors of 4 to 80 depending on the specific electron donor. The rate constants for hydrogen abstraction from an alcohol molecule by a free hydroxyl radical are also given in Table I since hole-scavenging is believed to be closely related to the activity of surficial hydroxyl radical in many cases. Even though *t*-butanol, which has the lowest *k*<sub>OH</sub> value, shows the lowest dechlorination rate, there does not appear to be a reasonable correlation between the CCl<sub>4</sub> dechlorination rates and *k*<sub>OH</sub>.

Some complexity arises when primary and secondary alcohols serve as electron donors since alcohols with  $\alpha$ -hydrogens can form  $\alpha$ -hydroxyalkyl radicals upon  $\alpha$ -H atom abstraction. These radical intermediates are strong one-electron reductants (reaction 14):<sup>25</sup>



The half-wave potentials  $E_{1/2}$  of oxidation of  $\alpha$ -hydroxyalkyl radicals have been determined to be -0.74 V for  $\cdot\text{CH}_2\text{OH}$ , -0.94 V for  $\text{CH}_3\text{CHOH}$  and -1.06 V for  $(\text{CH}_3)_2\text{COH}$  (vs. NHE) at pH 7.<sup>26</sup> All the potentials are negative enough to inject

electrons to the conduction band (current doubling) or directly reduce  $\text{CCl}_4$  as follows:<sup>27</sup>



The alcohols in Table I with the exception of *t*-butanol can reduce  $\text{CCl}_4$  through the above pathway, thus interpretation of the overall  $\text{CCl}_4$  reduction mechanism is complicated by this secondary effect. Even *t*-butanol can possibly lead to the formation of  $(\text{CH}_3)_2\text{COH}$  radical through a series of reactions in the presence of oxygen according to Schuchmann and Sonntag.<sup>28</sup> However, this effect, if any, does not seem to be significant in this system. Under air-saturation, reactions 15 - 18 compete with the addition of molecular oxygen to the  $\alpha$ -hydroxyalkyl radical. Using the experimental conditions employed in this paper and the literature rate constants ( $k(\cdot\text{CH}_2\text{OH} + \text{O}_2) = 4.9 \times 10^9 \text{ M}^{-1} \text{ s}^{-1}$  and  $k((\text{CH}_3)_2\text{COH} + \text{O}_2) = 4.2 \times 10^9 \text{ M}^{-1} \text{ s}^{-1}$ ),<sup>27</sup> we calculate that 38 % of the  $(\text{CH}_3)_2\text{COH}$  radicals are channeled via reaction 17 while only 0.5 % of the  $\cdot\text{CH}_2\text{OH}$  radicals proceed via reaction 15 in terms of homogeneous chemistry. However, we cannot rule out the possibility that reactions 16 and 18 are much faster than  $\text{O}_2$  addition in the heterogeneous system. More kinetic information is needed to distinguish between the current doubling activity (reactions 16 and 18) and the direct reaction with  $\text{CCl}_4$  (reactions 15 and 17) and to assess the effect of  $\text{O}_2$  on  $\text{CCl}_4$  reduction rate.

The relative reactivities of the electron donors at pH 2.8 increase in the order of  $\text{H}_2\text{O} < \text{tertiary alcohol} < \text{methanol} < \text{primary alcohol} < \text{secondary alcohol}$ . This ordering matches the order of the thermodynamic stability of the  $\alpha$ -hydroxyalkyl radical of each alcohol, which implies that the above order of dechlorination efficiency is determined primarily by the secondary reaction of  $\alpha$ -hydroxyalkyl radicals. Therefore, the highest dechlorination rate observed with 2-propanol can be attributed to the fast rate of reaction 17 (and possibly 18) while reactions 15 and 16 in the  $\text{CCl}_4/\text{methanol}$  system seem to be insignificant. However, the order of the dechlorination rates is drastically altered at pH 11. Under these conditions methanol is the most efficient electron donor while the rates with 2-propanol and 2-butanol are lower than those at pH 2.8. A similar reversal of the relative order in dechlorination rates is also found for methanol and 2-propanol systems as shown in Fig. 4.

In order to understand the pH-dependencies observed for the different alcohols, kinetic isotope effects in the methanol/ $\text{CCl}_4$  and 2-propanol/ $\text{CCl}_4$  systems at pH 2.8 and 11 were examined. These results are summarized in Table II. In an earlier study, Cunningham and Srijaranai<sup>6</sup> examined the photooxidation (acetone formation) of  $(\text{CH}_3)_2\text{CHOH}$  and  $(\text{CD}_3)_2\text{CDOD}$  on  $\text{TiO}_2$  and reported a small H-D kinetic-isotope effect. Our data at pH 2.8, which agree with their results, show little isotopic effects ( $k_{\text{H}}/k_{\text{D}} = 1.1$  for methanol and 1.3 for 2-propanol). However, the isotope effects at pH 11 show significant values around 2. In addition, the rate ratios  $v_{\text{pH}11}/v_{\text{pH}2.8}$  are significantly lower for  $\text{CD}_3\text{OD}$  (6.3) and  $(\text{CD}_3)_2\text{CDOD}$  (0.46) compared to  $\text{CH}_3\text{OH}$  (10.9) and  $(\text{CH}_3)_2\text{CHOH}$  (0.83).

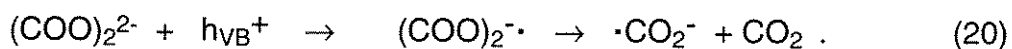
This somewhat puzzling phenomenon can be rationalized in terms of the competition between reactions 9 and 10 under acidic and basic conditions as

rate-determining steps. At pH 2.8, the reduction potential of CB electron is -0.27 V (according to eq. 13), which results in an unfavorable driving force for electron transfer to  $\text{CCl}_4$  ( $E_{1/2} = -0.51$  V).<sup>18c</sup> On the other hand, the oxidation potential of methanol,  $E^\circ(\cdot\text{CH}_2\text{OH}/\text{CH}_3\text{OH})$  is 0.93 V vs. NHE,<sup>29</sup> which results in a large driving force for hole transfer (VB hole oxidation potential, 2.93 V). On a semiconductor particle, the oxidation reaction by VB holes and the reduction reaction by CB electrons should proceed concurrently to satisfy the electroneutrality condition. Therefore, the overall  $\text{CCl}_4$  reduction rate is mainly limited by the slow CB electron transfer (reaction 9) at pH 2.8 and little H-D isotope effects in electron donors are observed. As pH increases to 11, the potentials of the CB electron and the VB hole are shifted to -0.75 V and 2.45 V, respectively. Then, the thermodynamic driving force for the electron transfer increases while the counterpart of the hole transfer decreases. As a result, the rate-limiting contribution from the electron-donor part (reaction 10) in the overall reduction rate cannot be neglected. If the hydrogen abstraction from the electron donors is rate-limiting, we expect significant H-D isotope effects for both methanol (2.1) and 2-propanol (2.0) according to the ratio,  $k_{\text{H}}/k_{\text{D}}$  in Table II. This interpretation is consistent with our results at pH 11. The lower ratio of rates,  $v_{\text{pH}11}/v_{\text{pH}2.8}$  in  $\text{CD}_3\text{OD}$  and  $(\text{CD}_3)_2\text{CDOD}$  than in  $\text{CH}_3\text{OH}$  and  $(\text{CH}_3)_2\text{CHOH}$  also suggests that hydrogen atom abstraction is rate-limiting to some extent at pH 11.

The lower absolute dechlorination rate in the 2-propanol system at pH 11 than at pH 2.8 can be understood in terms of the reduced hole oxidation potential. The reduced driving force of hole transfer makes the production rate of  $\alpha$ -hydroxyalkyl radicals decrease. Since the  $\alpha$ -hydroxyalkyl radical initiates reactions 17 and 18 which result in the release of additional chloride, the decrease of its production rate implies the decrease of the dechlorination rate.

This explains that the total CCl<sub>4</sub> dechlorination rate at pH 11 is lower than at pH 2.8 in the CCl<sub>4</sub>/secondary alcohol system.

Results for CCl<sub>4</sub> dechlorination in the presence of various organic acids as electron donors are summarized in Table III. The initial pH is adjusted to 6.0 ± 0.1 so that all acids are available in the dissociated form. We see that all of the organic acids except citric acid enhance the dechlorination rate relative to H<sub>2</sub>O. Hoffman et al.<sup>30</sup> have also reported that the quantum yield for the photocatalytic H<sub>2</sub>O<sub>2</sub> production on quantum-sized ZnO colloids was even lower than that of no electron donor system (i.e., H<sub>2</sub>O) when citrate was used as an electron donor. Citric acid is believed to form a strong surface complex through its multifunctional groups and thus preventing the CCl<sub>4</sub> molecule from approaching the reactive surface sites (>TiOH). Dechlorination rates with trifluoroacetate and oxalate, which do not have abstractable hydrogen atoms, are much lower than those of the other organic acids. These observations support the involvement of hydroxyl radicals in the hole-scavenging mechanism. This is also consistent with slower oxidation rate of trichloroacetic acid compared to monochloro- and dichloroacetic acid.<sup>3</sup> For these compounds, the direct hole transfer pathway is considered to be the only feasible pathway for the oxidation as suggested by Mao et al.:<sup>3</sup>



The hole scavenging efficiency of trifluoroacetate is expected to be quite low due to the low electron density at the carboxylate group while that of oxalate should be much higher. Accordingly, the CCl<sub>4</sub> dechlorination rate with oxalate is substantially higher than the CCl<sub>4</sub> dechlorination with trifluoroacetate.

The importance of the hydrogen-atom abstraction by hydroxyl radicals in the hole scavenging mechanism becomes clearer when we compare the reducing efficiencies of structurally-related electron donors: oxalate vs. malonate and trimethylacetate vs. isobutyrate. Malonate with its methylene group is susceptible to hydroxyl radical attack and thus induces higher dechlorination rates than oxalate. The presence of an  $\alpha$ -hydrogen, which is more easily abstractable by hydroxyl radicals than  $\beta$ -hydrogen, in isobutyrate may account for the slightly higher dechlorination rate in the  $\text{CCl}_4$ /isobutyrate system than in the  $\text{CCl}_4$ /trimethylacetate system.

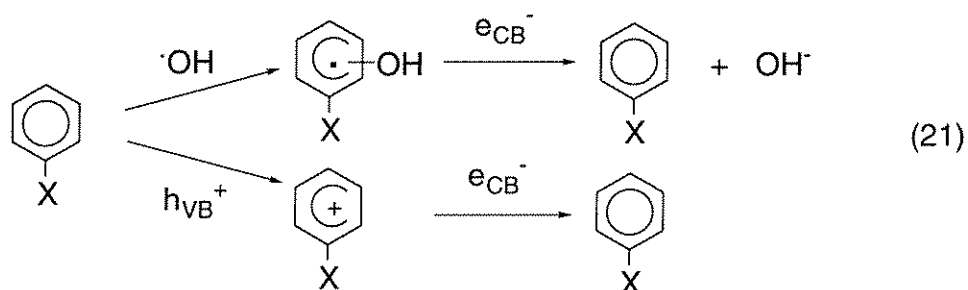
The dechlorination rates with various organic acids are plotted against the corresponding rate constants,  $k_{\text{OH}}$ , for the homogeneous bimolecular reactions of  $\cdot\text{OH}$  in Fig. 5. If the reaction of  $\cdot\text{OH}$  with electron donors is rate-limiting, there should be some degree of correlation, as shown in Fig. 5, between the heterogeneous  $\text{CCl}_4$  reduction rates and the rate constants,  $k_{\text{OH}}$ . The correlation does not seem to hold in the region of  $k_{\text{OH}} > 10^9 \text{ M}^{-1}\text{s}^{-1}$ . Similar correlations have been suggested for the oxidation of organic compounds by Turchi and Ollis.<sup>4a</sup> The correlation between the CB electron reaction and the reaction of electron donors with free  $\cdot\text{OH}$  becomes weaker as other parameters affecting the overall reaction prevail such as the secondary effect from the  $\alpha$ -hydroxyalkyl radicals (vide supra) which provide an additional reduction pathway. Due to this effect, we failed to find a correlation between CB electron reactivity and  $k_{\text{OH}}$  in the series of alcohols (Table I). Among organic acids in Table III, only formate and oxalate can lead to a radical intermediate,  $\cdot\text{CO}_2^-$  which may induce a secondary reduction reaction. The  $\cdot\text{CO}_2^-$  radical, however, is known to be non-reactive with  $\text{CCl}_4$  in a homogeneous solution.<sup>27</sup> The possible current doubling effect similar to reactions 16 and 18, which may enhance the  $\text{CCl}_4$  reduction efficiency, seems

to be insignificant considering that the efficiency of formate as an electron donor is somewhat low for its large  $k_{OH}$  value (Fig. 5).

It is interesting to note that monofluoroacetic acid, which has a rather slow hydrogen atom abstraction rate constant, shows the highest reduction rate. In a recent study, Pehkonen et al.<sup>31</sup> showed that fluoroacetate was the best electron donor among various halogenated acetic acids in the photoreduction of iron oxyhydroxides. Neither the hydroxyl-radical mechanism nor the direct hole-transfer mechanism can explain the abnormally high efficiency of fluoroacetate as an electron donor because the presence of a strongly electron-withdrawing fluorine adversely affects both its reaction with  $\cdot OH$  by destabilizing the carbon-centered free radical intermediate<sup>32</sup> and its reaction with  $h\nu_B^+$  by reducing the electron density at the carboxylate group. The high efficiency of fluoroacetate may be due to its tendency to form a strong surface complex with  $>TiOH$  sites.

The reduction efficiency of phenylacetate is much lower than that of acetate even though the  $k_{OH}$  of phenylacetate is much larger than the  $k_{OH}$  of acetate (Table III). In order to resolve this discrepancy, other benzene derivatives are tested as electron donors for the  $CCl_4$  dechlorination reaction. These compounds include: nitrobenzene, benzyl alcohol, aniline, benzaldehyde, benzonitrile, benzene, phenol, phenylacetic acid, benzenesulfonic acid, and benzoic acid. Measurements were performed with electron donor concentrations of 2 mM, pH 2.8 and with other conditions given in Table I. For these electron donors, the initial dechlorination rates are all less than  $0.5 \mu M \text{ min}^{-1}$ ; these rates were less than or equal to the no electron-donor ( $H_2O$ ) system. This result is not what is expected based on the hydroxyl-radical mechanism because the reactions of all the benzene derivatives with hydroxyl radicals are nearly diffusion-limited ( $k_{OH}$  ranging  $2 - 9 \times 10^9 \text{ M}^{-1}\text{s}^{-1}$ ).<sup>24</sup> If surface sorption of electron

donors is critical for efficient hole scavenging, then the low surface affinity of aromatic compounds may account for their low reactivity. However, considering that benzene derivatives with a variety of functional groups, which may induce inner sphere complexing (e.g.,  $-\text{OH}$ ,  $-\text{CO}_2\text{H}$ ) at  $>\text{TiOH}$  sites or favorable electrostatic interactions ( $-\text{SO}_3^-$ ) at the surface, are tested, the low surface affinity does not seem to be the single major source of the low reactivity of these compounds. More plausible explanation for the low hole-scavenging efficiency of benzene derivatives is the short-circuit reactions shown below.



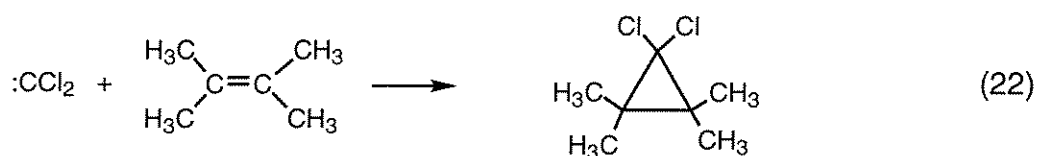
Unlike the other radical species involved in the reactions of alcohols and organic acids, the radical (or cation) species formed from the aromatic ring through the  $\cdot\text{OH}$  (or hole) reaction is highly resonance-stabilized and relatively long-lived. This makes it highly probable that the surface-adsorbed aromatic radicals (or cations) successively react with CB electrons to give no net change and enhanced recombination. This presents a good example how surface chemistry complicates the overall redox process where the simple analogs of homogeneous radical chemistry are inadequate.

**Intermediates and Photodegradation Mechanism of  $\text{CCl}_4$ .** In Figs. 6, 7, and 8 the time-dependent formation/ disappearance of the observed reaction intermediates and products are shown. The degradations of  $\text{CCl}_4$  in oxygenated and deoxygenated suspensions with 2-propanol are compared in Fig. 6 (at pH 2.7) and in Fig. 7 (at pH 12.4). In the suspension of pH 2.7 (both oxygenated

and deoxygenated),  $\text{CHCl}_3$ ,  $\text{C}_2\text{Cl}_4$ , and  $\text{C}_2\text{Cl}_6$  are formed as stable intermediates. It is interesting to note that  $\text{O}_2$  has little influence on reaction rates or product distributions although it does result in slightly slower rates of degradation. The same trend is observed with *t*-butanol (Fig. 8) which does not have secondary effects due to the  $\alpha$ -hydroxyalkyl radicals. Even though oxygen is a potential competitive electron acceptor with  $\text{CCl}_4$  and thus is expected to reduce the dechlorination rates of  $\text{CCl}_4$  (reaction 9), its presence was considered essential for the mineralization of  $\text{CCl}_4$  based on the results from previous radiolysis studies (reaction 4).<sup>16b</sup> However, our results show that  $\text{CCl}_4$  can be fully mineralized in the absence of dissolved oxygen. These observations suggest alternative mechanisms for the complete degradation of  $\text{CCl}_4$ .

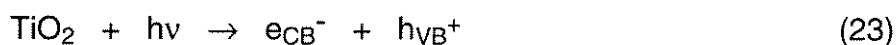
One possible pathway may involve a two-electron process leading to the formation of dichlorocarbene as shown in reactions 5 and 6. At the light intensity employed in this study ( $1.46 \times 10^{-3}$  einstein  $\text{L}^{-1} \text{min}^{-1}$ ) approximately 1600  $\text{e}^-/\text{h}^+$  pairs per particle per second can be generated assuming an average particle size of 30 nm. Considering that the CB electron concentration is significant even after  $\sim 10$  ms after a photoexcitation due to the slow interfacial electron transfer,<sup>33</sup> the steady-state concentration of CB electrons is well above 1 electron per particle under these conditions. Consequently, a simultaneous two-electron transfer or two consecutive one-electron transfers to  $\text{CCl}_4$  at the particle interface may be possible. In addition, the two-electron transfer to  $\text{CCl}_4$  is known to be thermodynamically more favorable than the one-electron transfer.<sup>17</sup> Bahnemann et al.<sup>12</sup> have also shown that halothane is reduced by a two-electron transfer on colloidal  $\text{TiO}_2$ . The detection of  $\text{C}_2\text{Cl}_4$  during photodegradation supports the dichlorocarbene mechanism (two-electron process) because the recombination reaction of dichlorocarbenes leads to the formation of  $\text{C}_2\text{Cl}_4$ .

Further proof of the formation of dichlorocarbene during the photolysis was obtained by directly trapping the dichlorocarbene through an addition reaction to alkene:<sup>34</sup>

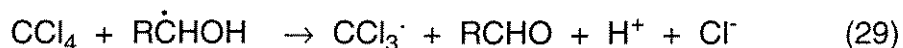
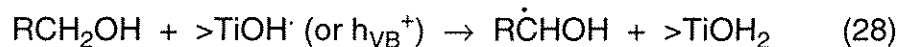
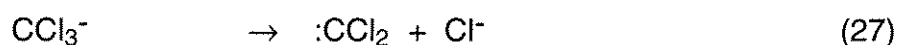
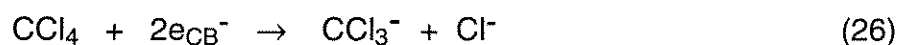


The *trapped* dichlorocarbene, 1,1-dichloro-2,2,3,3-tetramethylcyclopropane, was detected by GC/MS. Details on this reaction will be presented in a separate publication.<sup>35</sup> Dichlorocarbenes are known to hydrolyze rapidly to yield carbon monoxide and formate; formate is then oxidized to  $\text{CO}_2$ .<sup>36,37</sup> Thus, it is possible to degrade  $\text{CCl}_4$  completely in a strictly anoxic environment. We also detected formate ions from  $\text{CCl}_4$ /2-propanol system by ion chromatography even though it was not clear whether the formate originated from  $\text{CCl}_4$  or 2-propanol. Based on these results, we propose the following mechanism for the photoreductive degradation of  $\text{CCl}_4$  in the presence of alcohols:

*charge-pair generation:*



*initial charge transfer:*

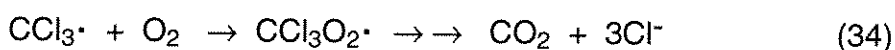


*intermediate formation:*

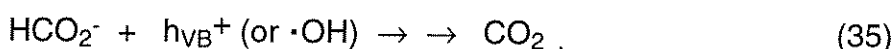
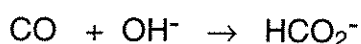
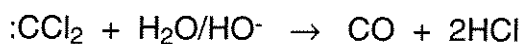


*mineralization to CO<sub>2</sub>:*

*with oxygen* <sup>16b</sup>



*without oxygen* <sup>37</sup>



In the presence of oxygen the competition between reactions 25 and 34 determines the branching ratio of the one-electron and two-electron pathways. Even though oxygen addition in reaction 34 is near the diffusion-limit ( $k(\text{CCl}_3\cdot + \text{O}_2) = 3.3 \times 10^9 \text{ M}^{-1}\text{s}^{-1}$ )<sup>11</sup> in the homogeneous solution, a finite residence time of  $\text{CCl}_3\cdot$  on the colloid surface in heterogeneous systems makes reaction 25 compete with reaction 34. Whether the reaction proceeds via an one-electron or two-electron transfer may depend on parameters such as light intensity, particle size, dissolved oxygen concentration, electron donor, and pH. This complex aspect of the one- and two-electron transfer process will be discussed in detail.<sup>35</sup> The fact that we did not detect any intermediates at pH 12.4 (Fig. 7) suggests that two-electron transfer is favored at this pH. Since the hydrolysis of dichlorocarbene is base-catalyzed,<sup>37</sup> it is quickly hydrolyzed at pH 12.4 with little chance of forming  $\text{C}_2\text{Cl}_4$  through reaction 33. The disappearance of the intermediates,  $\text{CHCl}_3$  and  $\text{C}_2\text{Cl}_4$ , is slow in the presence of excess hole scavengers (Fig. 6) because their degradation is hole-initiated. Fast degradation

of  $C_2Cl_6$  under the same conditions (Fig. 6) indicates that it is degraded through a reduction pathway similar to  $CCl_4$ .

## **Acknowledgments**

We are grateful to ARPA and ONR {N0014-92-J-1901} for financial support. We appreciate the help from Inez Hua, Patrick Lang, Scot Martin, Janet Kesselman and Nicole Peill in various aspects of this research. Comments from anonymous reviewers were valuable.

## References

- (1) Serpone, N., Pelizzetti, E., Eds. *Photocatalysis - Fundamentals and Applications*; Wiley Interscience: New York, 1989.
- (2) Ollis, D.F.; Al-Ekabi, H., Eds. *Photocatalytic Purification and Treatment of Water and Air*, Elsevier: Amsterdam, 1993.
- (3) Mao, Y.; Schöneich, C.; Asmus, K.-D. *J. Phys. Chem.* **1991**, *95*, 10080.
- (4) (a) Turchi, C.S.; Ollis, D.F. *J. Catal.* **1990**, *122*, 178. (b) Ollis, D.F.; Hsiao, C.-Y.; Budiman, L.; Lee, C.L. *ibid.* **1984**, *88*, 89. (c) Hsiao, C.-Y.; Lee, C.-L.; Ollis, D.F. *ibid.* **1983**, *82*, 418. (d) Pruden, A.L.; Ollis, D.F. *Environ. Sci. Technol.* **1983**, *17*, 628.
- (5) Kormann, C.; Bahnemann, D.W.; Hoffmann, M.R. *Environ. Sci. Technol.* **1991**, *25*, 494.
- (6) Cunningham, J.; Srijaranai, S. *J. Photochem. Photobiol. A: Chem.* **1988**, *43*, 329.
- (7) Micic, O.I.; Zhang, Y.; Cromack, K.R.; Trifunac, A.D.; Thurnauer, M.C. *J. Phys. Chem.* **1993**, *97*, 13284.
- (8) Stafford, U.; Gray, K.A.; Kamat, P.V. *J. Phys. Chem.* **1994**, *98*, 6343.
- (9) Mills, A.; Morris, S.; Davies, R. *J. Photochem. Photobiol. A: Chem.* **1993**, *70*, 183.
- (10) Chemseddine, A.; Boehm, H.P. *J. Mol. Catal.* **1990**, *60*, 295.
- (11) Lal, M.; Schöneich, C.; Mönig, J.; Asmus, K.-D. *Int. J. Radiat. Biol.* **1988**, *54*, 773.
- (12) Bahnemann, D.W.; Mönig, J.; Chapman, R. *J. Phys. Chem.* **1987**, *91*, 3782.
- (13) Hilgendorff, M.; Hilgendorff, M.; Bahnemann, D.W. submitted to *Environmental Aspects of Electrochemistry and Photoelectrochemistry*:

Proceedings of the 183rd Meeting of the Electrochemical Society, Yoneyama, H.; Hori, Y.; Haynes, R.; Tomkiewicz, M. (Eds.), 1993.

(14) (a) Choi, W.; Termin, A.; Hoffmann, M.R. *Angew. Chem. Int. Ed. Engl.* **1994**, *33*, 1091. (b) Choi, W.; Termin, A.; Hoffmann, M.R. *J. Phys. Chem.* **1994**, *98*, 13669.

(15) Filby, W.G.; Mintas, M.; Güsten, H. *Ber. Bunsenges. Phys. Chem.* **1981**, *85*, 189.

(16) (a) Asmus, K.-D.; Bahnemann, D.; Krischer, K.; Lal, M.; Mönig, J. *Life. Chem. Rep.* **1985**, *3*, 1. (b) Mönig, J.; Bahnemann, D.; Asmus, K.-D. *Chem.-Biol. Interactions* **1983**, *45*, 15. (c) Köster, R.; Asmus, K.-D. *Z. Naturforsch* **1971**, *26b*, 1104.

(17) Criddle, C.S.; McCarty, P.L. *Environ. Sci. Technol.* **1991**, *25*, 973.

(18) (a) Lambert, F.L.; Hasslinger, B.L.; Franz, R.N.,III *J. Electrochem. Soc.: Electrochem. Sci. Technol.* **1975**, *122*, 737. (b) Wawzonek, S.; Duty, R.C. *J. Electrochem. Soc.* **1961**, *108*, 1135. (c) Kolthoff, I.M.; Lee, T.S.; Stocesova, D.; Parry, E.P. *Anal. Chem.* **1950**, *22*, 521.

(19) (a) Gälli, R.; McCarty, P.L. *Appl. Environ. Microbiol.* **1989**, *55*, 837. (b) Castro, C.E.; Wade, R.S.; Belser, N.O. *Biochemistry* **1985**, *24*, 204.

(20) Heller, H.G.; Langan, J.R. *J. Chem. Soc. Perkin Trans.* **1981**, *2*, 341.

(21) Stumm, W.; Morgan, J.J. *Aquatic Chemistry*, 2nd ed.; Wiley-Interscience: New York, 1981.

(22) Grätzel, M. *Heterogeneous Photochemical Electron Transfer Reactions*, CRC Press: Boca Raton, Florida, USA, 1987.

(23) Prairie, M.R.; Evans, L.R.; Stange, B.M.; Martinez, S.L. *Environ. Sci. Technol.* **1993**, *27*, 1776.

(24) (a) Buxton, G.V.; Greenstock, C.L.; Helman, W.P.; Ross, A.B. *J. Phys. Chem. Ref. Data* **1988**, *17*, 513. (b) Farhataziz; Ross, A.B. *Selected Specific*

- Rates of Reactions of Transients from Water in Aqueous Solution. III. Hydroxyl Radical and Perhydroxyl Radical and Their Radical Ions*, NSRDS-NBS 59, National Bureau of Standards, 1977.
- (25) Mönig, J.; Asmus, K.-D. *J. Chem. Soc. Perkin Trans. II* **1984**, 2057.
- (26) Lilie, V.J.; Beck, G.; Henglein, A. *Ber. Bunsenges. Phys. Chem.* **1971**, 75, 458.
- (27) Ross, A.B.; Neta, P. *Rate Constants for Reactions of Aliphatic Carbon-Centered Radicals in Aqueous Solution*, NSRDS-NBS 70, National Bureau of Standards, 1982.
- (28) Schuchmann, M.N.; Sonntag, C.v. *J. Phys. Chem.* **1979**, 83, 780.
- (29) The potential is calculated from the polarographic half wave potential,  $E_{1/2} = -0.74$  V (vs. NHE) for the half-reaction of  $\text{HCHO} + e^- + \text{H}^+ \rightarrow \cdot\text{CH}_2\text{OH}$  and  $E^\circ = 0.19$  V for the half-reaction of  $\text{HCHO} + 2e^- + 2\text{H}^+ \rightarrow \text{CH}_3\text{OH}$ .
- (30) Hoffman, A.J.; Carraway, E.R.; Hoffmann, M.R. *Environ. Sci. Technol.* **1994**, 28, 776.
- (31) Pehkonen, S.O.; Siefert, R.; Hoffmann, M.R. submitted to *Environ. Sci. Technol.*
- (32) Anbar, M.; Meyerstein, D.; Neta, P. *J. Chem. Soc. B* **1966**, 742.
- (33) Martin, S.T.; Herrmann, H.; Choi, W.; Hoffmann, M.R. *J. Chem. Soc. Faraday Trans.* **1994**, 90, 3315.
- (34) Doering, W.v.E.; Henderson, W.A., Jr. *J. Am. Chem. Soc.* **1958**, 80, 5274.
- (35) Choi, W.; Hoffmann, M.R., *J. Phys. Chem.* **1996**, 100, 2161.
- (36) Kirmse, W. *Organic Chemistry - A Series of Monographs Vol. 1 Carbene Chemistry*, Academic Press: New York, 1964.
- (37) Robinson, E.A. *J. Chem. Soc.* **1961**, 1663.

**Table I. CCl<sub>4</sub> Dechlorination<sup>a</sup> Rates with Various Alcohols Serving as Electron Donors**

electron donors 0.1 M	d[Cl <sup>•</sup> ]/dt, μM min <sup>-1</sup> pH 2.8, (Φ <sub>Cl<sup>•</sup></sub> (%) <sup>b</sup> )	d[Cl <sup>•</sup> ]/dt, μM min <sup>-1</sup> pH 11, (Φ <sub>Cl<sup>•</sup></sub> (%) <sup>b</sup> )	k <sub>OH</sub> <sup>c</sup> (M <sup>-1</sup> s <sup>-1</sup> )
none (H <sub>2</sub> O)	0.6 (0.3)	0.8 (0.4)	
methanol, CH <sub>3</sub> OH	5.9 (2.8)	64.1 (30.5)	9.7 x 10 <sup>8</sup>
ethanol, CH <sub>3</sub> CH <sub>2</sub> OH	24.5 (11.7)	43.3 (20.6)	1.9 x 10 <sup>9</sup>
<i>n</i> -propanol, CH <sub>3</sub> (CH <sub>2</sub> ) <sub>2</sub> OH	18.5 (8.8)	31.7 (15.1)	2.8 x 10 <sup>9</sup>
2-propanol, (CH <sub>3</sub> ) <sub>2</sub> CHOH	46.0 (21.9)	38.0 (18.1)	1.9 x 10 <sup>9</sup>
<i>n</i> -butanol, CH <sub>3</sub> (CH <sub>2</sub> ) <sub>3</sub> OH	17.0 (8.1)	26.0 (12.4)	4.2 x 10 <sup>9</sup>
2-butanol, CH <sub>3</sub> CH <sub>2</sub> CHOHCH <sub>3</sub>	31.1 (14.8)	24.0 (11.4)	3.1 x 10 <sup>9</sup>
<i>tert</i> -butanol, (CH <sub>3</sub> ) <sub>3</sub> COH	4.5 (2.1)	3.2 (1.5)	6.0 x 10 <sup>8</sup>

<sup>a</sup> at the condition of [CCl<sub>4</sub>]<sub>0</sub> = 5.1 mM, [TiO<sub>2</sub>] = 0.5 g/L, I = 2.1 x 10<sup>-4</sup> einstein L<sup>-1</sup>min<sup>-1</sup> (at λ = 320 nm, FWHM 15 nm). <sup>b</sup> Φ<sub>Cl<sup>•</sup></sub> (%) = 100 x (d[Cl<sup>•</sup>]/dt)/I. <sup>c</sup> bimolecular rate constants (per molecule) of hydrogen abstraction by a free hydroxyl radical (ref. 24a).

**Table II. Kinetic Isotope Effects on the Rate of Photocatalytic CCl<sub>4</sub> Dechlorination<sup>a</sup> with Methanol and 2-propanol**

electron donor 0.1 M	$v_{Cl}$ ( $\mu\text{M min}^{-1}$ ) pH 2.8	$v_{Cl}$ ( $\mu\text{M min}^{-1}$ ) pH 11	$v_{pH11}/v_{pH2.8}$	$v_H/v_D$ pH 2.8	$v_H/v_D$ pH 11
CH <sub>3</sub> OH	5.9	64.1	10.9	1.1	1.9
CD <sub>3</sub> OD	5.5	34.4	6.3		
(CH <sub>3</sub> ) <sub>2</sub> CHOH	46.0	38.0	0.83	1.3	2.3
(CD <sub>3</sub> ) <sub>2</sub> CDOD	35.1	16.3	0.46		
CH <sub>3</sub> OH + ·OH → H <sub>2</sub> O + ·CH <sub>2</sub> OH			$k_H^b = 3.0 \times 10^8 \text{ M}^{-1} \text{ s}^{-1}$	$k_H/k_D = 2.1$	
CD <sub>3</sub> OH + ·OH → HDO + ·CD <sub>2</sub> OH			$k_D^b = 1.4 \times 10^8 \text{ M}^{-1} \text{ s}^{-1}$		
(CH <sub>3</sub> ) <sub>2</sub> CHOH + ·OH → H <sub>2</sub> O + (CH <sub>3</sub> ) <sub>2</sub> COH			$k_H^b = 1.6 \times 10^9 \text{ M}^{-1} \text{ s}^{-1}$	$k_H/k_D = 2.0$	
(CH <sub>3</sub> ) <sub>2</sub> CDOH + ·OH → HDO + (CH <sub>3</sub> ) <sub>2</sub> COH			$k_D^b = 7.9 \times 10^8 \text{ M}^{-1} \text{ s}^{-1}$		

<sup>a</sup> at the condition of [CCl<sub>4</sub>]<sub>0</sub> = 5.1 mM, [TiO<sub>2</sub>] = 0.5 g/L, I = 2.1 × 10<sup>-4</sup> einstein L<sup>-1</sup> min<sup>-1</sup> (at λ = 320 nm FWHM 15 nm). <sup>b</sup> bimolecular rate constants (per H-atom) estimated from the original data (per molecule) in ref. 24.

**Table III. CCl<sub>4</sub> Dechlorination<sup>a</sup> Rates with Various Organic Acids as Electron Donors**

electron donors (2 mM)	d[Cl <sup>-</sup> ]/dt (μM min <sup>-1</sup> ) (Φ <sub>Cl<sup>-</sup></sub> (%) <sup>b</sup> )	k <sub>OH</sub> <sup>c</sup> (M <sup>-1</sup> s <sup>-1</sup> )
none (H <sub>2</sub> O)	0.15 (0.07)	
formate, HCO <sub>2</sub> <sup>-</sup>	6.7 (3.2)	3.2 x 10 <sup>9</sup>
acetate, CH <sub>3</sub> CO <sub>2</sub> <sup>-</sup>	4.9 (2.3)	8.5 x 10 <sup>7</sup>
citrate, <sup>-</sup> O <sub>2</sub> CCH <sub>2</sub> C(OH)(CO <sub>2</sub> H)CH <sub>2</sub> CO <sub>2</sub> <sup>-</sup>	0.0 (0.0)	5.0 x 10 <sup>7</sup>
oxalate, (CO <sub>2</sub> <sup>-</sup> ) <sub>2</sub>	1.8 (0.9)	7.7 x 10 <sup>6</sup>
malonate, CH <sub>2</sub> (CO <sub>2</sub> <sup>-</sup> ) <sub>2</sub>	6.5 (3.1)	3.0 x 10 <sup>8</sup>
propionate, CH <sub>3</sub> CH <sub>2</sub> CO <sub>2</sub> <sup>-</sup>	8.1 (3.9)	8.2 x 10 <sup>8</sup>
butyrate, CH <sub>3</sub> (CH <sub>2</sub> ) <sub>2</sub> CO <sub>2</sub> <sup>-</sup>	4.7 (2.2)	1.85 x 10 <sup>9</sup>
isobutyrate, (CH <sub>3</sub> ) <sub>2</sub> CHCO <sub>2</sub> <sup>-</sup>	8.6 (4.1)	1.3 x 10 <sup>9</sup>
trimethylacetate, (CH <sub>3</sub> ) <sub>3</sub> CCO <sub>2</sub> <sup>-</sup>	6.2 (3.0)	1.5 x 10 <sup>9</sup>
monofluoroacetate, FCH <sub>2</sub> CO <sub>2</sub> <sup>-</sup>	16.7 (8.0)	3.0 x 10 <sup>7</sup>
difluoroacetate, F <sub>2</sub> CHCO <sub>2</sub> <sup>-</sup>	2.7 (1.3)	
trifluoroacetate, F <sub>3</sub> CCO <sub>2</sub> <sup>-</sup>	0.25 (0.1)	2 x 10 <sup>5</sup>
phenylacetate, C <sub>6</sub> H <sub>5</sub> CH <sub>2</sub> CO <sub>2</sub> <sup>-</sup>	1.1 (0.5)	7.9 x 10 <sup>9</sup>

<sup>a</sup> at the condition of [CCl<sub>4</sub>]<sub>0</sub> = 5.1 mM, [TiO<sub>2</sub>] = 0.5 g/L, pH 6.0 ± 0.2, I = 2.1 x 10<sup>-4</sup> einstein L<sup>-1</sup> min<sup>-1</sup> (at λ = 320 nm, FWHM 15 nm).

<sup>b</sup> Φ<sub>Cl<sup>-</sup></sub> (%) = 100 x (d[Cl<sup>-</sup>]/dt)/I. <sup>c</sup> bimolecular rate constants of reaction of free hydroxyl radicals with these carboxylates (ref. 24).

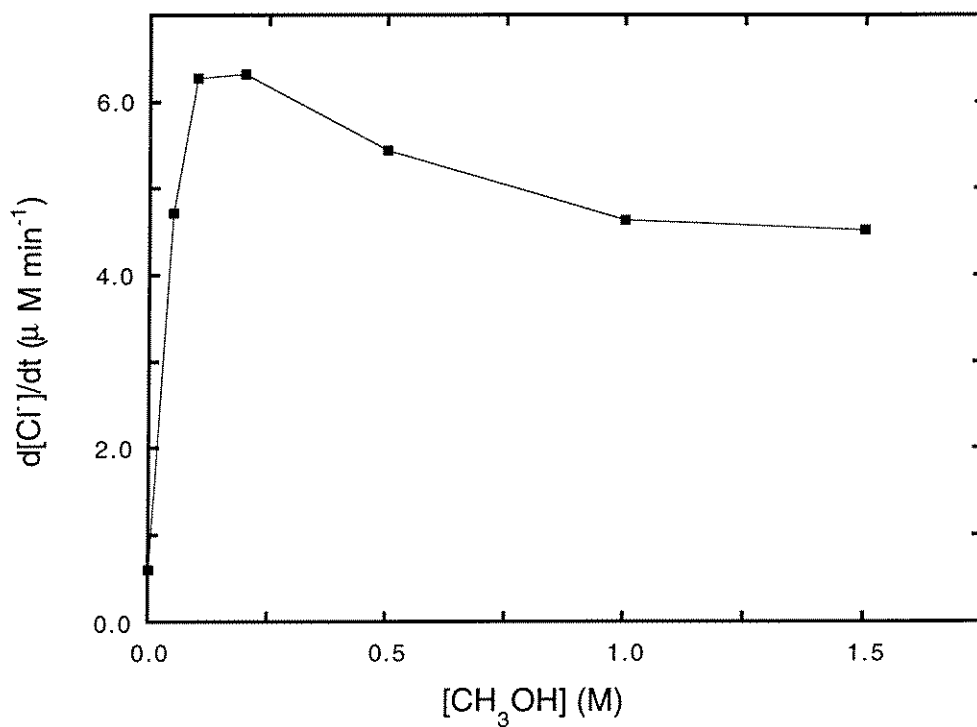


**Figure 1.**  $\text{CCl}_4$  dechlorination rates as a function of added methanol concentration where  $[\text{CCl}_4]_0 = 5.1 \text{ mM}$ ,  $\text{pH} = 2.8 \pm 0.1$ ,  $[\text{TiO}_2] = 0.5 \text{ g/L}$ ,  $I = 2.1 \times 10^{-4} \text{ einstein L}^{-1} \text{ min}^{-1}$  (at  $\lambda = 320 \text{ nm}$ , FWHM 15 nm), and  $[\text{O}_2]_{\text{diss}} \sim 0.2 \text{ mM}$  (air-equilibrated).

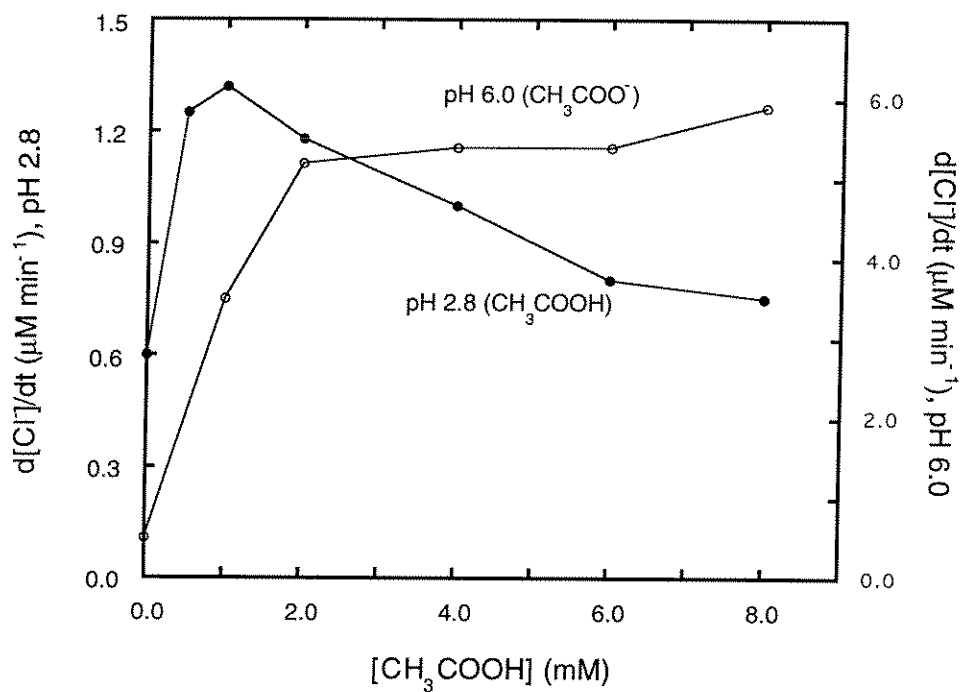


**Figure 2.** CCl<sub>4</sub> dechlorination rates as a function of added acetate concentration at an initial pH of 2.8 (●) and 6.0 (○). Other conditions are the same with those of Fig. 1.

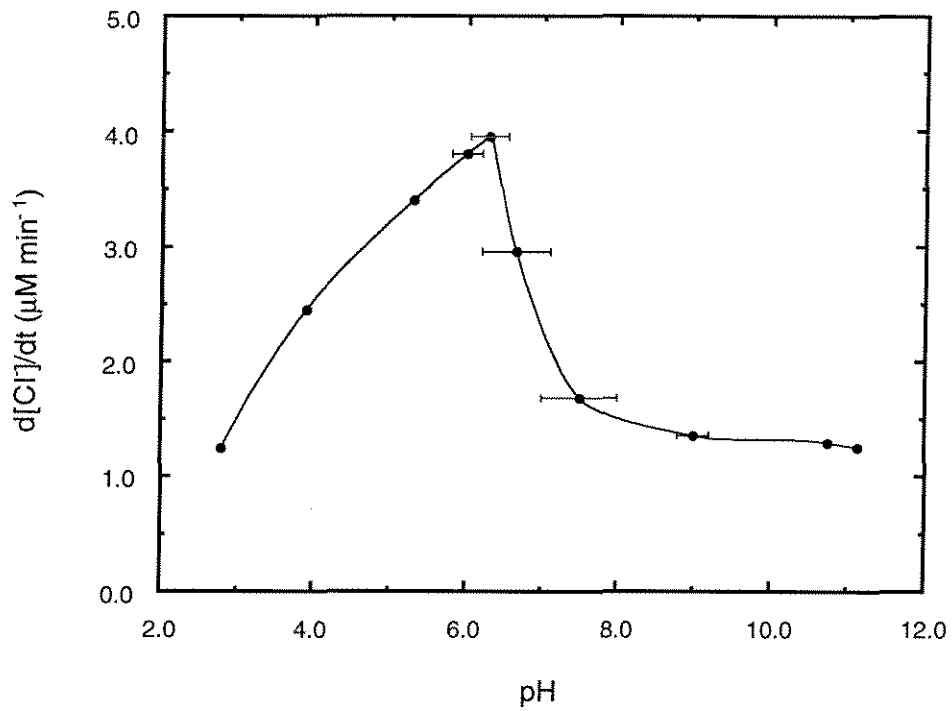


**Figure 3.** CCl<sub>4</sub> dechlorination rates as a function of pH in the presence of 1 mM of sodium acetate. Other conditions are the same with those of Fig.1.

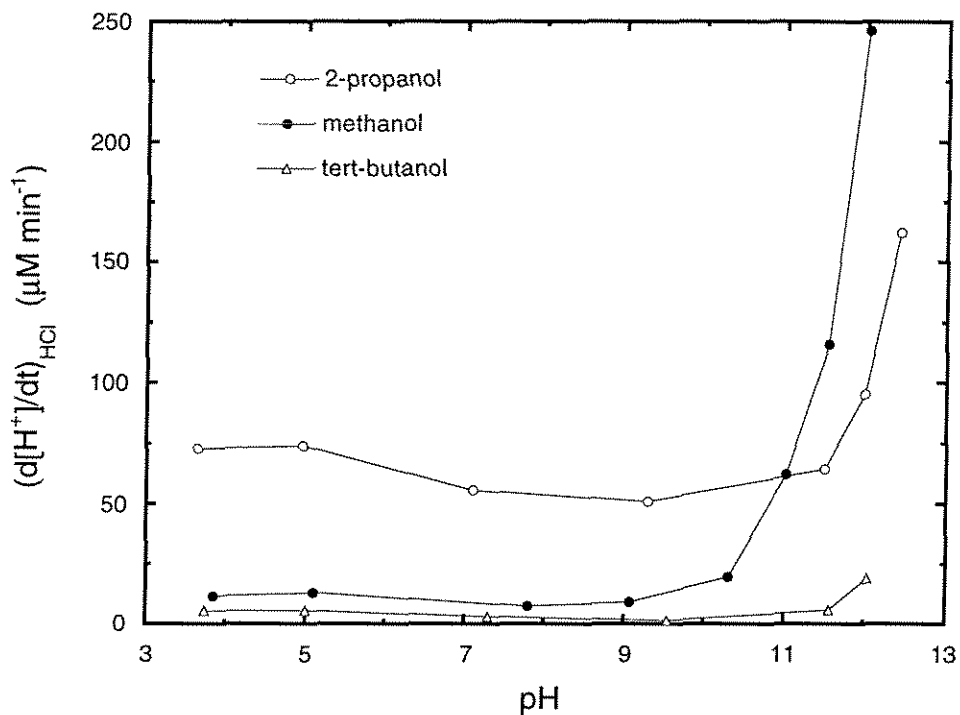


**Figure 4.** Rates of acid generation (corrected by eq. 6) from  $\text{CCl}_4$  degradation as a function of pH with 0.1 M of *tert*-butanol ( $\Delta$ ), methanol ( $\bullet$ ), and 2-propanol (o). The pH was maintained constant within  $\pm 0.05$  during each separate photolysis. Other conditions are the same with those of Fig. 1.

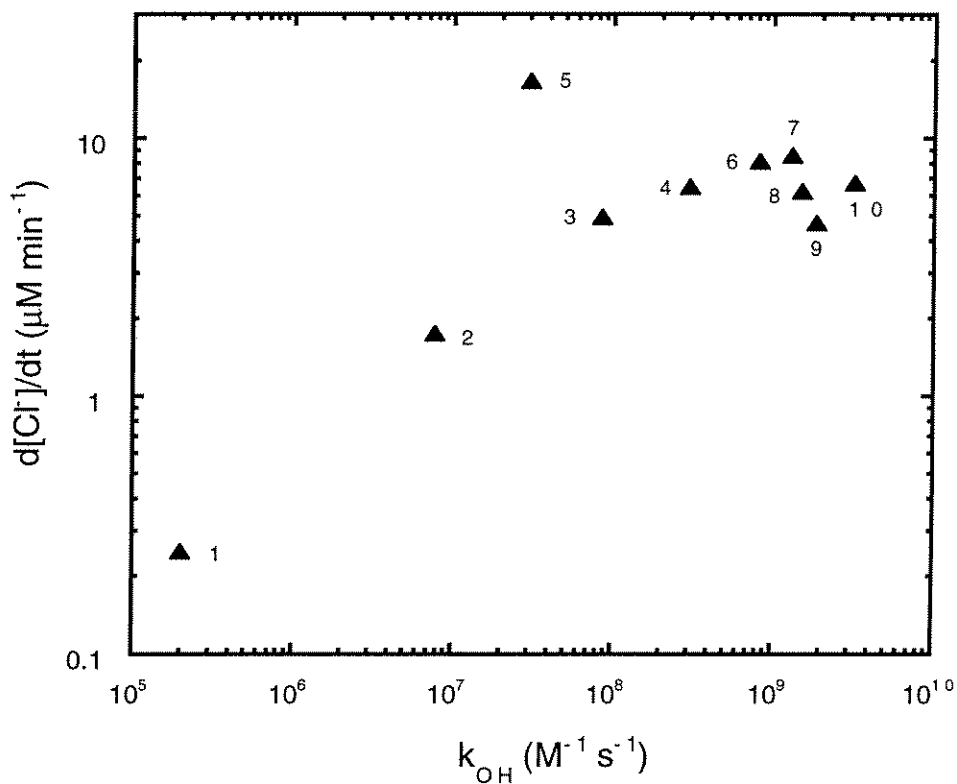


**Figure 5.** Plot of the rates of  $CCl_4$  dechlorination with aliphatic carboxylic acids against the  $k_{OH}$  from Table III. The corresponding numbers refer to 1, trifluoroacetate; 2, oxalate; 3, acetate; 4, malonate; 5, monofluoroacetate; 6, propionate; 7, isobutyrate; 8, trimethylacetate; 9, butyrate; 10, formate.

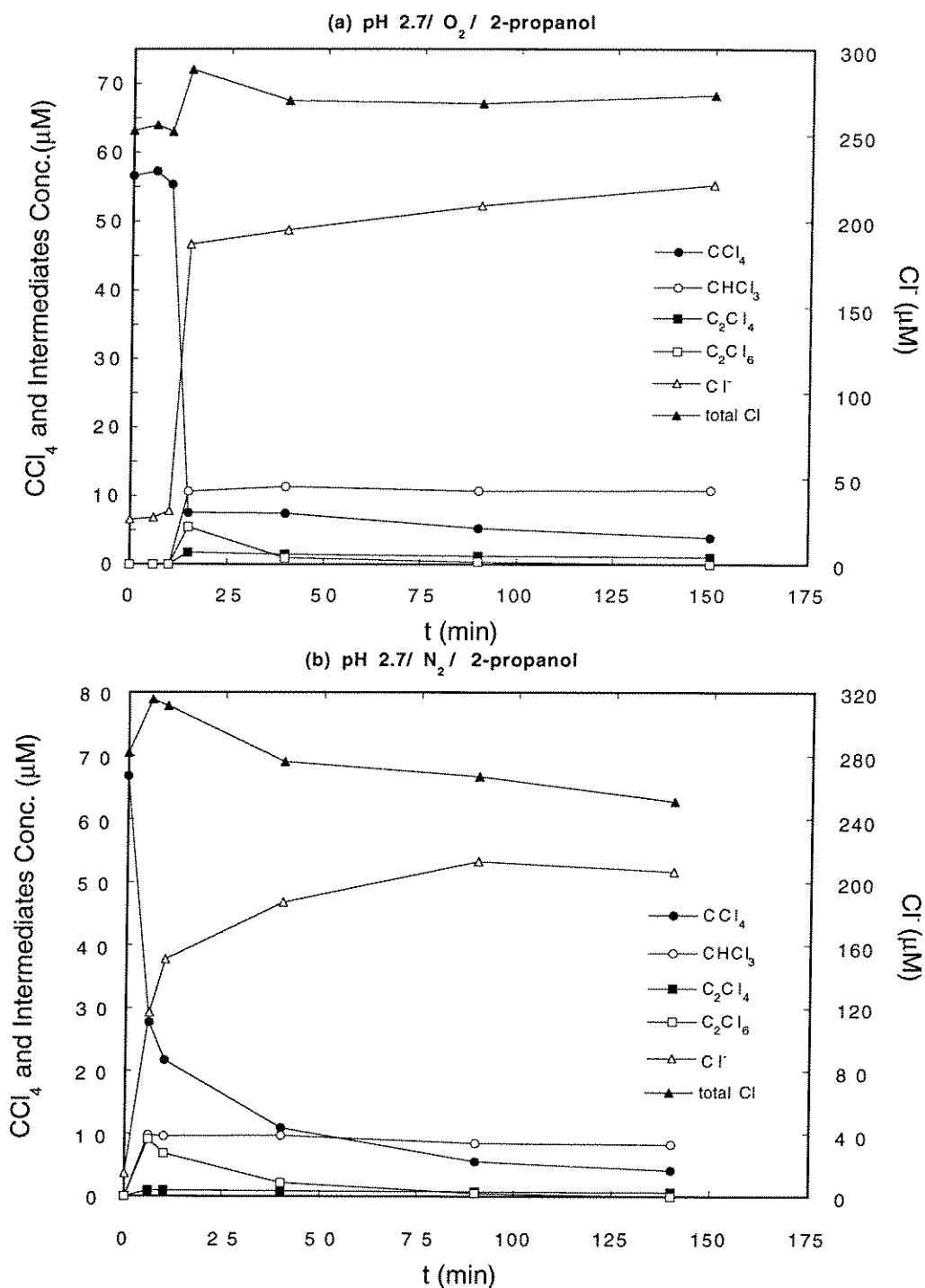


**Figure 6.** CCl<sub>4</sub> degradation at pH 2.7 and the production of Cl<sup>-</sup> and intermediates in the presence of 2-propanol (0.1 M) in (a) an oxygenated and (b) a deoxygenated suspension. [TiO<sub>2</sub>] = 0.5 g/L, and I = 1.46 × 10<sup>-3</sup> einstein L<sup>-1</sup> min<sup>-1</sup> (310 - 400 nm).

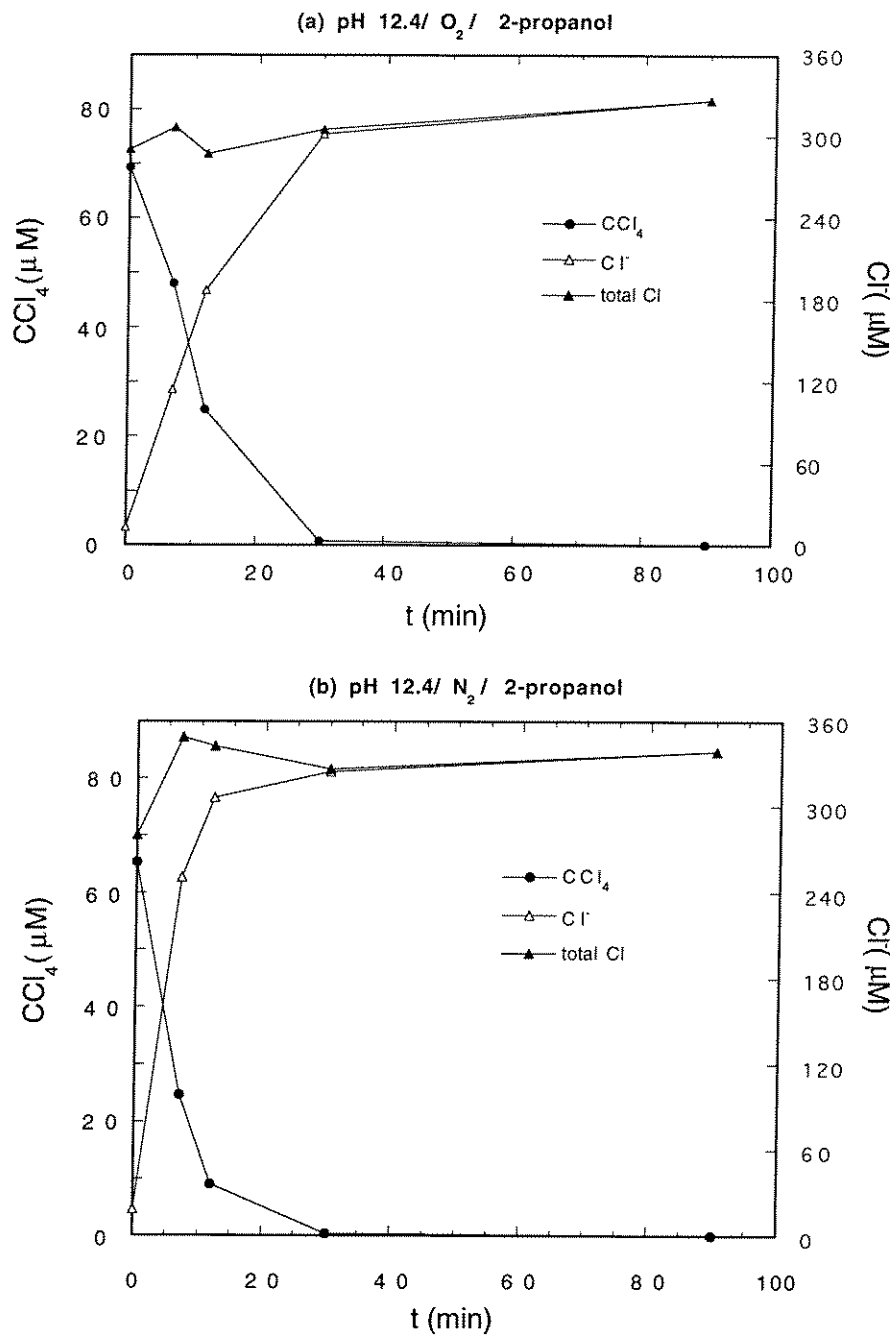


**Figure 7.** CCl<sub>4</sub> degradation at pH 12.4 and the production of Cl<sup>-</sup> and intermediates in the presence of 2-propanol (0.1 M) in (a) an oxygenated and (b) a deoxygenated suspension under the same condition of Fig.6.

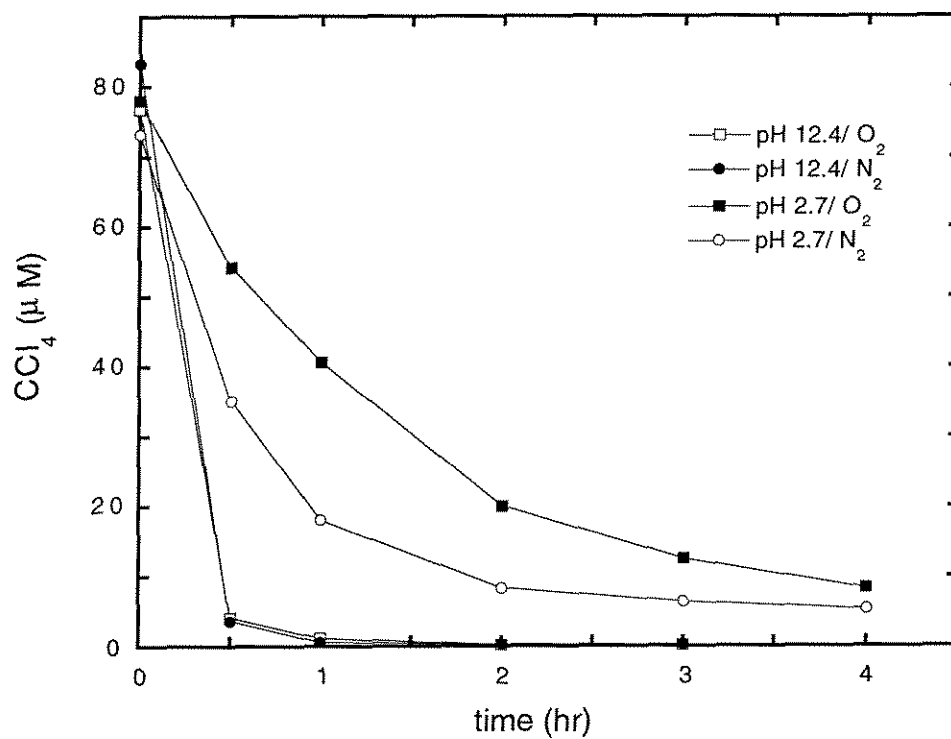


**Figure 8.**  $\text{CCl}_4$  degradation with *tert*-butanol (0.1 M) in the oxygenated and deoxygenated suspensions at both pH 2.7 and pH 12.4. The other conditions are the same with those of Fig. 6.

## Chapter 4

### Kinetics and Mechanism of CCl<sub>4</sub> Photoreductive Degradation on TiO<sub>2</sub>: The Role of Trichloromethyl Radical and Dichlorocarbene

[ The text of this chapter appears in: W. Choi and M.R. Hoffmann *Journal of Physical Chemistry* **1996**, *100*, 2161 - 2169.]

## Abstract

The mechanism of photoreduction of  $\text{CCl}_4$  on illuminated  $\text{TiO}_2$  surfaces was investigated by selectively trapping transient free radical intermediates. Dichlorocarbene and trichloromethyl radical were trapped with 2,3-dimethyl-2-butene during the photocatalytic degradation of  $\text{CCl}_4$ . The rate of formation of trapped  $:\text{CCl}_2$  and  $\cdot\text{CCl}_3$  was found to be a function of  $[\text{H}_2\text{O}]$ , pH,  $[\text{CCl}_4]$ , the nature of the dissolved gas, and light intensity. Dissolved oxygen was not essential for the degradation of  $\text{CCl}_4$ . The production rate of trapped dichlorocarbene showed light intensity dependencies of second, first, and half order with progressively increasing light intensity. A two-electron photoreductive pathway (via dichlorocarbene formation) was found to be the dominant mechanism leading to the full degradation of  $\text{CCl}_4$ . Since dichlorocarbene is hydrolyzed under basic conditions, the pH and water concentration were found to be integral parameters controlling the complete degradation of  $\text{CCl}_4$  to  $\text{CO}$ ,  $\text{CO}_2$ , and  $\text{HCl}$ . Kinetic equations describing the formation of trapped dichlorocarbene were derived from a proposed mechanism. The comparison of the predicted rate expression to the observed data suggested that the observed two-electron transfer occurred consecutively.

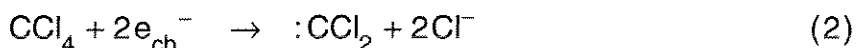
## Introduction

Semiconductor photocatalysis has been intensively studied and investigated for a wide variety of applications such as water splitting<sup>1</sup>, organic chemical synthesis<sup>2</sup>, metal recovery<sup>3</sup> and water and air treatment.<sup>4</sup> Among the wide band-gap semiconductors, TiO<sub>2</sub> is the most widely used due to its outstanding photostability.<sup>5</sup> In particular, its application to hazardous waste remediation has emerged as a viable technology.

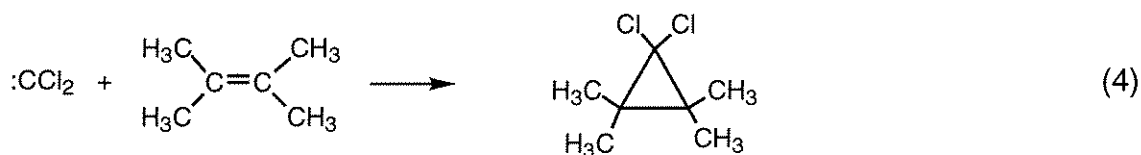
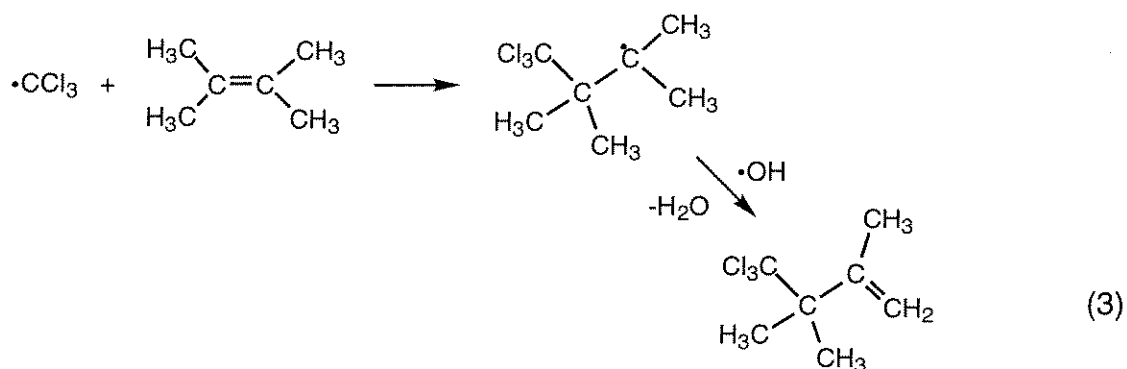
In colloidal TiO<sub>2</sub>, both the photogenerated electrons and holes are likely transferred to substrates at the solid/liquid interface.<sup>6</sup> While hole-transfer reactions (i.e., photooxidation) have been widely studied due to the strong oxidation potential ( $E^0 = +2.7$  V vs. NHE at pH 7) of the valence-band edge of TiO<sub>2</sub>, electron-transfer reactions have been investigated primarily as an auxiliary step to minimize charge-pair recombination. Not many studies on chemistry induced by photo-electron transfer on TiO<sub>2</sub> are found.<sup>6-10</sup>

Carbon tetrachloride degradation is initiated by a one-electron reduction step that may be followed by a series of oxidation or reduction steps. The degradation of CCl<sub>4</sub> has been studied using  $\gamma$ -ray radiolysis,<sup>11</sup> TiO<sub>2</sub> photocatalysis,<sup>7b</sup> sonolysis,<sup>12</sup> electrolysis,<sup>13-14</sup> and photolysis on MgO.<sup>15</sup> In addition, CCl<sub>4</sub> reduction is known to occur in aquatic environments in the presence of mineral surfaces<sup>16</sup> and on iron powders.<sup>17</sup> In a recent study,<sup>18</sup> we demonstrated that CCl<sub>4</sub> can be photochemically degraded through the mechanism involving photoreduction by conduction-band electrons in the presence of TiO<sub>2</sub> and suitable electron donors. Based upon the fact that CCl<sub>4</sub> was found to be fully degraded in the absence of dissolved oxygen,<sup>18</sup> we also suggested that the initial electron transfer process may involve both one- and

two-electron transfer reactions. The one-electron and two-electron steps result in the formation of trichloromethyl radical and dichlorocarbene as intermediates, respectively. Both pathways result in the release of chloride ions (dissociative electron capture).



In this study, we present direct evidence for competing one- and two-electron transfer steps to  $\text{CCl}_4$  by trapping the short-lived intermediates. The transient intermediates were trapped using 2,3-dimethyl-2-butene as follows:



The product of reaction 3,  $\text{C}_7\text{H}_{11}\text{Cl}_3$  (4,4,4-trichloro-2,3,3-trimethyl-1-butene) will be referred as "TCCI3" and that of reaction 4,  $\text{C}_7\text{H}_{12}\text{Cl}_2$  (1,1-dichloro-2,2,3,3-tetramethylcyclopropane) as "TCCI2". In this paper, we examine the kinetics of the formation of TCCI3 and TCCI2 and propose a mechanism for  $\text{CCl}_4$  photodegradation consistent with our kinetic observations.

## Experimental Section

Titanium dioxide (Degussa P25), which is a known mixture of 80% anatase and 20% rutile with an average particle size of 30 nm and a reactive surface area of  $\sim 50 \text{ m}^2/\text{g}$ , was used as a photocatalyst without further treatment.  $\text{TiO}_2$  concentrations were maintained at 0.5 g/L in all experiments. To explore the effects of dissolved gas (Fig. 4), the particle suspensions were bubbled with  $\text{O}_2$ , air and  $\text{N}_2$ , respectively, for 30 - 40 mins before addition of the trapping agent and  $\text{CCl}_4$ . The pH of the suspension was adjusted with 1 N  $\text{HClO}_4$  or 1 N  $\text{NaOH}$ .  $\text{CCl}_4$  (Baker) and 2,3-dimethyl-2-butene (Aldrich) were used as received.

Steady-state photolyses were performed with a 1000-W Xe arc lamp (Spindler and Hoyer). Light was filtered through a 10-cm IR water filter and a UV band pass filter (310 - 400 nm, Corning). The filtered light was focused onto a 35 mL quartz reactor cell loaded with  $\text{TiO}_2$  suspension. Head space above the suspension was minimized. Light intensity measurements were performed by chemical actinometry using (E)  $\alpha$ -(2,5-dimethyl-3-furylethylidene) (isopropylidene) succinic anhydride (Aberchrome 540).<sup>19</sup> The typical light intensity was  $\sim 1.4 \times 10^{-3} \text{ einstein L}^{-1} \text{ min}^{-1}$ . Two types of photolysis experiments were carried out. Detection of  $\text{TCCl}_3$  and  $\text{TCCl}_2$  was carried out in a water/acetonitrile mixture in order to increase the solubility of 2,3-dimethyl-2-butene (trap) and  $\text{CCl}_4$  up to 100 mM and 10 mM, respectively. Water concentrations were varied from 0 to 10 M. In order to investigate the degradation of  $\text{CCl}_4$ , photolyses were carried out in aqueous suspensions in the presence of methanol and 2-propanol (0.1 M) as electron donors. The desired concentrations of  $\text{CCl}_4$  in water were prepared by dilution of a saturated  $\text{CCl}_4$  stock solution (5.1 mM).

Sample aliquots were obtained with a 1 mL-syringe, filtered through a 0.45  $\mu\text{m}$ -nylon filter, and injected into a 2.5 mL glass vial with a PTFE/silicone septum-lined threaded cap.  $\text{CCl}_4$  and intermediates were extracted with 0.5 mL of pentane immediately after sampling. Sample vials were stored at 4  $^\circ\text{C}$  in the dark up to 48 hrs before analysis.  $\text{CCl}_4$  degradation, the formation of intermediates, and the formation of products were followed chromatographically with a Hewlett-Packard (HP) 5880A Gas Chromatograph equipped with a  $^{63}\text{Ni}$  electron capture detector and a HP-5 column (crosslinked 50% PhMe silicone, 25m x 0.32 mm x 1.05  $\mu\text{m}$ ). Nitrogen was used as the carrier gas. For the detection and identification of  $\text{TCCl}_3$  and  $\text{TCCl}_2$ , a HP 5890 II Gas Chromatograph with a HP-5 column serially connected to a HP 5965B Infrared Detector (IRD) and a HP 5972A Mass Selective Detector (MSD) was used. The carrier gas, in this case, was helium. The GCs were calibrated daily with external standards and duplicate measurements were made for each sample. The bottom aqueous phase (or water/acetonitrile phase) in the sampling vial was analyzed by ion-exchange chromatography (IC) for  $\text{Cl}^-$  ion. The IC system was a Dionex Bio-LC system equipped with a conductivity detector and a Dionex OmniPac PAX-500 column (8  $\mu\text{m}$ , 5 mm x 250 mm).

1,1-dichloro-2,2,3,3-tetramethylcyclopropane ( $\text{TCCl}_2$ ) was synthesized using the method of Doering and Henderson.<sup>20</sup> The product was a white powder having a melting range of 51.0 - 51.5  $^\circ\text{C}$ . No significant impurity was detected by GC/MS. Since authentic samples of 4,4,4-trichloro-2,3,3-trimethyl-1-butene ( $\text{TCCl}_3$ ) were not available, its quantification was prevented. However, analyses of mass and FTIR spectra provided sufficient information to identify the formation of  $\text{TCCl}_3$ . The formation of  $\text{TCCl}_2$  and  $\text{TCCl}_3$  was followed by monitoring mass

signals of  $m/e = 131$  and  $m/e = 165$ , respectively. These peaks represented fragment ions of the molecular ion less chlorine atom ( $m/e = M - 35$ ).

## Results

### Formation of TCCl<sub>2</sub> and TCCl<sub>3</sub> and Degradation of CCl<sub>4</sub>

The mass spectra of TCCl<sub>2</sub> and TCCl<sub>3</sub>, which were generated during the photolysis of CCl<sub>4</sub> in the presence of 2,3-dimethyl-2-butene (trap), are shown in Fig. 1. The molecular ion peak of TCCl<sub>2</sub> ( $m/e = 166$ ) was too weak to be detected at its in-situ concentration ( $< 5 \mu\text{M}$ ). However, the GC retention time and mass spectrum of TCCl<sub>2</sub> exactly matched those of the authentic compound. In the case of TCCl<sub>3</sub>, the relative intensity ratios of the chlorine isotope peaks at mass  $M$ ,  $M + 2$ , and  $M + 4$  were 3 : 3 : 1, which indicated that three chlorine atoms were contained in the molecular ion.<sup>21</sup> The presence of the terminal C=C double bond was confirmed by the FTIR spectrum which showed a C=C stretching vibration at  $1630 \text{ cm}^{-1}$  and olefinic C-H stretching vibration at  $3109 \text{ cm}^{-1}$ .

The production of TCCl<sub>2</sub> during photolysis was linear up to 30 min as shown in Fig. 2. TCCl<sub>3</sub> production showed a similar trend. Most of the data shown in this paper were reproducible within  $\pm 10\%$ . The production of trapped intermediates appeared to depend on  $[\text{H}_2\text{O}]$ . This effect is shown in Fig. 3. Production of both TCCl<sub>2</sub> and TCCl<sub>3</sub> increased with increasing water concentration up to 1M. However, further increases in the water concentration resulted in a reduced production of TCCl<sub>2</sub>, while TCCl<sub>3</sub> production continued to increase slowly. On the other hand, chloride production was found to be significant only in an excess of water (10 M). The production of Cl<sup>-</sup> at lower water concentrations ( $\leq 1 \text{ M}$ ) in Fig. 3 was negligible although the production of TCCl<sub>2</sub> and TCCl<sub>3</sub> was a clear indication of chloride production. The

corresponding chloride production to the formation of TCCl<sub>2</sub> at [H<sub>2</sub>O] = 1 M was ~7 μM. As for TCCl<sub>3</sub>, similar amount of chlorides were expected to be generated even though the concentration of TCCl<sub>3</sub> was not determined. Therefore, the total chloride production at [H<sub>2</sub>O] = 1 M may not exceed 20 μM, which is similar to *in-situ* chloride impurity concentration in the TiO<sub>2</sub> (Degussa P25) suspension. At such low [Cl<sup>-</sup>], titania surface can serve as buffer sites with retaining additional chlorides produced. Such a retention can be significant when the dielectric constant of the solution (mostly acetonitrile) is low.

Since dissolved O<sub>2</sub> is an alternative electron acceptor competing with CCl<sub>4</sub> and since it is known to react fast with ·CCl<sub>3</sub>, the effect of dissolved oxygen on the formation of TCCl<sub>2</sub> and TCCl<sub>3</sub> was investigated. In Fig. 4, the production of TCCl<sub>2</sub> and TCCl<sub>3</sub> in illuminated TiO<sub>2</sub> suspensions, which were sparged with nitrogen, air, and oxygen prior to photoirradiation, are compared. In the presence of O<sub>2</sub>, the apparent induction period increased with increasing [O<sub>2</sub>]. This trend is consistent with the effect of scavenging CB electrons by O<sub>2</sub>. The appearance of an induction period in the N<sub>2</sub>-saturated system can be attributed to surface adsorbed oxygen, which was not readily removed by purging alone. After the induction period, during which oxygen was consumed, the production rate of TCCl<sub>2</sub> and TCCl<sub>3</sub> in the O<sub>2</sub>-saturated system increased to the level of the oxygen-free system. In the case of TCCl<sub>2</sub> production, there was little difference between N<sub>2</sub>- and air-saturated solutions except for the initial induction period. However, TCCl<sub>3</sub> production in an air-saturated suspension was significantly delayed compared with its production in a N<sub>2</sub>-saturated suspension.

The influence of [CCl<sub>4</sub>]<sub>0</sub> on the production rates of TCCl<sub>2</sub> and TCCl<sub>3</sub> are compared for two different light intensities in Fig. 5. The production of TCCl<sub>2</sub> showed similar saturation behavior at both low (6.1 × 10<sup>-5</sup> einstein L<sup>-1</sup> min<sup>-1</sup>) and

high ( $1.4 \times 10^{-3}$  einstein  $L^{-1} \text{ min}^{-1}$ ) light intensities. However, the production rate of TCCl3 at the lower light intensity reached a saturation level sooner than the system at high light intensity. The solid lines are fits to a Langmuir-Hinshelwood equation ( $v = kK[\text{CCl}_4]/(1+K[\text{CCl}_4])$ ). The corresponding constants for TCCl2 are:  $k = 155.7 \text{ nM min}^{-1}$ ,  $K = 330 \text{ M}^{-1}$  for high light intensity and  $k = 11.2 \text{ nM min}^{-1}$ ,  $K = 200 \text{ M}^{-1}$  for low light intensity.

The production rates of TCCl2 are plotted as a function of light intensity in Fig. 6. Three distinct regions are apparent. Over a broad range, the light intensity dependence changes from  $v_{\text{TCCl}_2} \propto I^{2.0}$  ( $I < 1.6 \times 10^{-4}$  einstein  $L^{-1} \text{ min}^{-1}$ ), to  $v_{\text{TCCl}_2} \propto I^{1.0}$  ( $1.6 \times 10^{-4} < I < 3.5 \times 10^{-4}$  einstein  $L^{-1} \text{ min}^{-1}$ ), and finally to  $v_{\text{TCCl}_2} \propto I^{0.5}$  ( $I > 3.5 \times 10^{-4}$  einstein  $L^{-1} \text{ min}^{-1}$ ). The measured rates in the third region appear to deviate from the square-root dependence. This may be due to light scattering losses in the turbid suspension at higher light intensities. The average photon fluxes per particle at  $I = 1.6 \times 10^{-4}$  and  $3.5 \times 10^{-4}$  einstein  $L^{-1} \text{ min}^{-1}$  (or  $1.8 \times 10^{-6}$  and  $3.9 \times 10^{-6}$  einstein  $\text{cm}^{-2} \text{ min}^{-1}$ ) are 176 and 385 photons / particle-sec, respectively (assuming an average particle size of 30 nm).

Such transition light intensities seem to vary with the experimental conditions. In our previous study<sup>22</sup> using the same photocatalyst (Degussa P25, 0.5 g/L), the photodegradation of chloroform showed the light-intensity order transition at  $6.87 \times 10^{-5}$  einstein  $L^{-1} \text{ min}^{-1}$ . As for  $\text{Fe}^{3+}$ -doped (0.5 atom%) quantum-sized  $\text{TiO}_2$ ,<sup>6b</sup> the same photoreaction showed the transition at  $5.5 \times 10^{-4}$  einstein  $L^{-1} \text{ min}^{-1}$ . In an isopropanol photooxidation study using pure rutile powder (10 g/L), Egerton and King<sup>23a</sup> reported the light-intensity order changed from first-order to half-order at  $1.2 \times 10^{-5}$  einstein  $L^{-1} \text{ min}^{-1}$ . On the other hand, Okamoto et al.<sup>23b</sup> showed that the light-intensity dependence of phenol

photooxidation using anatase (2 g/L) changed from first-order to half-order around  $(1.7 \sim 3.4) \times 10^{-5}$  einstein  $L^{-1} \text{ min}^{-1}$ .

The light intensity dependencies of TCCI3 production were also measured (data not shown due to the undetermined TCCI3 concentration) and showed the similar behavior of second, first, and half order transition with increasing the light intensity. Even though the production of TCCI3 requires only 1 electron (unlike TCCI2 which needs 2 electrons), it needs a hydroxyl radical (a hole-equivalent) instead (reaction 3). Therefore, the overall process of TCCI3 production is equivalent to the two-electron transfer in terms of the total number of charge transfer, which makes its light-intensity dependence indistinguishable from that of TCCI2.

The formation of products and intermediates in  $\text{TiO}_2/\text{UV}$ -catalyzed reactions often show a strong pH dependence. In order to investigate the effects of pH, the production rates of TCCI2, TCCI3, and  $\text{Cl}^-$  were measured as a function of pH (Fig. 7). The absolute pH values of the suspensions were not given on the abscissa of Fig. 7 since the reaction medium was a mixture of water and acetonitrile in which the proton activity was not measured.<sup>24</sup> However, the  $\log [\text{OH}^-]_{\text{add}}$  can be used as a surrogate for pH. The production rate of TCCI2 showed a maximum at  $\log [\text{OH}^-]_{\text{add}} \sim -4$  while that of TCCI3 monotonously decreased with increasing base concentration. Both production rates dropped quickly above  $\log [\text{OH}^-]_{\text{add}} > -3.5$ . On the other hand, the chloride production rate, which provides a measure of total  $\text{CCl}_4$  degradation, showed an anticorrelation with the production rate of TCCI2. The pH-dependent behavior was also investigated in an aqueous solution of  $\text{CCl}_4$  (Fig. 8.), which were measured using a pH-stat titration technique.<sup>18,25</sup> This technique measured the consumption rate of the standard base (NaOH 0.10N) titrant which was added to

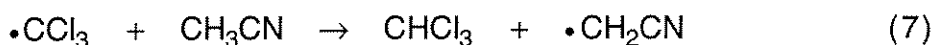
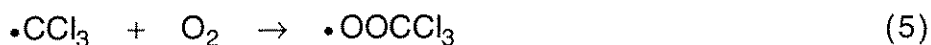
the reactor in order to maintain the pH of the system constant. The acid generation resulting from  $\text{CCl}_4$  degradation to  $\text{HCl}$ , which is equivalent to the base consumption during titration, can be considered as an indicator of  $\text{CCl}_4$  degradation. The acid generation rate showed a drastic increase above pH 10. This behavior is also seen for  $\text{Cl}^-$  production as shown in Fig. 7.

The product and intermediate analyses were also determined for photocatalytic  $\text{CCl}_4$  degradation in aqueous  $\text{TiO}_2$  suspensions at pH 2.7 (Fig. 9a) and pH 12.4 (Fig. 9b). At pH 2.7, intermediates such as  $\text{CHCl}_3$ ,  $\text{C}_2\text{Cl}_4$ , and  $\text{C}_2\text{Cl}_6$  were formed while no intermediates were detected at pH 12.4. The degradation of  $\text{CCl}_4$  was found to be much faster at pH 12.4 than at pH 2.7.

### ***Photochemical Mechanism of $\text{CCl}_4$ Degradation on $\text{TiO}_2$***

We propose a detailed mechanism of  $\text{CCl}_4$  photolysis in  $\text{TiO}_2$  suspension that is listed in Table I in order to interpret our results. The intermediate trap (2,3-dimethyl-2-butene) is symbolized "T"; DH indicates a suitable electron donor (i.e., trap, acetonitrile, alcohols) with abstractable hydrogen atoms. In this proposed mechanism, several assumptions are made: (i) adsorption equilibria for various intermediate species are omitted; (ii) only indirect hole transfers are considered; (iii) only recombination between free charge carriers is considered; (iv) the actual surficial reaction sites are not specified.<sup>26</sup> (For example, the bimolecular reaction of R23 can take place between two adsorbates (Hinshelwood-type) or between one adsorbate and the other in the solution (Rideal-type), or between both in the solution after desorption); (v) the degradation reaction of  $\text{TCCl}_2$  is not shown because it is negligible in the presence of excess hole scavengers such as the trap during the initial portions of the reaction.

In addition to the above assumptions, we have to keep in mind that the following reactions are in competition with reactions 3 and 4:



As a result of this competition, only a small fraction of  $\bullet\text{CCl}_3$  and  $:\text{CCl}_2$  generated during the photolysis was trapped effectively. The relative trapping efficiency was optimized by using a high concentration of 2,3-dimethyl-2-butene (e.g., 0.1 M).

### ***Kinetic Analysis of TCCl2 Formation***

From the mechanism of Table I, the observed TCCl2 production rate (Figs. 5 and 6) can be expressed as (R23)

$$\frac{d[\text{TCCl}_2]}{dt} = k_{R23}[:\text{CCl}_2][\text{T}]. \quad (10)$$

Since the initial rates of TCCl2 formation were measured after the induction period, reaction steps involving dissolved oxygen (R5 and R18) can be ignored. The reverse reaction of R12 is not considered because the chloride production is small during the initial period. Three different cases of electron transfers to  $\text{CCl}_4$  are treated separately: (i) sequential one-electron (free  $e_{cb}^-$ ) transfers (R7 and R9); (ii) a simultaneous two-electron (free  $e_{cb}^-$ ) transfer (R11); (iii) sequential one-electron (trapped electron,  $>\text{Ti}^{\text{III}}$ ) transfers (R8 and R10). The derived kinetic rate equations for each case under two extreme conditions of the low and high light intensities are summarized in Table II. We present the derivation of the

kinetic expression for TCCl<sub>2</sub> production for only Case (iii) since it represents the most complex mechanism.

The concentration of :CCl<sub>2</sub> during the photolysis can be assumed to be in steady-state according to eq 11:

$$k_{R12}[\text{CCl}_3^-] = k_{R23}[:\text{CCl}_2][\text{T}] + k_{R25}[:\text{CCl}_2][\text{H}_2\text{O}] + 2k_{R22}[:\text{CCl}_2]^2. \quad (11)$$

The term reflecting the bimolecular recombination of :CCl<sub>2</sub> is negligible relative to the other terms such that

$$[:\text{CCl}_2] = \frac{k_{R12}[\text{CCl}_3^-]}{k_{R23}[\text{T}] + k_{R25}[\text{H}_2\text{O}]} = k_a[\text{CCl}_3^-] \quad (12)$$

$$\text{where } k_a = \frac{k_{R12}}{k_{R23}[\text{T}] + k_{R25}[\text{H}_2\text{O}]}.$$

Similar steady-state analysis for [CCl<sub>3</sub><sup>-</sup>] yields:

$$\frac{d[\text{CCl}_3^-]}{dt} = k_{R10}[\cdot\text{CCl}_3][>\text{Ti}^{\text{III}}] - k_{-R10}[\text{CCl}_3^-] - k_{R12}[\text{CCl}_3^-] - k_{R21}[\text{CCl}_3^-][\text{H}^+] \approx 0$$

$$[\text{CCl}_3^-] = \frac{k_{R10}[\cdot\text{CCl}_3][>\text{Ti}^{\text{III}}]}{k_{-R10} + k_{R12} + k_{R21}[\text{H}^+]} = f_3([\text{H}^+])[\cdot\text{CCl}_3][>\text{Ti}^{\text{III}}] \quad (13)$$

$$\text{where } f_3([\text{H}^+]) = \frac{k_{R10}}{k_{-R10} + k_{R12} + k_{R21}[\text{H}^+]}.$$

The corresponding steady-state treatment for  $\cdot\text{CCl}_3$  yields

$$\frac{d[\cdot\text{CCl}_3]}{dt} = k_{R8}[\text{CCl}_{4,\text{ad}}][>\text{Ti}^{\text{III}}] - k_{R10}[\cdot\text{CCl}_3][>\text{Ti}^{\text{III}}] + k_{-R10}[\text{CCl}_3^-] \quad (14)$$

$$- 2k_{R16}[\cdot\text{CCl}_3]^2 - [\cdot\text{CCl}_3]\sum k_i[\text{S}_i] \approx 0$$

where  $k_i$  and  $\text{S}_i$  refer to the reactions that deplete  $\cdot\text{CCl}_3$  such as R17-19. Since the  $[\cdot\text{CCl}_3]^2$  term is negligible, we can rewrite eq 14 as

$$[\bullet\text{CCl}_3] = \frac{k_{R8}[\text{CCl}_{4,\text{ad}}][>\text{Ti}^{\text{III}}] + k_{R10}[\text{CCl}_3^-]}{k_{R10}[>\text{Ti}^{\text{III}}] + \sum k_i[\text{S}_i]} \quad (15)$$

When the back-reaction rate of R10 is slow compared to the rate of R8, eq 15 can be simplified to

$$[\bullet\text{CCl}_3] = \frac{k_{R8}[\text{CCl}_{4,\text{ad}}][>\text{Ti}^{\text{III}}]}{k_{R10}[>\text{Ti}^{\text{III}}] + \sum k_i[\text{S}_i]} \quad (16)$$

The trapped electron,  $>\text{Ti}^{\text{III}}$ , concentration is given by

$$\begin{aligned} \frac{d[>\text{Ti}^{\text{III}}]}{dt} = & k_{R6}[\text{Ti}^{\text{IV}}][e_{\text{cb}}^-] - k_{R6}[>\text{Ti}^{\text{III}}] - k_{R8}[\text{CCl}_{4,\text{ad}}][>\text{Ti}^{\text{III}}] \\ & - k_{R10}[\bullet\text{CCl}_3][>\text{Ti}^{\text{III}}] + k_{R10}[\text{CCl}_3^-] \approx 0 \end{aligned} \quad (17)$$

$$[>\text{Ti}^{\text{III}}] = \frac{k_{R6}[\text{Ti}^{\text{IV}}][e_{\text{cb}}^-] + k_{R10}[\text{CCl}_3^-]}{k_{R6} + k_{R8}[\text{CCl}_{4,\text{ad}}] + k_{R10}[\bullet\text{CCl}_3]} \quad (18)$$

The second term in the numerator of eq 18 can be neglected because the electron trapping reaction (R6) is very fast compared to the reverse reaction of R10.<sup>27</sup> The third term in the denominator of eq 18 is much smaller than the second term since the steady-state concentration of trichloromethyl radical should be much lower than the adsorbed  $\text{CCl}_4$  concentration. Therefore, eq 18 is reduced to

$$[>\text{Ti}^{\text{III}}] = \frac{k_{R6}[\text{Ti}^{\text{IV}}][e_{\text{cb}}^-]}{k_{R6} + k_{R8}[\text{CCl}_{4,\text{ad}}]} \quad (19)$$

The steady-state concentration of free charge-carriers under illumination can be related to the absorbed light intensity,  $I_{\text{abs}}$  as follows:<sup>26</sup>

$$\frac{d[h_{vb}^+]}{dt} = I_{abs} - k_{R13}[h_{vb}^+][H_2O] - k_{R15}[h_{vb}^+][e_{cb}^-] \approx 0 \quad (20)$$

$$I_{abs} = k_{R13}[e_{cb}^-][H_2O] + k_{R15}[e_{cb}^-]^2 \quad (\text{by assuming } [h_{vb}^+] \approx [e_{cb}^-]) \quad (21)$$

for low light intensities

$$[e_{cb}^-] = \frac{I_{abs}}{k_{R13}[H_2O]} = \frac{I_{abs}}{k'_{R13}} \quad (\text{where } k'_{R13} = k_{R13}[H_2O]) \quad (22)$$

and for high light intensities

$$[e_{cb}^-] = \left( \frac{I_{abs}}{k_{R15}} \right)^{1/2} \quad (23)$$

Combining eqs 10, 12, 13, 16, 19, 22, and 23 yields

for low light intensities:

$$\frac{d[TCCl_2]}{dt} = k_{3L} I_{abs}^2 \frac{\frac{k_{R8}}{k_{-R6}} [CCl_{4,ad}]}{\left( 1 + \frac{k_{R8}}{k_{-R6}} [CCl_{4,ad}] \right)^2} \quad (24)$$

$$\text{where } k_{3L} = \frac{k_a k_{R23} k_{R6}^2 f_3([H^+])}{k'_{R13}{}^2 k_{-R6} \sum k_i [S_i]} [Ti^{IV}]^2 [T]$$

and for high light intensities:

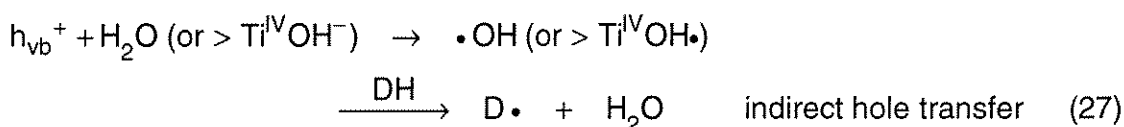
$$\frac{d[TCCl_2]}{dt} = k_{3H} I_{abs}^{1/2} \frac{\frac{k_{R8}}{k_{-R6}} [CCl_{4,ad}]}{\left( 1 + \frac{k_{R8}}{k_{-R6}} [CCl_{4,ad}] \right)} \quad (25)$$

$$\text{where } k_{3H} = \frac{k_a k_{R23} k_{R6} f_3([H^+])}{k_{R10} k_{R15}^{1/2}} [Ti^{IV}] [T].$$

## Discussion

From our experimental results, we conclude that both  $\cdot\text{CCl}_3$  and  $:\text{CCl}_2$  are formed via one- and two-electron reductions of  $\text{CCl}_4$  on illuminated  $\text{TiO}_2$  surfaces. Similar observations of distinct 1- and 2-electron pathways were made by Bahnemann et al.<sup>7a</sup> during the photoreduction of haloethane (2-bromo-2-chloro-1,1,1-trifluoroethane). However, they noted that the presence of surficial Pt deposits on the  $\text{TiO}_2$  was essential for the two-electron reduction pathway to occur.

The effect of water on the production rate of  $\text{TCCl}_2$  and  $\text{TCCl}_3$  (Fig. 3) can be interpreted in terms of the role of the hydroxyl radical in the hole scavenging mechanism. Efficient hole scavenging is essential for maximizing conduction-band electron transfer since most of photogenerated electrons in the colloidal  $\text{TiO}_2$  system recombine with holes. Two hole scavenging mechanisms are currently being discussed among researchers: direct and indirect hole transfers<sup>28,29</sup>

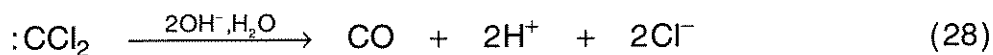


where D and DH represent electron donors. The trap (2,3-dimethyl-2-butene) can serve as an electron donor for both direct and indirect hole transfer. However, the data in Fig. 3 indicate that indirect hole transfer, which involves water molecules and surficial hydroxyl radicals, is a more efficient hole-scavenging pathway. Adding *t*-butanol or 2-propanol as additional hole scavengers had little effect on the production rate of  $\text{TCCl}_2$  and  $\text{TCCl}_3$ . Similar

conclusions, which were based on H-D kinetic isotope effects, were drawn previously.<sup>18,28</sup> When  $[\text{H}_2\text{O}] \geq 1 \text{ M}$ , the hole scavenging efficiency leveled off.

Since  $\text{Cl}^-$  production was negligible over the range of  $0.0 \text{ M} < [\text{H}_2\text{O}] < 1.0 \text{ M}$  in which the production of  $\text{TCCl}_2$  and  $\text{TCCl}_3$  was rapid (Fig.3), most of  $:\text{CCl}_2$  and  $\cdot\text{CCl}_3$  radicals were trapped with no further degradation. However, when  $[\text{H}_2\text{O}] = 10 \text{ M}$ , the  $[\text{Cl}^-]$  yield was  $200 \mu\text{M}$  which corresponded to  $\sim 50 \mu\text{M}$   $\text{CCl}_4$  degraded. This implies that  $\text{CCl}_4$  degradation is significant only with the presence of excess amount of water. The principal role of water in  $\text{CCl}_4$  degradation does not seem to be as a source of hydroxyl radicals since the hole-scavenging efficiency leveled off at  $[\text{H}_2\text{O}] \geq 1 \text{ M}$ . This indicates that the hydrolysis of the intermediate,  $:\text{CCl}_2$  may play a primary role in the complete degradation of  $\text{CCl}_4$ .

Dichlorocarbene is known to undergo hydrolysis (reaction 8) while trichloromethyl radical does not. The hydrolysis reaction of dichlorocarbene has been studied in detail by Robinson<sup>30</sup> who proposed the following mechanism:

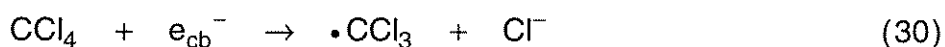


As  $[\text{H}_2\text{O}]$  increases, reaction 28 competes effectively with the trapping reaction 4. As a result, the  $[\text{TCCl}_2]$  decreased as  $[\text{H}_2\text{O}]$  increased from 1 M to 10 M while  $[\text{TCCl}_3]$  continued to increase (Fig. 3). The rapid increase in the  $\text{CCl}_4$  degradation rate at high pH, as shown in Figs. 7 and 8, can be attributed primarily to the base-catalyzed reaction of eq 28.

In our previous study,<sup>18</sup> we attributed the enhanced rate of  $\text{CCl}_4$  reduction at high pH solely to the larger thermodynamic driving force of CB electron

transfer to  $\text{CCl}_4$ , which is a result of normal Nernstian behavior. However, this study indicates a more complex process. Increasing TCCl2 production coincides with decreasing TCCl3 production at  $\log [\text{OH}^-]_{\text{add}} < -4.0$  (Fig. 7). In this region, total chloride production from reductive dechlorination and hydrolysis remains constant. The fate of  $\cdot\text{CCl}_3$  should be independent of pH. This implies that a larger thermodynamic driving force for CB electron transfer increasingly favors a two-electron transfer over an one-electron transfer to  $\text{CCl}_4$ . For the range of  $\log [\text{OH}^-]_{\text{add}} > -3.5$ , however, both the production of TCCl2 and TCCl3 rapidly decrease with a concurrent increase in total  $\text{Cl}^-$  production.

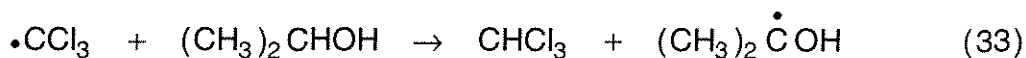
The two electron transfer represented by the reaction of eq 2 can be broken into several steps as follows:



Reaction of eq 32 has been shown to be the rate determining step in the basic hydrolysis of chloroform.<sup>31</sup> If the photogenerated dichlorocarbene is rapidly scavenged by reaction 28 at high pH, the equilibrium of reaction 32 shifts to the right side of the equation. Sequentially, so does that of reaction 31. As a result, we can expect more trichloromethyl radicals to lead to dichlorocarbene with increasing pH. However, we cannot expect TCCl2 production to increase continuously with pH, as is shown in Fig. 7, because the hydrolysis reaction (reaction 28) starts to compete with reaction 4. From the above argument, we can say that increasing pH has a dual effect on  $\text{CCl}_4$  degradation. One part of this effect is the shift in the CB electron potential to a more negative value according to a Nernstian behavior, which results in an increase in the electron-transfer rate and the other part is an increase in the rate of hydrolysis of

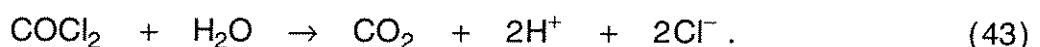
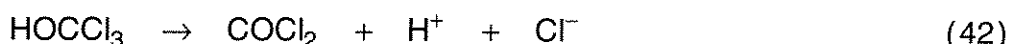
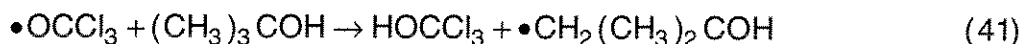
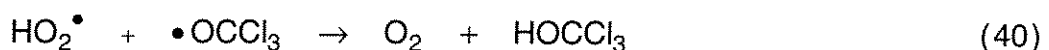
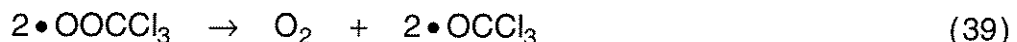
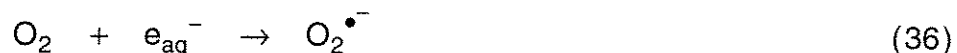
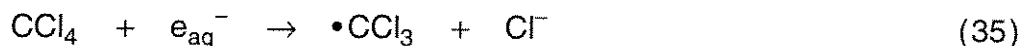
dichlorocarbene. This latter effect leads to the full degradation of  $\text{CCl}_4$  and favors dichlorocarbene formation over trichloromethyl radical formation by shifting the equilibria of reactions 31 and 32.

The relative effect of pH on intermediate formation (Fig. 9) is consistent with the data shown in Fig. 7. The intermediates are formed at pH 2.7, where both  $\text{TCCl}_2$  and  $\text{TCCl}_3$  are detected, but they are absent at pH 12.4, where neither  $\text{TCCl}_2$  nor  $\text{TCCl}_3$  are seen. Hexachloroethane ( $\text{C}_2\text{Cl}_6$ ) and perchloroethylene ( $\text{C}_2\text{Cl}_4$ ) are formed through the recombination of two trichloromethyl radicals (reaction 6) and two dichlorocarbenes (reaction 9), respectively. Chloroform ( $\text{CHCl}_3$ ) could be formed through two pathways:



Since all of the chlorinated intermediates were derived from either  $\text{:CCl}_2$  or  $\bullet\text{CCl}_3$ , their formation should be directly correlated with the formation of  $\text{TCCl}_2$  and  $\text{TCCl}_3$ . At pH 12.4, trapped conduction-band electron transfer to  $\text{CCl}_4$  seems to lead to the formation of dichlorocarbene, which is then rapidly hydrolyzed with little chance of recombination.

Oxygen also plays a dual role. It competes as an electron acceptor with  $\text{CCl}_4$  and it serves as a reactant (reaction 5), which is essential for the release of three  $\text{Cl}^-$  ions from trichloromethyl radical. The proposed mechanism for this pathway based on pulse radiolysis of  $\text{CCl}_4$  is as follows:<sup>11</sup>



Since the production of TCCl3 in the presence of air is retarded relative to TCCl2 (Fig. 4), we conclude that either  $\cdot\text{CCl}_3$  or the intermediate carbon centered radical in reaction 3 is scavenged by oxygen addition to some extent while  $\cdot\text{CCl}_2$  is not. Therefore, some of the  $\text{CCl}_4$  could be degraded completely by following reactions 35 - 43. However, reactions 35 - 43 do not seem to be the dominant pathway for  $\text{CCl}_4$  degradation in the UV/TiO<sub>2</sub> system for the following reasons: (i) carbon tetrachloride is fully degraded in the absence of dissolved oxygen; (ii) the total chloride production is significant only in the presence of excess water and at high pH; (iii) the relative distribution of the intermediates and their pH dependence can not be explained by a mechanism involving only the trichloromethyl radical. The two-electron transfer to  $\text{CCl}_4$  and the subsequent hydrolysis of dichlorocarbene seem to be a main path for  $\text{CCl}_4$  degradation in the UV/TiO<sub>2</sub> system.

The resulting kinetic expressions for Case (i) and (iii) (from Table II) predict the observed light intensity dependence of TCCl2 production: the production rate is proportional to  $I_{\text{abs}}^2$  at low light intensities and  $I_{\text{abs}}^{1/2}$  at high light intensities. However, Case (ii) which involves the simultaneous two-electron

transfer does not explain the square-root dependence of TCCl<sub>2</sub> production at high light intensities. Based on this analysis, CCl<sub>4</sub> appears to be reduced through sequential one-electron transfers instead of a simultaneous two-electron transfer.

The initial TCCl<sub>2</sub> production rates (Fig. 5a) show an apparent Langmuir-Hinshelwood type kinetics with respect to the initial CCl<sub>4</sub> concentration. Even though both Cases (i) and (iii) predict the observed light intensity dependence, they have different [CCl<sub>4</sub>] dependencies. Case (i) shows that the reaction rate will be proportional to [CCl<sub>4,ad</sub>] under both low and high light intensities. On the other hand, Case (iii) predicts that the concentration dependence should be different between the low and high light intensity conditions especially at higher CCl<sub>4</sub> concentrations. The production rates under the low-intensity irradiation should start to decrease at higher CCl<sub>4</sub> concentration according to Case (iii). This behavior can be rationalized in terms of the competition for limited trapped electrons between  $\cdot\text{CCl}_3$  and CCl<sub>4</sub>. However, the low intensity limit of Case (iii) is not consistent with the experimental observations (Fig. 5a) because we failed to see any significant difference in the concentration dependence between the low and high light intensity cases. However, we cannot rule out the possibility that Case (iii) is operative at high light intensities. We note that the high intensity limit of Case (iii) takes the typical form of Langmuir-Hinshelwood kinetics.

Based upon the above argument, we conclude that the reduction of CCl<sub>4</sub> proceeds through consecutive *free* electron transfers at low light intensities (Case (i)) and through the consecutive *trapped* or *free* electron transfers at high light intensities (Cases (i) and (iii)). Even though Rothenberger et al.<sup>27</sup> showed that the electron trapping was a very rapid process ( $\tau < 30$  ps) in colloidal (diameter 12nm) particles of TiO<sub>2</sub> in aqueous solution where there were no added electron

donors and acceptors, the *free* electron transfer at the interface could be possible in the present colloidal system which drastically differs from that of Rothenberger et al.. The photoinduced charge-transfer at the semiconductor/ liquid interface is strongly influenced by various parameters such as the colloid surface condition, the presence of electron donors and acceptors, and the size and the crystallinity of the semiconductor particle.<sup>27,32</sup> With excess amount of electron donors (traps) and acceptors (CCl<sub>4</sub> and O<sub>2</sub>) available on the surface, the interfacial *free* electron transfer may compete with the fast electron trapping at the surface site.

## Conclusions

Photoinduced electron transfer to CCl<sub>4</sub> on colloidal TiO<sub>2</sub> surfaces is shown to involve both one-electron and two-electron reduction pathways producing ·CCl<sub>3</sub> and :CCl<sub>2</sub>, respectively as intermediates. Even though both pathways lead to the degradation of CCl<sub>4</sub>, the two-electron reduction appears to be the principal pathway leading to the complete degradation. Since the two-electron pathway involves the formation of dichlorocarbene, which readily undergoes base-catalysed hydrolysis, pH is found to be a critical experimental variable that controls the rate of degradation of CCl<sub>4</sub>. At high pH, the degradation rate is greatly enhanced and no intermediates (e.g., C<sub>2</sub>Cl<sub>4</sub> and C<sub>2</sub>Cl<sub>6</sub>) are detected. The presence of water is essential for the degradation of CCl<sub>4</sub> because it provides an efficient hole scavenging pathway and because it is critical for the hydrolysis of dichlorocarbene. Comparing the results of a kinetic model derived from a proposed mechanism to the observed light-intensity dependence indicates that the two-electron transfer pathway is a consecutive electron-electron transfer and not a single 2-electron transfer. The mechanism of CCl<sub>4</sub> degradation proposed in this work may provide useful information for further studies of the photoreduction of perhalogenated organic compounds in TiO<sub>2</sub>/UV systems.

## **Acknowledgments**

Financial support from Advanced Research Projects Agency (ARPA) and the Office of Naval Research (ONR) {N0014-92-J-1901} under the auspices of the Department of Defense - University Research Initiative Program (DOD-URI) is gratefully acknowledged.

## References

- (1) Grätzel, M. *Acc. Chem. Res.* **1981**, *14*, 376.
- (2) Fox, M.A. *Acc. Chem. Res.* **1983**, *16*, 314.
- (3) (a) Borgarello, E.; Serpone, N.; Emo, G.; Harris, R.; Pelizzetti, E.; Minero, C. *Inorg. Chem.* **1986**, *25*, 4499. (b) Foster, N.S.; Noble, R.D.; Koval, C.A. *Environ. Sci. Technol.* **1993**, *27*, 350.
- (4) (a) Ollis, D.F.; Al-Ekabi, H., Eds. *Photocatalytic Purification and Treatment of Water and Air*, Elsevier: Amsterdam, 1993. (b) Hoffmann, M.R.; Martin, S.T.; Choi, W.; Bahnemann, D.W. *Chem. Rev.* **1995**, *95*, 69.
- (5) Frank, S.N.; Bard, A.J. *J. Phys. Chem.* **1977**, *81*, 1484.
- (6) (a) Choi, W.; Termin, A.; Hoffmann, M.R. *Angew. Chem. Int. Ed. Engl.* **1994**, *33*, 1091. (b) Choi, W.; Termin, A.; Hoffmann, M.R. *J. Phys. Chem.* **1994**, *98*, 13669.
- (7) (a) Bahnemann, D.W.; Mönig, J.; Chapman, R. *J. Phys. Chem.* **1987**, *91*, 3782. (b) Hilgendorff, M.; Hilgendorff, M.; Bahnemann, D.W. In *Environmental Aspects of Electrochemistry and Photoelectrochemistry*, Tomkiewicz, M., Haynes, R., Yoneyama, H., Hori, Y., Eds.; The Electrochemical Society: Pennington, 1993; pp 112-121.
- (8) Chemseddine, A.; Boehm, H.P. *J. Mol. Catal.* **1990**, *60*, 295.
- (9) Filby, W.G.; Mintas, M.; Güsten, H. *Ber. Bunsenges. Phys. Chem.* **1981**, *85*, 189.
- (10) Moser, J.; Grätzel, M. *J. Am. Chem. Soc.* **1983**, *105*, 6547.
- (11) (a) Asmus, K.-D.; Bahnemann, D.; Krischer, K.; Lal, M.; Mönig, J. *Life. Chem. Rep.* **1985**, *3*, 1. (b) Mönig, J.; Bahnemann, D.; Asmus, K.-D. *Chem.-Biol. Interactions* **1983**, *45*, 15. (c) Köster, R.; Asmus, K.-D. *Z. Naturforsch* **1971**, *26b*, 1104.

- (12) Bhatnagar, A.; Cheung, H.M. *Environ. Sci. Technol.* **1994**, *28*, 1481.
- (13) Criddle, C.S.; McCarty, P.L. *Environ. Sci. Technol.* **1991**, *25*, 973.
- (14) (a) Lambert, F.L.; Hasslinger, B.L.; Franz, R.N.,III *J. Electrochem. Soc.: Electrochem. Sci. Technol.* **1975**, *122*, 737. (b) Wawzonek, S.; Duty, R.C. *J. Electrochem. Soc.* **1961**, *108*, 1135. (c) Kolthoff, I.M.; Lee, T.S.; Stocesova, D.; Parry, E.P. *Anal. Chem.* **1950**, *22*, 521.
- (15) Zhou, X.-L.; Cowin, J.P. submitted to *J. Phys. Chem.*
- (16) (a) Kriegman-King, M.R.; Reinhard, M. *Environ. Sci. Technol.* **1992**, *26*, 2198. (b) Kriegman-King, M.R.; Reinhard, M. *Environ. Sci. Technol.* **1994**, *28*, 692. (c) Hooker, P.D.; Klabunde, K.J. *Environ. Sci. Technol.* **1994**, *28*, 1243.
- (17) Matheson, L.J.; Tratnyek, P.G. *Environ. Sci. Technol.* **1994**, *28*, 2045.
- (18) Choi, W.; Hoffmann, M.R. *Environ. Sci. Technol.* **1995**, *29*, 1646.
- (19) Heller, H.G.; Langan, J.R. *J. Chem. Soc. Perkin Trans.* **1981**, *2*, 341.
- (20) Doering, W.v.E.; Henderson, W.A., Jr. *J. Am. Chem. Soc.* **1958**, *80*, 5274.
- (21) Biemann, K. *Mass Spectrometry - Organic Chemical Applications*, McGraw Hill: New York, 1962.
- (22) Martin, S.T.; Herrmann, H.; Choi, W.; Hoffmann, M.R. *J. Chem. Soc., Faraday Trans.* **1994**, *90*, 3315.
- (23) (a) Egerton, T.A.; King, C.J. *J. Oil Col. Chem. Assoc.* **1979**, *62*, 386. (b) Okamoto, K.-I.; Yamamoto, Y.; Tanaka, H.; Itaya, A. *Bull. Chem. Soc. Jpn.* **1985**, *58*, 2023.
- (24) Westcott, C.C. *pH Measurements*, Academic Press: Orlando, 1978.
- (25) Kormann, C.; Bahnemann, D.W.; Hoffmann, M.R. *Environ. Sci. Technol.* **1991**, *25*, 494.
- (26) Turchi, C.S.; Ollis, D.F. *J. Catal.* **1990**, *122*, 178.
- (27) Rothenberger, G.; Moser, J.; Grätzel, M.; Serpone, N.; Sharma, D.K. *J. Am. Chem. Soc.* **1985**, *107*, 8054.

- (28) Cunningham, J.; Srijaranai, S. *J. Photochem. Photobiol. A.: Chem.* **1988**, *43*, 329.
- (29) Stafford, U.; Gray, K.A.; Kamat, P.V. *J. Phys. Chem.* **1994**, *98*, 6343.
- (30) Robinson, E.A. *J. Chem. Soc.* **1961**, 1663.
- (31) Kirmse, W. *Organic Chemistry - A Series of Monographs Vol. 1 Carbene Chemistry*, Academic Press: New York, 1964.
- (32) Frei, H.; Fitzmaurice, D.J.; Grätzel, M. *Langmuir* **1990**, *6*, 198.

**Table I.** Elementary Reaction Steps of CCl<sub>4</sub> Photolysis in UV-Irradiated TiO<sub>2</sub>.

Photoexcitation	$\text{TiO}_2 \xrightarrow{h\nu} e_{\text{cb}}^- + h_{\text{vb}}^+$	R1
Adsorption	$\text{CCl}_4 + >S (\text{surface site}) \leftrightarrow \text{CCl}_{4,\text{ad}}$	R2
	$\text{O}_2 + >S \leftrightarrow \text{O}_{2,\text{ad}}$	R3
	$\text{T} + >S \leftrightarrow \text{T}_{\text{ad}}$	R4
Electron transfer	$\text{O}_{2,\text{ad}} + e_{\text{cb}}^- \leftrightarrow \text{O}_2^-$	R5
	$>\text{Ti}^{\text{IV}} + e_{\text{cb}}^- \leftrightarrow >\text{Ti}^{\text{III}} (\equiv e_{\text{tr}}^-)$	R6
	$\text{CCl}_{4,\text{ad}} + e_{\text{cb}}^- \rightarrow \cdot\text{CCl}_3 + \text{Cl}^-$	R7
	$\text{CCl}_{4,\text{ad}} + >\text{Ti}^{\text{III}} \rightarrow \cdot\text{CCl}_3 + \text{Cl}^-$	R8
	$\cdot\text{CCl}_3 + e_{\text{cb}}^- \leftrightarrow \text{CCl}_3^-$	R9
	$\cdot\text{CCl}_3 + >\text{Ti}^{\text{III}} \leftrightarrow \text{CCl}_3^-$	R10
	$\text{CCl}_{4,\text{ad}} + 2e_{\text{cb}}^- \rightarrow \text{CCl}_3^- + \text{Cl}^-$	R11
	$\text{CCl}_3^- \leftrightarrow \text{:CCl}_2 + \text{Cl}^-$	R12
Hole transfer	$h_{\text{vb}}^+ + \text{H}_2\text{O} (\text{or } >\text{TiOH}) \rightarrow \cdot\text{OH} (\text{or } >\text{TiOH}\cdot) + \text{H}^+$	R13
	$\cdot\text{OH} + \text{DH} \rightarrow \text{D}\cdot + \text{H}_2\text{O}$	R14
Recombination	$e_{\text{cb}}^- + h_{\text{vb}}^+ \rightarrow \text{TiO}_2$	R15
Intermediate and product formation	$2\cdot\text{CCl}_3 \rightarrow \text{C}_2\text{Cl}_6$	R16
	$\cdot\text{CCl}_3 + \text{DH} \rightarrow \text{CHCl}_3 + \text{D}\cdot$	R17
	$\cdot\text{CCl}_3 + \text{O}_2 \rightarrow \cdot\text{OCCl}_3$	R18
	$\cdot\text{CCl}_3 + \text{T} \rightarrow \cdot\text{TCCl}_3$	R19
	$\cdot\text{TCCl}_3 + \cdot\text{OH} \rightarrow \text{TCCl}_3 + \text{H}_2\text{O}$	R20
	$\text{CCl}_3^- + \text{H}^+ \rightarrow \text{CHCl}_3$	R21
	$2\text{:CCl}_2 \rightarrow \text{C}_2\text{Cl}_4$	R22
	$\text{:CCl}_2 + \text{T} \rightarrow \text{TCCl}_2$	R23
	$\cdot\text{OCCl}_3 \rightarrow \text{CO}_2 + 3\text{Cl}^-$	R24
	$\text{:CCl}_2 + \text{H}_2\text{O}/\text{OH}^- \rightarrow \text{CO} + 2\text{HCl}$	R25
	$\text{CO} + \text{OH}^- \rightarrow \text{HCOO}^-$	R26
$\text{HCOO}^- + \cdot\text{OH} \rightarrow \text{CO}_2$	R27	

**Table II.** Kinetic Rate Equations of TCCl<sub>2</sub> Production for Three Different Cases of Electron Transfers to CCl<sub>4</sub>.

Cases	d[TCCl <sub>2</sub> ]/dt	
	low light intensities	high light intensities
I. CCl <sub>4,ad</sub> + e <sub>cb</sub> <sup>-</sup> •CCl <sub>3</sub> + e <sub>cb</sub> <sup>-</sup>	$k_{1L} I_{\text{abs}}^2 [\text{CCl}_{4,\text{ad}}]$ where $k_{1L} = \frac{k_a k_{R23} k_{R7} f_1 ([\text{H}^+])^a}{k'_{R13} \sum k_i [S_i]} [\text{T}]$	$k_{1H} I_{\text{abs}}^{1/2} [\text{CCl}_{4,\text{ad}}]$ where $k_{1H} = \frac{k_a k_{R23} k_{R7} f_1 ([\text{H}^+])}{k_{R9} k_{R15}^{1/2}} [\text{T}]$
II. CCl <sub>4,ad</sub> + 2e <sub>cb</sub> <sup>-</sup>	$k_{2L} I_{\text{abs}}^2 [\text{CCl}_{4,\text{ad}}]$ where $k_{2L} = \frac{k_a k_{R23} f_2 ([\text{H}^+])^b}{k'_{R13} \sum k_i [S_i]} [\text{T}]$	$k_{2H} I_{\text{abs}} [\text{CCl}_{4,\text{ad}}]$ where $k_{2H} = \frac{k_a k_{R23} f_2 ([\text{H}^+])}{k_{R15}} [\text{T}]$
III. CCl <sub>4,ad</sub> + > Ti <sup>III</sup> •CCl <sub>3</sub> + > Ti <sup>III</sup>	$k_{3L} I_{\text{abs}}^2 \frac{\frac{k_{R8}}{k_{-R6}} [\text{CCl}_{4,\text{ad}}]}{\left(1 + \frac{k_{R8}}{k_{-R6}} [\text{CCl}_{4,\text{ad}}]\right)^2}$ where $k_{3L} = \frac{k_a k_{R23} k_{R6}^2 f_3 ([\text{H}^+])^c}{k'_{R13} \sum k_i [S_i]} [\text{Ti}^{\text{IV}}]^2 [\text{T}]$	$k_{3H} I_{\text{abs}}^{1/2} \frac{\frac{k_{R8}}{k_{-R6}} [\text{CCl}_{4,\text{ad}}]}{\left(1 + \frac{k_{R8}}{k_{-R6}} [\text{CCl}_{4,\text{ad}}]\right)}$ where $k_{3H} = \frac{k_a k_{R23} k_{R6} f_3 ([\text{H}^+])}{k_{R10} k_{R15}^{1/2}} [\text{Ti}^{\text{IV}}] [\text{T}]$

$${}^a f_1 ([\text{H}^+]) = \frac{k_{R9}}{k_{-R9} + k_{R12} + k_{R21} [\text{H}^+]} \cdot {}^b f_2 ([\text{H}^+]) = \frac{k_{R11}}{k_{-R9} + k_{R12} + k_{R21} [\text{H}^+]}$$

$${}^c f_3 ([\text{H}^+]) = \frac{k_{R10}}{k_{-R10} + k_{R12} + k_{R21} [\text{H}^+]}$$

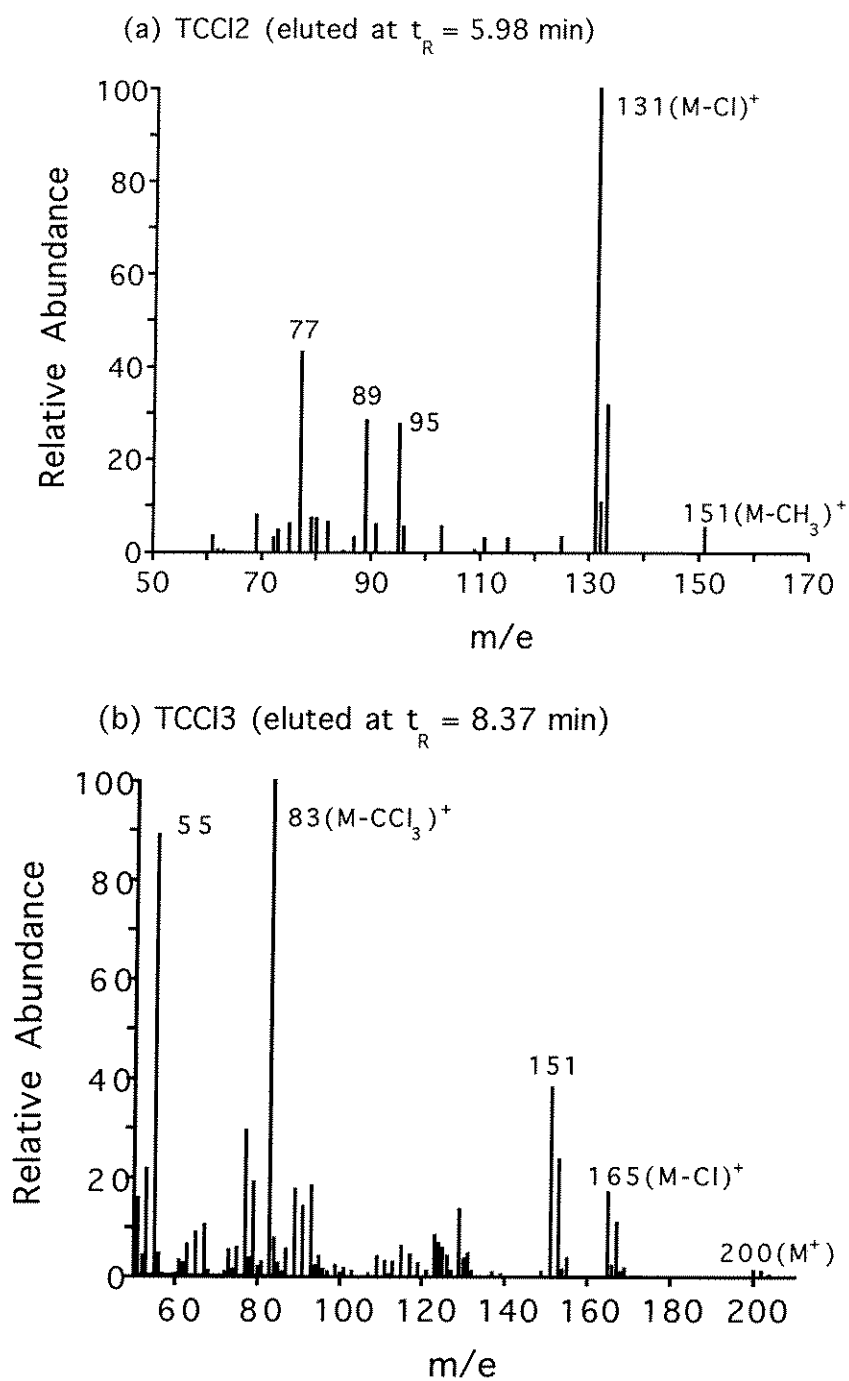


**Figure 1.** Mass spectra (extracted from a GC total ion chromatogram) of (a) TCCI2 and (b) TCCI3 which were generated during the  $CCl_4$  photolysis in the presence of  $TiO_2$  and traps. The mass signal intensities were normalized.

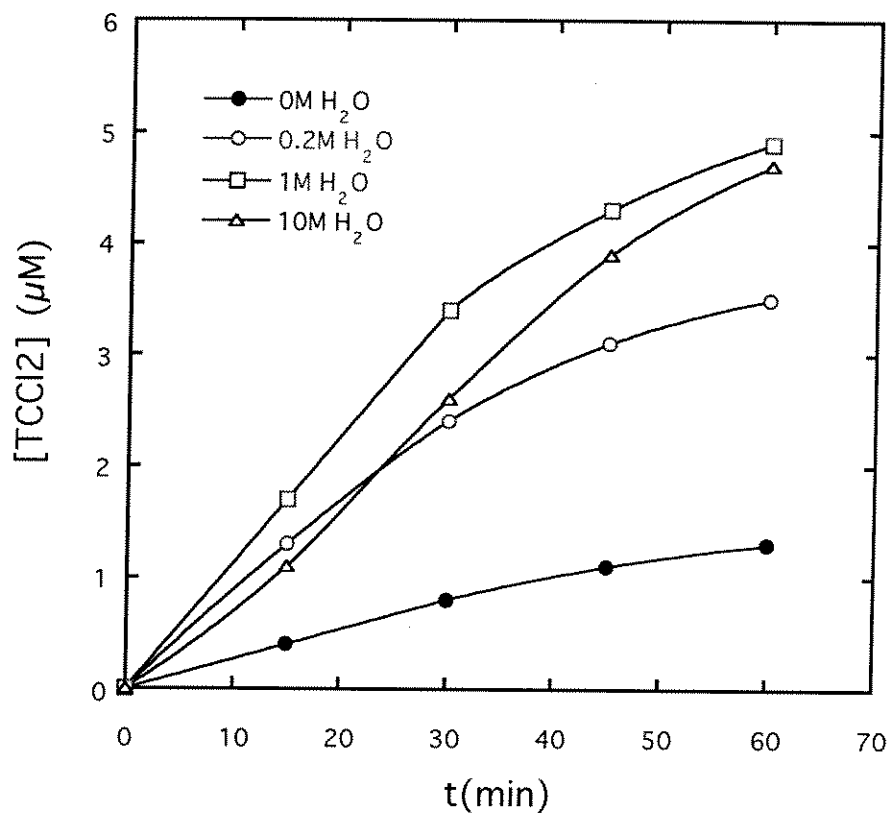


**Figure 2.** The time-dependent production of TCCl<sub>2</sub> during the photolysis with varying amount of water (0, 0.2, 1, and 10 M). The experimental conditions were: [CCl<sub>4</sub>]<sub>0</sub> = 5 mM, [TiO<sub>2</sub>] = 0.5 g L<sup>-1</sup>, I = 1.43 × 10<sup>-3</sup> einstein L<sup>-1</sup> min<sup>-1</sup> (310 < λ < 400 nm), [Trap] = 0.1 M, air-equilibration, and no pH adjustment.

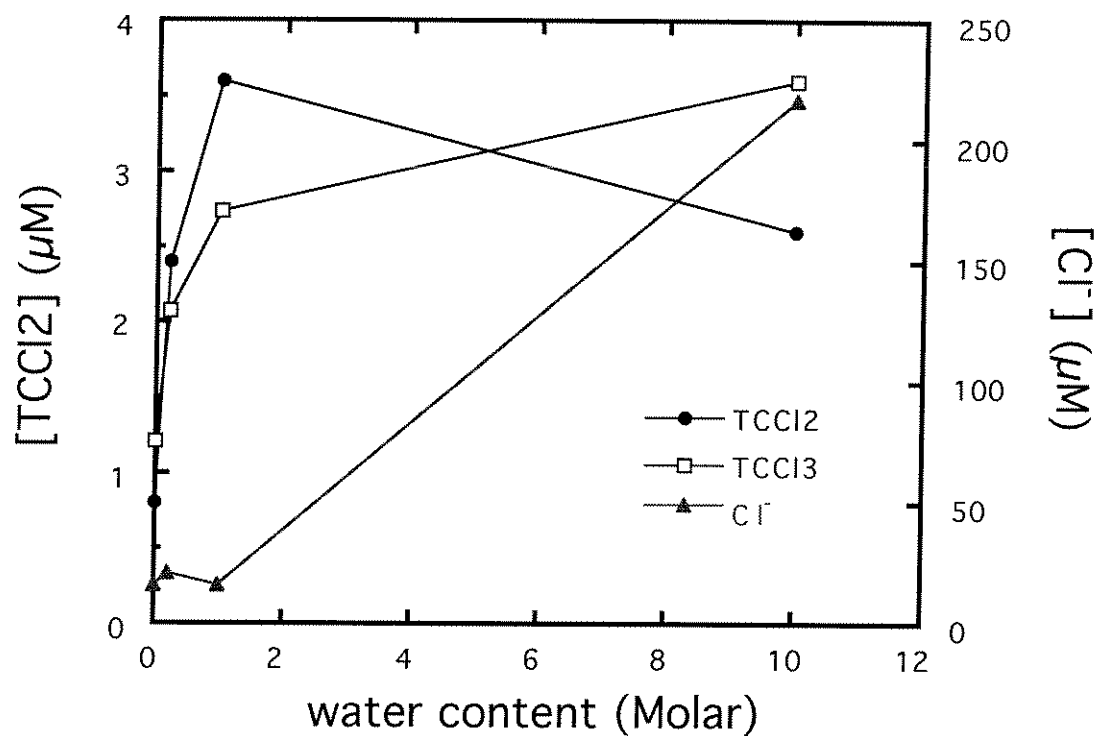


**Figure 3.** The comparison of the production of TCCl<sub>2</sub>, TCCl<sub>3</sub>, and chloride after 30 min irradiation as a function of water concentration in TiO<sub>2</sub> suspension. Other experimental conditions were the same to those of Fig. 2. The concentration of TCCl<sub>3</sub> was not determined.

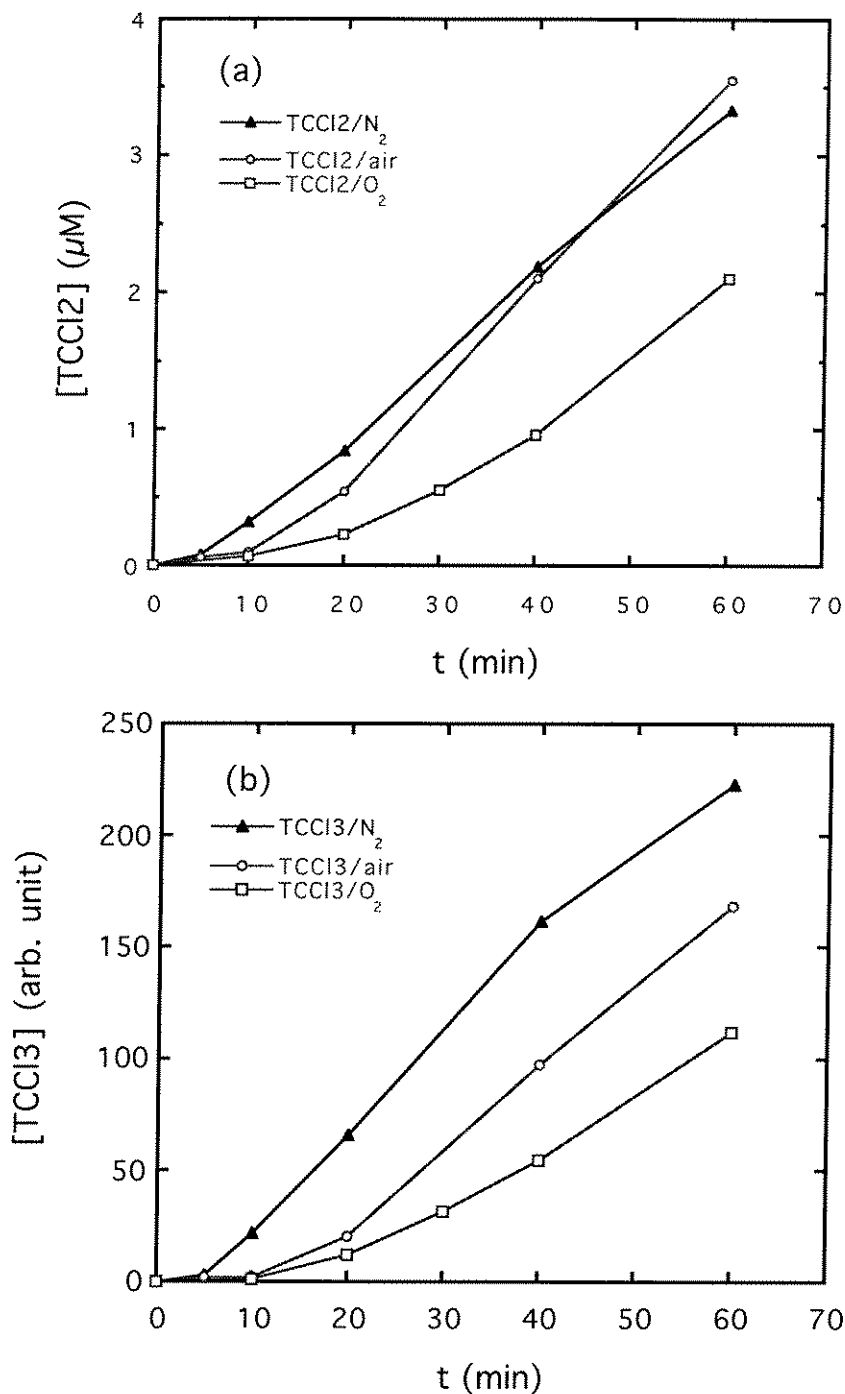


**Figure 4.** The productions of (a) TCCI2 and (b) TCCI3 as a function of irradiation time in TiO<sub>2</sub> suspensions saturated with N<sub>2</sub>, air, and O<sub>2</sub> gases before irradiation. Water concentration was 10 molar and other experimental conditions were the same to those of Fig. 2.

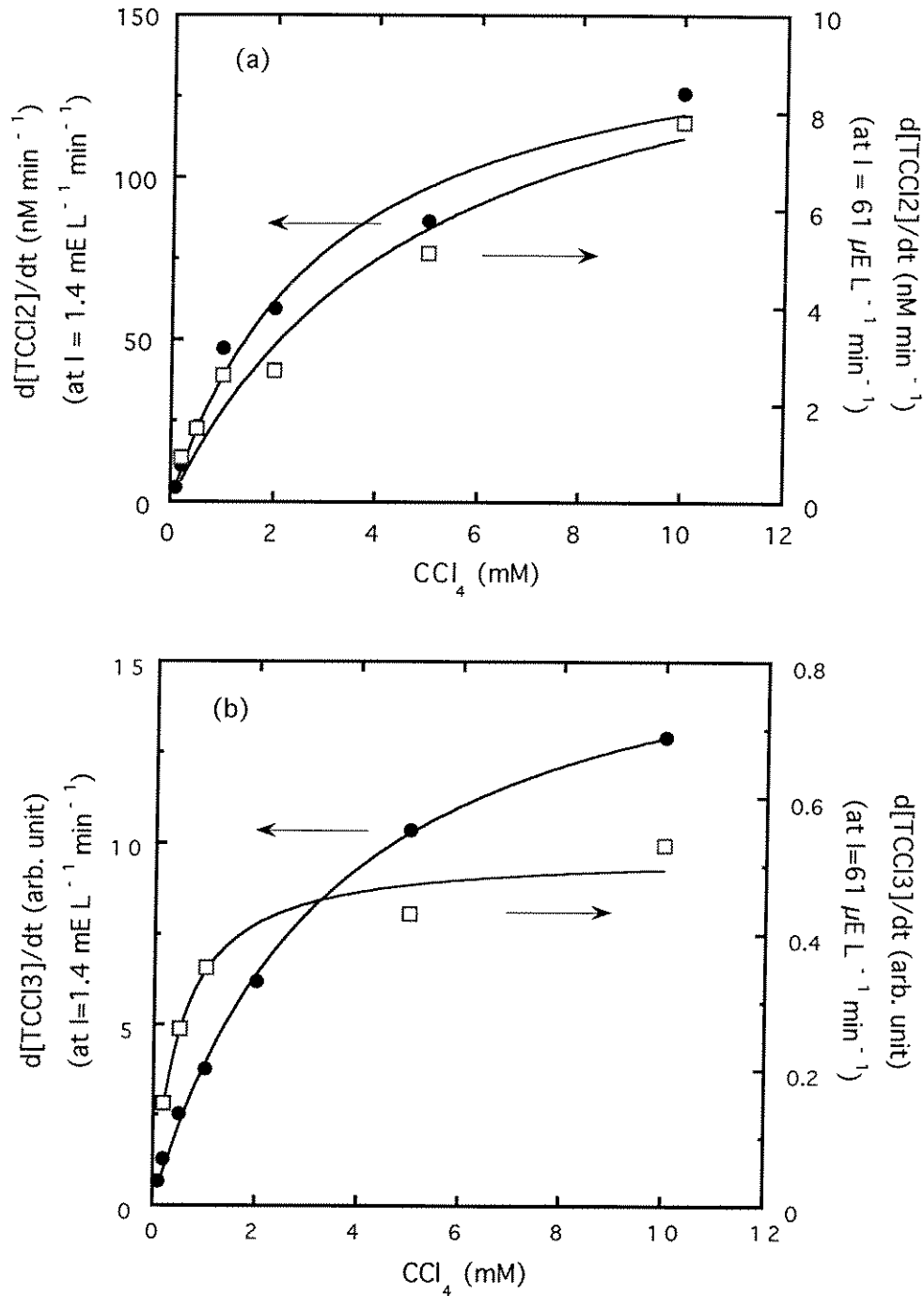


**Figure 5.** The production of (a) TCCl<sub>2</sub> and (b) TCCl<sub>3</sub> as a function of initial CCl<sub>4</sub> concentration. The concentration dependences are compared at two different light intensities (1.4 mE L<sup>-1</sup> min<sup>-1</sup> vs. 61 μE L<sup>-1</sup> min<sup>-1</sup>). Water concentration was 10 molar and other experimental conditions were the same to those of Fig. 2.

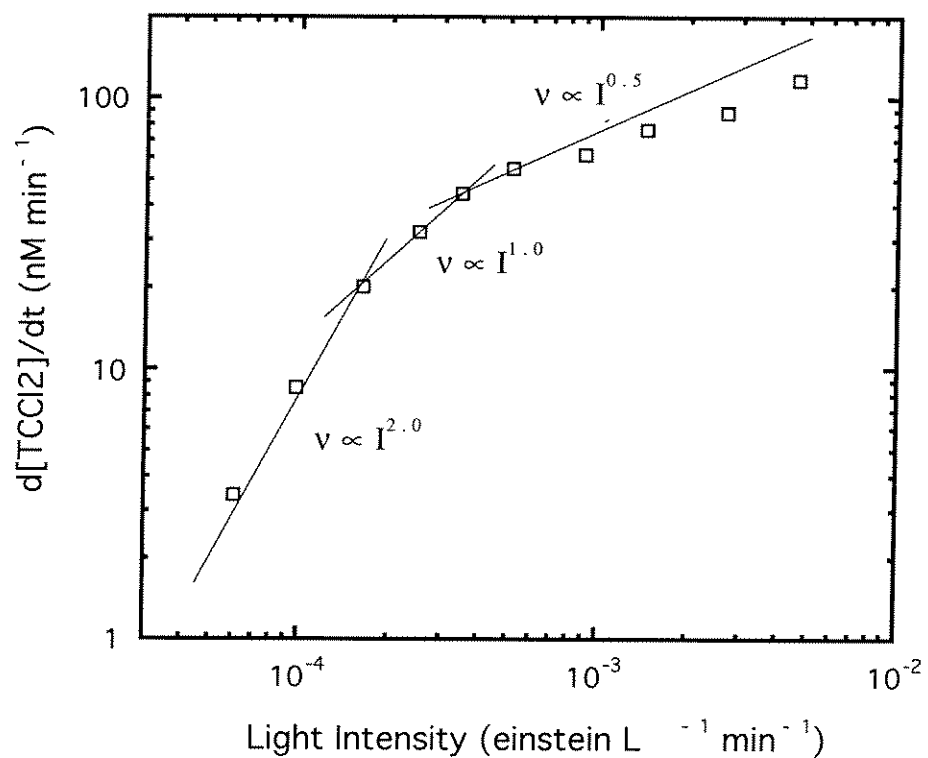


**Figure 6.** Light intensity dependence of TCCI2 production rate under the same experimental conditions of Fig. 2. Water concentration was 10 molar. The solid lines represent the light-intensity dependence of  $I^{2.0}$ ,  $I^{1.0}$ , and  $I^{0.5}$ , respectively.

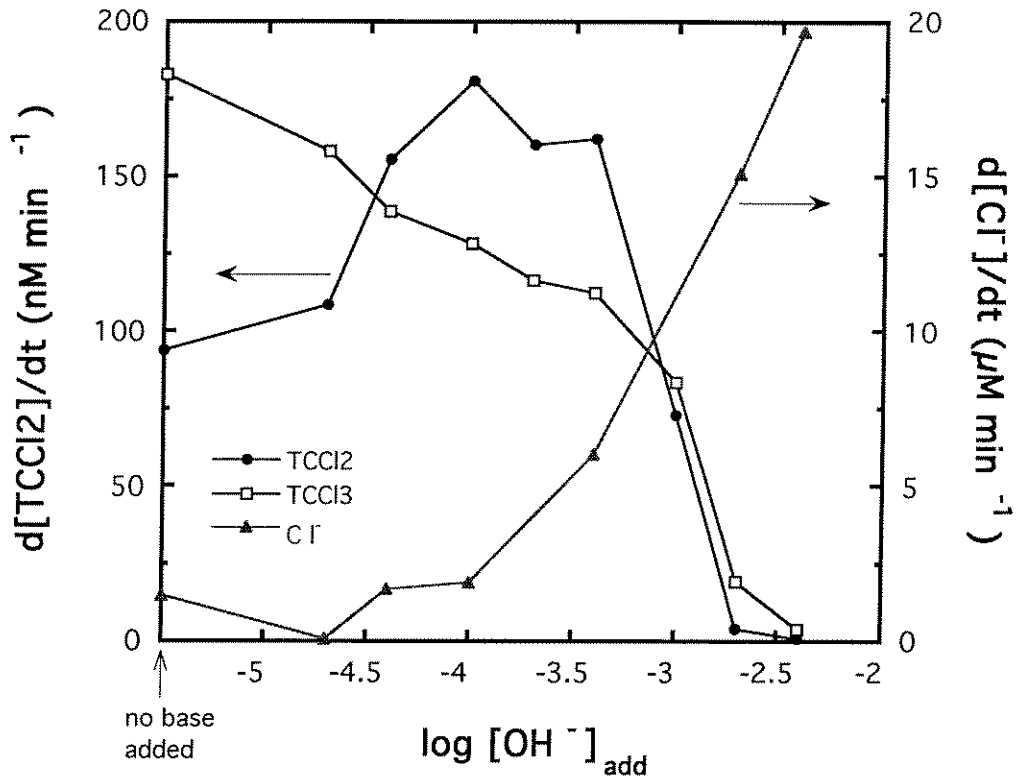


**Figure 7.** The pH (relative scale) dependence of the production rate of TCCl<sub>2</sub>, TCCl<sub>3</sub>, and chloride in the TiO<sub>2</sub> suspension having the same condition of Fig. 2. Water concentration was 10 molar. The production rate of TCCl<sub>3</sub> is relative.

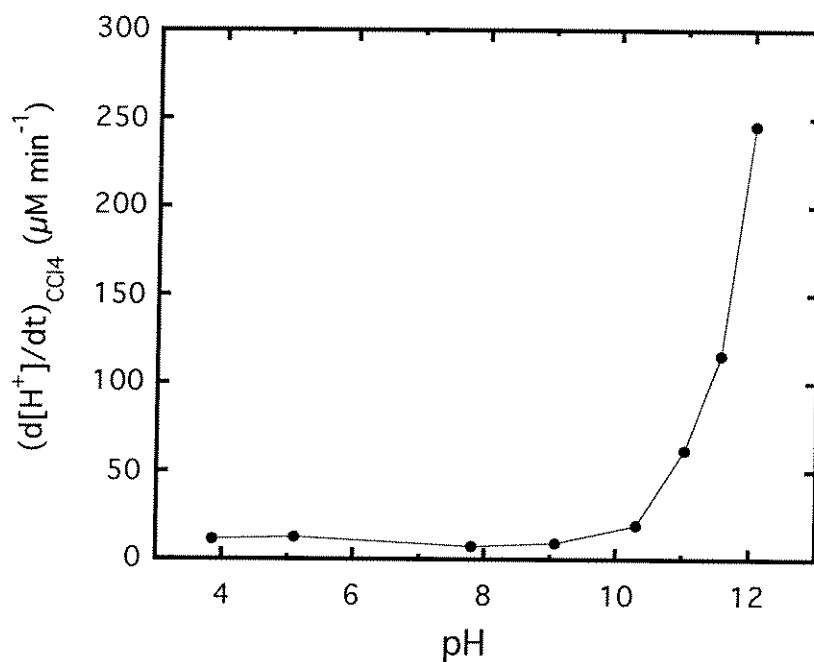


**Figure 8.** The pH dependence of  $\text{CCl}_4$  degradation, which were measured by monitoring the acid generation rate, in an aqueous  $\text{TiO}_2$  suspension where  $[\text{CCl}_4]_0 = 5.1 \text{ mM}$ ,  $[\text{TiO}_2] = 0.5 \text{ g L}^{-1}$ ,  $I = 2.1 \times 10^{-4} \text{ einstein L}^{-1} \text{ min}^{-1}$  ( $\lambda = 320 \pm 10 \text{ nm}$ ),  $[\text{CH}_3\text{OH}] = 0.1 \text{ M}$ , and air-equilibration.

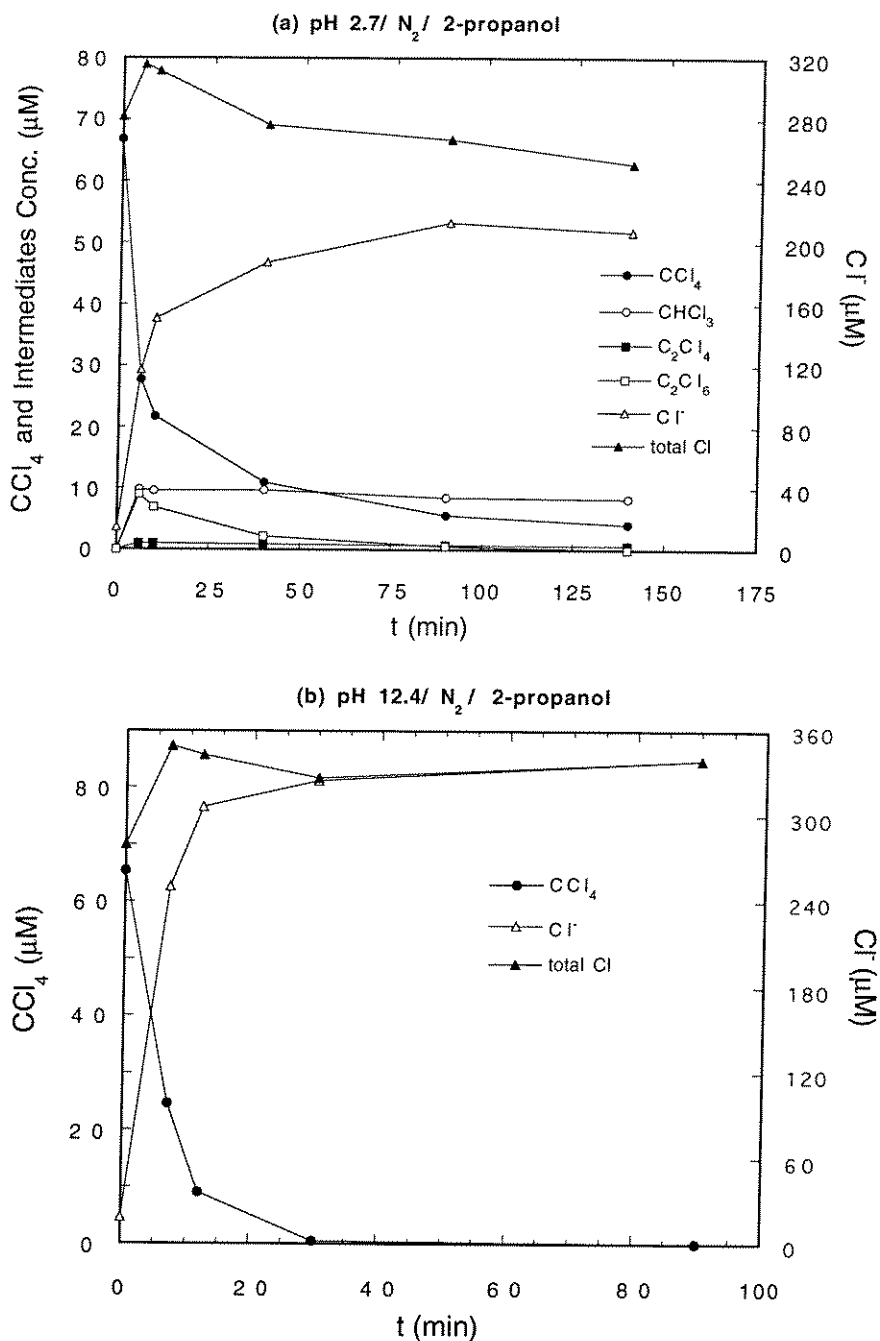


**Figure 9.** The degradation of  $\text{CCl}_4$  and the production of intermediates and chloride in an aqueous  $\text{TiO}_2$  suspension at (a) pH 2.7 and (b) pH 12.4. Other experimental conditions were  $[\text{TiO}_2] = 0.5 \text{ g L}^{-1}$ ,  $I = 1.46 \times 10^{-3} \text{ einstein L}^{-1} \text{ min}^{-1}$  ( $310 < \lambda < 400 \text{ nm}$ ),  $[(\text{CH}_3)_2\text{CHOH}] = 0.1 \text{ M}$ , and  $\text{N}_2$  saturation prior to light illumination.

## Chapter 5

A Novel Photocatalytic Mechanism for  $\text{CHCl}_3$  and  $\text{CHBr}_3$  Degradation  
and the Fate of Photogenerated Trihalomethyl Radicals on  $\text{TiO}_2$

[ The text of this chapter has been submitted to *Environmental Science & Technology* (W. Choi and M.R. Hoffmann) in February, **1996**.]

## Abstract

The photocatalytic degradation of  $\text{CHCl}_3$ ,  $\text{CHBr}_3$ ,  $\text{CCl}_4$ , and  $\text{CCl}_3\text{CO}_2^-$  is investigated in aqueous  $\text{TiO}_2$  suspensions. A common intermediate, the trihalomethyl radical, is involved in the degradation of each substrate except for  $\text{CCl}_3\text{CO}_2^-$ .  $\text{CHCl}_3$  and  $\text{CHBr}_3$  are degraded into carbon monoxide and halide ions in the absence of dissolved oxygen. The anoxic degradation proceeds through a dihalocarbene intermediate, which is produced by sequential reactions of the haloform molecule with a valence band hole and a conduction band electron. Carbon dioxide and halide ion are formed as the primary products during  $\text{CHCl}_3$  degradation in the presence of oxygen. Under these conditions, the trihalomethyl radicals react rapidly with dioxygen. At  $\text{pH} > 11$ , degradation of the haloforms is enhanced dramatically. This enhancement is ascribed to "*photoenhanced hydrolysis*". The secondary reactions of the trichloromethyl radical generated during  $\text{CCl}_4$  photolysis is strongly influenced by the nature of the electron donors. Both  $\bullet\text{CCl}_3$  and  $\text{Cl}^-$  production increase substantially when 2-propanol is present as an electron donor. A new photocatalytic mechanism for  $\text{CCl}_3\text{CO}_2^-$  degradation, which involves the formation of a dichlorocarbene intermediate, is proposed.

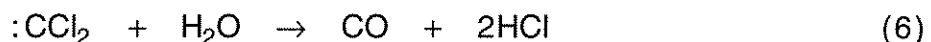
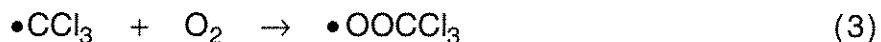
## Introduction

Halogenated organic compounds are the most frequent and important chemical contaminants in a wide range of environments. In addition, their general toxicity raises serious concerns about their impacts on human health. The degradation of halogenated compounds is known to proceed through a series of free radical reactions. TiO<sub>2</sub> photocatalysis, which has been demonstrated to be effective for mineralization of a variety of organic compounds,<sup>1-3</sup> involves the production of free radicals on the illuminated TiO<sub>2</sub> surface. However, our knowledge about the fate of carbon-centered radicals generated during photocatalysis is far from complete.

The reaction mechanisms in heterogeneous radical chemistry are often different from their homogeneous counterparts due to the influence of the solid surface.<sup>4</sup> However, many suggested mechanisms for photocatalytic reactions are inferred from well-documented homogeneous reactions. Previous studies<sup>5,6</sup> proposed a photocatalytic mechanism for CHCl<sub>3</sub> degradation, which was based on the reaction of trichloromethyl peroxy radical (Cl<sub>3</sub>COO•) whose chemistry was well understood from homogeneous radiolysis.<sup>7-10</sup> Trichloromethyl radicals in oxygenated aqueous solutions react rapidly with dioxygen (*vide infra*, eq 3) at a rate near the diffusion limit ( $k = 3.3 \times 10^9 \text{ M}^{-1}\text{s}^{-1}$ ).<sup>10</sup>

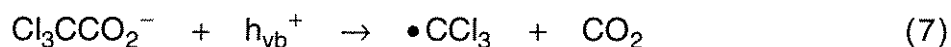
Our recent studies<sup>11,12</sup> on the photocatalytic reduction of CCl<sub>4</sub>, however, demonstrated that •CCl<sub>3</sub> on the TiO<sub>2</sub> surface could react not only with an oxygen molecule but also directly with a conduction-band electron (eq 4). The •CCl<sub>3</sub> radical can be formed on TiO<sub>2</sub> surface via CHCl<sub>3</sub> oxidation through valence band (VB) hole transfer (eq 1) or from CCl<sub>4</sub> reduction through conduction band (CB)

electron transfer (eq 2). The subsequent reactions of  $\bullet\text{CCl}_3$  should follow similar pathways in both systems.



The above argument opens up the possibility for recognition of a new  $\text{CHCl}_3$  degradation pathway, in which there is a redox-mediated short circuiting of the VB holes and CB electrons. The new pathway could make the photocatalytic degradation of  $\text{CHCl}_3$  possible in the absence of dissolved oxygen by producing CO instead of  $\text{CO}_2$  as a final product (eq 6).

In order to test the possibility of the alternative mechanism (eqs 1, 4, and 6), the photocatalytic degradation of  $\text{CHCl}_3$  is reexamined. In this work, we explore evidence for this novel photocatalytic mechanism for  $\text{CHCl}_3$  and  $\text{CHBr}_3$  photooxidation. Reactions of trichloromethyl radical, which are generated from the  $\text{CCl}_4$ /electron donor system, are compared to those of  $\text{CHCl}_3$  system in an attempt to ascertain the general fate of the trihalomethyl radical on illuminated  $\text{TiO}_2$ . In addition, trichloromethyl radical generation from trichloroacetate photooxidation via a photo-Kolbe process (eq 7)<sup>1,13,14</sup> is investigated.



## Experimental Section

**Materials, Apparatus, and Operation.** Degussa (P25) TiO<sub>2</sub>, which is known to be a mixture of 80% anatase and 20% rutile with an average particle size of 30 nm and B.E.T. surface area of ~50 m<sup>2</sup>/g,<sup>15</sup> was used as a photocatalyst without further treatment. All TiO<sub>2</sub> suspensions were prepared at a concentration of 0.5 g/L in water purified with a Milli-Q UV Plus system (resistivity, 18.2 MΩ·cm). The TiO<sub>2</sub> suspension was dispersed by simultaneous sonication and shaking in an ultrasonic cleaning bath (Branson 5200). The suspension was then bubbled with O<sub>2</sub>, N<sub>2</sub>, or a mixture (O<sub>2</sub>/N<sub>2</sub>) at a fixed ratio for an hour before addition of the organic substrate. The suspension was stirred magnetically throughout each experiment. Saturated solutions of CCl<sub>4</sub> (5 mM), CHCl<sub>3</sub> (63 mM), and CHBr<sub>3</sub> (12 mM) were prepared by stirring in an excess of each organic liquid in water and solutions of a desired concentration were then prepared by dilution. For anoxic (i.e., oxygen free) photodegradation experiments separate saturated stock solutions were prepared under nitrogen. Fresh stock solutions of CHBr<sub>3</sub> were made daily because of its slow hydrolytic decomposition. The pH of the suspension was adjusted with 1 N HClO<sub>4</sub> or 1 N NaOH and was measured before and after the irradiation. CCl<sub>4</sub> (Baker), CHCl<sub>3</sub> (Baker), CCl<sub>3</sub>COONa (Aldrich), and CHBr<sub>3</sub> (Aldrich) were used as received.

Irradiations were performed with a 1000-W Xe arc lamp (Spindler and Hoyer) operated at 910 W. Light was filtered through a 10-cm IR water filter and, when light intensities needed to be measured, a UV band pass filter (310 - 400 nm, Corning). The filtered light was focused through a convex lens onto a reactor cell loaded with the TiO<sub>2</sub> suspension. Light intensity measurements were performed by chemical actinometry using (E)-α-(2,5-dimethyl-3-furylethylidene)

(isopropylidene) succinic anhydride (Aberchrome 540).<sup>16</sup> A typical light intensity through a UV band pass filter was  $\sim 1.4 \times 10^{-3}$  einstein L<sup>-1</sup> min<sup>-1</sup>.

Two distinct types of photolysis experiments were carried out. One set of experiments were focused on the formation of halogenated intermediates and halide ions and the disappearance of substrate compounds as a function of irradiation time; another set on the determination of gaseous CO and CO<sub>2</sub> generation after 2-hr of irradiation. The two sets of photolysis experiments were performed in different reactors as described below.

**Photolysis and Analysis of Halogenated Compounds and Halide Ions.** For the experiments in which halogenated intermediates and halide ions were determined, a 35 mL quartz reactor cell was used. After gas saturation, reagents (an aliquot of the saturated stock solution and alcohols as an electron donor for CCl<sub>4</sub> degradation) were added into the reactor with minimal head space through a rubber septum. Light was irradiated through a UV-band pass filter.

Sample aliquots were obtained with a 1 mL-syringe, filtered through a 0.45  $\mu$ m-nylon filter, and injected into a 2.5 mL glass vial having a screwtop cap and a Teflon-faced septum. Halogenated compounds and their degradation intermediates were extracted with 0.5 mL of pentane immediately after sampling. Sample vials were stored at 4 °C in the dark up to 48 hrs before analysis. The degradation and formation of halogenated compounds and intermediates were followed chromatographically with a Hewlett-Packard (HP) 5880A gas chromatograph (GC) equipped with a <sup>63</sup>Ni electron capture detector and a HP-5 column (crosslinked 50% PhMe silicone, 25m x 0.32 mm x 1.05  $\mu$ m). Nitrogen was used as the carrier gas. The GCs were calibrated daily with external standards (CCl<sub>4</sub>, CHCl<sub>3</sub>, CHBr<sub>3</sub>, C<sub>2</sub>Cl<sub>4</sub>, and C<sub>2</sub>Cl<sub>6</sub>) and duplicate measurements

were made for each sample. The formation of perbromoethylene ( $C_2Br_4$ ) whose authentic standard was not available was identified with a GC (HP 5890 II) connected to a mass selective detector (HP 5972A). The aqueous phase in the sampling vial was analyzed by ion-exchange chromatography (IC) for halide ions. The IC system was a Dionex Bio-LC system equipped with a conductivity detector and a Dionex OmniPac PAX-500 column ( $8\ \mu\text{m} \times 5\ \text{mm} \times 250\ \text{mm}$ ).

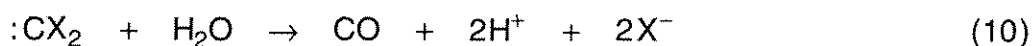
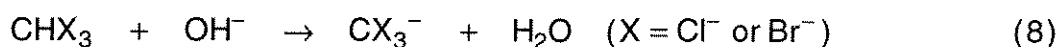
**Photolysis and Analysis of Gaseous Products.** The experiments determining CO and  $CO_2$  used a pyrex reactor with a total volume of 100 mL. The pyrex reactor was connected to a gas collection tube (total volume 145 mL, Ace Glass) through a glass joint, which was evacuated with a closed stopcock. After  $N_2$  or  $O_2$  purging, 0.5 mL of  $CHCl_3$  or  $CCl_4$  was added directly into the suspension. By the end of photolysis, most of  $CHCl_3$  dissolved into the aqueous suspension while excess  $CCl_4$  droplets remained at the bottom of the reactor. A He-filled balloon was then attached to a top opening of the reactor in order to collect gaseous product evolved during the photolysis. The full band irradiation (with no filter) lasted for two hours. At the end of each photolysis, the evacuated gas collection tube was filled with the gas mixture in the balloon and taken for GC analysis. Two aliquots of 1 mL aqueous phase were sampled, filtered, and injected into the same glass vial described above. In order to drive aqueous carbonate species into the gas phase (for  $CO_2$  analysis), 100  $\mu\text{L}$  of concentrated sulfuric acid was added. The vial was then shaken and left for at least 30 min for equilibration before GC analysis. Standard solutions of sodium carbonate for  $CO_2$  analysis were prepared by the same method.

The  $Cl^-$  production after the photolysis was measured with an Orion chloride ion-selective electrode (Model 96-17B). Gaseous samples from the gas collecting tube and the head space of the glass vials were analyzed by a GC

(Carle AGC series 400) equipped with a thermal conductivity detector and columns of Porapak QS and 5 Å molecular sieve particles. Helium was used as the carrier gas. Duplicate measurements were made for each sample with an injection volume of 20 µL. Standards of gaseous CO and CO<sub>2</sub> were made by mixing each gas with He at known ratios in the gas collecting tube. The total numbers of CO and CO<sub>2</sub> molecules generated during the photolysis were calculated by using Henry's law constants based on the assumption of liquid-gas equilibrium.

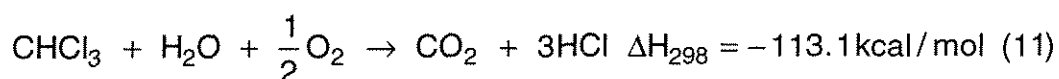
## Results

Results of the photocatalytic degradations of CHCl<sub>3</sub> and CHBr<sub>3</sub> in the absence of dissolved oxygen are shown in Figure 1. Even though dioxygen was considered to be essential for the degradation of these compounds,<sup>5,6,17,18</sup> they were decomposed slowly in the O<sub>2</sub>-free photocatalytic systems. The small amount of oxygen that remains even after vigorous nitrogen purging can be responsible for this degradation. However, the linearity of halide production over the whole irradiation period indicates that the contribution of the residual oxygen to total halide production is insignificant. In particular, the degradation rates were greatly enhanced at pH 12 for both CHCl<sub>3</sub> and CHBr<sub>3</sub>. Although CHCl<sub>3</sub> and CHBr<sub>3</sub> can be degraded through base-catalyzed hydrolysis (eqs 8-10) in the absence of light,<sup>19,20</sup> the hydrolysis rate at pH 12 is small compared to the net photolysis rate as shown in Figure 1.



The measured quantum yields for the halide production were  $\Phi_{\text{CHCl}_3} = 0.021$  ( $\text{CHCl}_3$  at pH 12),  $\Phi_{\text{CHCl}_3} = 0.0034$  ( $\text{CHCl}_3$  at pH 5),  $\Phi_{\text{CHBr}_3} = 0.018$  ( $\text{CHBr}_3$  at pH 12), and  $\Phi_{\text{CHBr}_3} = 0.0019$  ( $\text{CHBr}_3$  at pH 5).

The effects of the dissolved oxygen concentration on the photolysis rate of  $\text{CHCl}_3$  are shown in Figures 2 and 3. These results show that  $\text{O}_2$  increases the net dechlorination rate. The stoichiometry for the complete mineralization of  $\text{CHCl}_3$  to  $\text{CO}_2$  in the presence of oxygen is:<sup>5,17</sup>



For  $\text{CHCl}_3$  photodegradation in an air-saturated solution (Figure 2), the  $\text{Cl}^-$  production, however, went beyond the level of concentration which corresponded to the stoichiometric consumption of dissolved  $\text{O}_2$ . This result is not consistent with the observations of Kormann et al.<sup>5</sup> They observed that  $[\text{Cl}^-]$  increased linearly up to  $\sim 1.4$  mM, at which point the chloride production rate abruptly decreased to a much smaller value as the  $\text{O}_2$  was depleted.

The normal effect of  $[\text{O}_2]$  on the dechlorination rate (Figure 3) exhibited Langmuirian dependence<sup>21,22</sup> except that the dechlorination rate was non-zero at  $[\text{O}_2] = 0.0$  mM. The data of Figure 3 are fitted to the following equation:

$$\frac{d[\text{Cl}^-]}{dt} = k_{\text{Cl}} \frac{K_{\text{O}_2}[\text{O}_2]}{1 + K_{\text{O}_2}[\text{O}_2]} + k_{\text{Cl},0} \quad (12)$$

where  $k_{\text{Cl}}$  is a photodechlorination rate constant in the presence of dissolved oxygen,  $K_{\text{O}_2}$  is a photochemical equivalent of  $\text{O}_2$  adsorption constant, and  $k_{\text{Cl},0}$  is a photodechlorination rate in the absence of dissolved oxygen. The fitted values were:  $k_{\text{Cl}} = 11.5 \mu\text{M min}^{-1}$ ,  $K_{\text{O}_2} = 3.4 \times 10^3 \text{ M}^{-1}$  and  $k_{\text{Cl},0} = 3.4 \mu\text{M min}^{-1}$ . Mills et al.<sup>23</sup> reported a value of  $K_{\text{O}_2} = 3.6 \times 10^3 \text{ M}^{-1}$  in a  $\text{TiO}_2$  (Degussa P25)/ 4-

chlorophenol system while Okamoto et al.<sup>24</sup> obtained  $K_{O_2} = 8.9 \times 10^3 \text{ M}^{-1}$  in a  $\text{TiO}_2$  (anatase)/ phenol system. However, a value of  $K_{O_2} = (1.3 \pm 0.7) \times 10^5 \text{ M}^{-1}$ , which Kormann et al.<sup>5</sup> reported for a  $\text{TiO}_2$  (Degussa P25)/ chloroform system, appears to be an overestimate.

The pH-dependent dechlorination rates and formation of intermediates during  $\text{CHCl}_3$  degradation are compared between  $\text{O}_2$  and  $\text{N}_2$  saturated suspensions in Figure 4. Production of  $\text{Cl}^-$  in  $\text{O}_2$ -saturated solutions increased exponentially at  $\text{pH} > 10$ , while the  $\text{N}_2$ -saturated systems showed a moderate increase in  $[\text{Cl}^-]$ . The calculated extent of hydrolysis<sup>25</sup> of  $\text{CHCl}_3$  as a function of pH (dotted line in Figure 4a) shows that the  $\text{Cl}^-$  production from hydrolysis was about 100 times smaller than that due to photolysis. However, the qualitative exponential behavior of pH-dependent base hydrolysis rate resembles that of photolysis. The formation of  $\text{C}_2\text{Cl}_6$  and  $\text{C}_2\text{Cl}_4$  (Figure 4b) was only significant at  $\text{pH} > 11.5$ , and their concentrations were higher in  $\text{N}_2$ -saturated solutions than in  $\text{O}_2$ -saturated solutions.

Due to the high substrate concentration (6 mM) used in this study, dimerization products of the intermediate radicals were detected (eqs 13-15).



The time-dependent production of the dimerized products from  $\text{CHCl}_3$  and  $\text{CHBr}_3$  degradation at pH 12 are shown in Figure 5. Both  $\text{C}_2\text{Cl}_6$  and  $\text{C}_2\text{Cl}_4$  from  $\text{CHCl}_3$  degradation were detected as intermediates while only  $\text{C}_2\text{Br}_4$  (not  $\text{C}_2\text{Br}_6$ ) was detected from  $\text{CHBr}_3$  degradation. The concentration of  $\text{C}_2\text{Cl}_6$  reached its maximum in 1 hr. The concentrations of  $\text{C}_2\text{Cl}_4$  and  $\text{C}_2\text{Br}_4$  rose continuously. In

control reactions, which were performed in the dark, a trace amount of  $C_2Br_4$  and  $0.2 \mu M C_2Cl_4$  were formed after 2.5 hr from a dimerization of hydrolytically produced dihalocarbenes (eqs 8,9).

In order to examine the possibility of trichloromethyl radical production during trichloroacetate photooxidation (eq 7),  $C_2Cl_6$  and  $C_2Cl_4$  were sought as intermediates from the photolysis of trichloroacetate on  $TiO_2$ . No  $C_2Cl_6$  was detected throughout the photolysis runs listed in Table I. However, a trace of  $C_2Cl_4$  was found in some cases. Few differences in the dechlorination rates were found under  $O_2$  and  $N_2$ ; this observation is consistent to those of Chemseddine and Boehm.<sup>14</sup> The dechlorination rates gradually increased with lowering pH.

In our previous study,<sup>11</sup> we reported that the photoreductive decomposition of  $CCl_4$  on  $TiO_2$  was strongly dependent on the nature of the electron donors. In order to investigate how the electron donor affects the fate of trichloromethyl radical (generated through eq 2) on  $TiO_2$ , the production of chloride and chlorinated intermediates ( $CHCl_3$ ,  $C_2Cl_6$ , and  $C_2Cl_4$ ), which are derived from the trichloromethyl radical, were measured in the  $CCl_4$ /electron donor system and summarized in Table II. The intermediate formation varied greatly as a function of the specific electron donor. The addition of 2-propanol resulted in enhanced concentration of intermediates, while methanol showed a moderate effect. *Tert*-butanol had little effect.

The production of  $CO_2$ ,  $CO$ , and  $Cl^-$  from the photolysis of  $CHCl_3$  is compared in Table III.  $CO$  was found as the main product of chloroform photolysis in the absence of  $O_2$  and at high pH. At  $pH < 11$  and in the absence of dissolved oxygen,  $CHCl_3$  degradation was slow. In  $O_2$ -saturated suspensions,

on the other hand,  $\text{CO}_2$  was determined to be the principle product and CO the minor product even at high pH. At low pH and under  $\text{N}_2$ -saturation, the analytical method was not accurate and sensitive enough to distinguish between background  $\text{CO}_2$  and photogenerated  $\text{CO}_2$  and CO. The stoichiometric balance between chlorides and gaseous products was reasonable. However, the  $\text{Cl}^-$  level was consistently a little higher than the sum of CO and  $\text{CO}_2$ ; this result suggests the presence of other intermediates.

Similar analyses for  $\text{CCl}_4$  are presented in Table IV. Both CO and  $\text{CO}_2$  were detected as photolysis products. In addition, photolysis of the added electron donors in the absence of  $\text{CCl}_4$  did not produce detectable levels of CO. Therefore, CO appears to have originated directly from  $\text{CCl}_4$  degradation. Even though the chloride production under  $\text{O}_2$  saturation was about doubled from that under  $\text{N}_2$  saturation,  $\text{CO}_2$  generation was enhanced more substantially in the  $\text{O}_2$ -saturated system. Based on this observation, it appears that the majority of evolved  $\text{CO}_2$  originated from the electron donor oxidation and not from  $\text{CCl}_4$  reduction. The sum of total CO and an undetermined fraction of total  $\text{CO}_2$  (which came from  $\text{CCl}_4$ ) accounts for only a small fraction of total  $\text{Cl}^-$ . In the present photolysis system, where excess  $\text{CCl}_4$  droplets remained at the bottom of reactor, most of chlorinated radical intermediates seemed to react with the electron donor or to be scavenged into the  $\text{CCl}_4$  liquid phase, thus preventing their subsequent degradation.

## Discussion

Experimental results presented above clearly show that  $\text{CHCl}_3$  and  $\text{CHBr}_3$  are photocatalytically degraded into CO in the absence of dissolved oxygen. These results are consistent with a "short-circuit" mechanism which involves

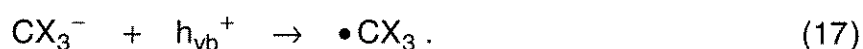
reactions of  $\text{CHCl}_3$  with a VB hole (or  $\bullet\text{OH}$ ) (eq 1) and a CB electron (eq 4). The overall stoichiometry for this degradation pathway can be written as:



However, this reaction (eq 16) is preferred thermodynamically only under anoxic conditions. In  $\text{O}_2$ -saturated suspensions, most of the  $\bullet\text{CCl}_3$  radicals react with  $\text{O}_2$  (eq 3) to produce  $\text{CO}_2$  as suggested previously.<sup>5,8</sup> Therefore, the heterogeneously photogenerated trichloromethyl radical exhibits two branching pathways; the branching ratio is dependent on the availability of dioxygen on the surface.

Even though both pathways involving the trichloromethyl radical lead to the full degradation of  $\text{CHCl}_3$ , several experimental observations can not be readily explained by these alternative mechanisms. For example, the  $\text{CHCl}_3$  dechlorination rates (Figure 4a) increase exponentially at  $\text{pH} > 10$  in  $\text{O}_2$ -saturated suspensions while  $d[\text{Cl}^-]/dt$  rises slowly in  $\text{N}_2$ -saturated suspensions. Similar behavior was reported for the kinetics of  $\text{CCl}_4$  dechlorination on  $\text{TiO}_2$ .<sup>11,12</sup> In that case, the enhanced rates were attributed to an increase in the rate of CB electron transfer and the base-catalyzed hydrolysis of dichlorocarbene. The same general arguments can be applied to the reactions of eq 4 and eq 6. However, there is no reason why these effects should be enhanced in  $\text{O}_2$ -saturated suspensions. In addition,  $\text{CO}_2$  production (Table III) in the presence of  $\text{O}_2$  was enhanced significantly at high pH. Furthermore, the rates of formation of  $\text{C}_2\text{Cl}_6$  and  $\text{C}_2\text{Cl}_4$  (Figure 4b) also show exponential increases above pH 11. However, during  $\text{CCl}_4$  photoreduction the same intermediates were shown to decrease at high pH.<sup>11,12</sup> This trend is supported by the data presented in Table II.

In order to account for these observations, a third mechanistic pathway for  $\text{CHCl}_3$  and  $\text{CHBr}_3$  degradation is proposed. Even though the base-catalyzed hydrolyses of the haloforms (eqs 8-10) are much slower than the corresponding photolysis rates (Figures 1 and 4a), they do increase exponentially with pH. The rate-determining steps in the hydrolyses involve the release of a halide ion from a trihalocarbanion (eq 9).<sup>19</sup> On the photoilluminated  $\text{TiO}_2$  surface, however, an alternative pathway for a trihalocarbanion is possible as follows:



The observed polarographic cathodic wave of trichloromethyl radical ( $\bullet\text{CCl}_3 + e^- \rightarrow \text{CCl}_3^-$ ) has a half-wave potential of  $E_{1/2} \approx 0.0$  V (vs NHE).<sup>26</sup> Since the VB hole potential of  $\text{TiO}_2$  (at pH 7) is +2.7 V, there is a large thermodynamic driving force for the reaction of eq 17. When  $\text{O}_2$  is present, the  $\bullet\text{CX}_3$  radical is rapidly scavenged via eqs 3 and 5. As a consequence, the equilibrium deprotonation step (eq 8) is shifted to the right. This, in turn, results in an increase in the rates of  $\text{CHCl}_3$  degradation and intermediate formation with increasing pH. In the absence of  $\text{O}_2$ , the  $\bullet\text{CX}_3$  radical reacts with a CB electron to form  $:\text{CX}_2$  (eq 4); this pathway is consistent with the slower increase of  $\text{Cl}^-$  production in  $\text{N}_2$ -saturated systems as shown in Figure 4a. Since the above phenomenon is closely related to the net effects of base-catalyzed hydrolysis, we name the process "photoenhanced hydrolysis".

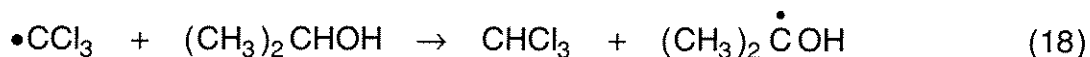
The proposed photocatalytic mechanisms for  $\text{CHCl}_3$  and  $\text{CHBr}_3$  degradation on  $\text{TiO}_2$  are summarized in Figure 6. The mechanism of Fig. 6a represents photooxidation in the presence of dissolved oxygen, as proposed by Kormann et al.<sup>5</sup> This mechanism is the major pathway for a haloform degradation under normal conditions in which oxygen is present and hydrolysis is

negligible ( $\text{pH} < 10$ ). The mechanism of Fig. 6b becomes a major contributor under anoxic conditions. The rate of this reaction in the absence of oxygen is much slower than that achieved in pathway "a" because there is no efficient CB electron scavengers available except for the transient, trihalomethyl radicals. When a sufficient amount of oxygen is present at the  $\text{TiO}_2$  surface, the mechanisms of Fig. 6a and 6b proceed concurrently. The experimental observation (Figure 2) that  $\text{Cl}^-$  generation in an air-saturated  $\text{TiO}_2$  suspension was linear beyond the stoichiometric consumption of  $\text{O}_2$  supports this argument. At higher pH, the rate of dehalogenation can be increased due to enhancement in both the CB electron-transfer pathway and dihalocarbene hydrolysis. The mechanism of Fig. 6c becomes important only when deprotonation of the haloform (eq 8) occurs at  $\text{pH} > 10$ . When oxygen is present, the acceleration of the degradation rate is dramatic. Without oxygen the degradation pathway is similar to the mechanism of Fig. 6b. However, at this time, it is not clear how much of the net anoxic degradation can be attributed to mechanisms "b" and "c", respectively. The intrinsic hydrolysis pathway of Fig. 6d is insignificant under the conditions employed in this study. For example, the hydrolysis rate is only comparable to the photolysis rate at nominal pH values above 14.<sup>25</sup>

In contrast to the  $\text{CHCl}_3$  system, the trichloromethyl radical in  $\text{CCl}_4$  photoreduction appears only in the presence of appropriate electron donors. Since the electron donors (ROH) scavenge VB holes efficiently and induce secondary reactions through the formation of  $\alpha$ -hydroxyalkyl radicals,<sup>11,27,28</sup> the chemistry of  $\bullet\text{CCl}_3$  with efficient electron donors is substantially different from that of  $\bullet\text{CCl}_3$  radical generated without electron donors. As shown in Table II, the specific electron donors have a strong influence on the production of  $\text{Cl}^-$  and

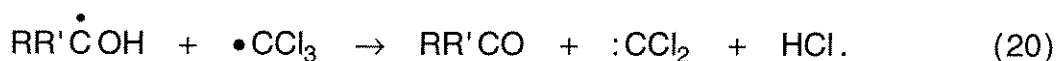
chlorinated hydrocarbon intermediates. The relative effect of a wide range of electron donors on  $\text{CCl}_4$  dechlorination has been discussed previously.<sup>11</sup>

The rates of formation of chlorinated hydrocarbon intermediates and  $\text{Cl}^-$  are enhanced substantially when 2-propanol is employed as an electron donor (Table II). This effect can be explained by the following chain propagation steps:



Considering the bond strength of  $\text{H-C}(\text{CH}_3)_2\text{OH}$  ( $91 \pm 1$  kcal/mol) and  $\text{H-CCl}_3$  ( $94 \pm 1$  kcal/mol),<sup>29</sup> this chain propagation sequence reaction is energetically feasible. With methanol C-H bond strength of  $94 \pm 2$  kcal/mol, the chain propagation of eqs 18 and 19 should be less efficient as seen experimentally. The chain propagation of eqs 18 and 19 is inoperative in the  $\text{CCl}_4/t$ -butanol system because  $t$ -butanol does not form  $\alpha$ -hydroxyalkyl radicals. The extent of chain propagation in our study seems to be limited due to the competition from  $\text{O}_2$  addition to the carbon-centered radicals.

The net production of  $\text{C}_2\text{Cl}_6$  in the  $\text{CCl}_4/\text{ROH}$  systems is less than that of  $\text{C}_2\text{Cl}_4$  while the  $\text{CHCl}_3$  system showed the opposite trend. At pH 12, only traces of  $\text{C}_2\text{Cl}_6$  were found (Table II) in contrast with its dramatic increase in the  $\text{CHCl}_3$  system at the same pH (Figure 4b). This behavior is consistent with the following secondary reaction induced by the electron donor (eq 20):<sup>27</sup>



The oxidation potentials of  $\bullet\text{CH}_2\text{OH}$  ( $-0.74$  V vs NHE) and  $\bullet\text{C}(\text{OH})(\text{CH}_3)_2$  ( $-1.06$  V)<sup>27</sup> are strong enough to directly reduce  $\bullet\text{CCl}_3$  (0.0 V). The reduced surface

concentration of  $\bullet\text{CCl}_3$  results in fewer net dimerizations to produce  $\text{C}_2\text{Cl}_6$  while at the same time  $\text{:CCl}_2$  dimerization to produce  $\text{C}_2\text{Cl}_4$  is enhanced.

The above arguments suggest that the fate of trichloromethyl radical generated from  $\text{CCl}_4$  on photoilluminated  $\text{TiO}_2$  is largely determined by the nature of the specific electron donor. Production of  $\alpha$ -hydroxyalkyl radicals results in complex secondary reactions with surficial trichloromethyl radicals. The specific electron donors (i.e., alcohols), which were originally introduced primarily to scavenge VB holes, play a key role in determination of the actual reaction path for  $\bullet\text{CCl}_3$ .

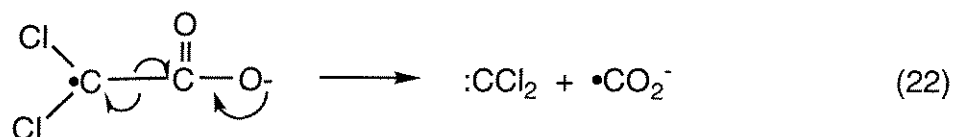
In general, photocatalytic degradation of organic compounds on illuminated  $\text{TiO}_2$  is thought to be initiated through hydrogen atom abstraction by surface-bound  $\bullet\text{OH}$  radical.<sup>13,14</sup> Therefore, organic compounds having no abstractable hydrogen atoms such as  $\text{CCl}_4$  and  $\text{CCl}_3\text{CO}_2^-$  exhibit much slower overall degradation rates.<sup>13,14,18,30</sup> In the case of  $\text{CCl}_3\text{CO}_2^-$ , the slow degradation rates were attributed to either the photo-Kolbe reaction (eq 7)<sup>1,13,14</sup> and/or the photoreduction by CB electrons (eq 21)<sup>14,31</sup> although it is not clear which was the predominant pathway mechanism.



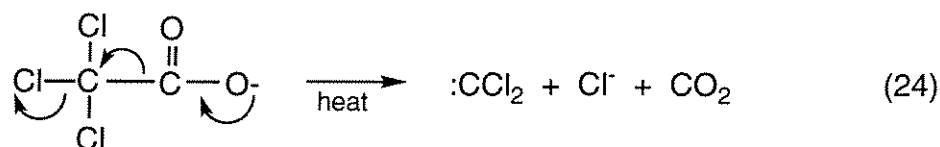
Supporting evidence for the photo-Kolbe mechanism is that  $\text{CO}_2$  is formed from trichloroacetate degradation in  $\text{N}_2$ -saturated  $\text{TiO}_2$  suspensions.<sup>14</sup> On the other hand, Chemseddine and Boehm<sup>14</sup> reported that  $\text{CO}_2$  production under  $\text{N}_2$  decreased in the order of  $\text{CCl}_3\text{CO}_2^- > \text{CHCl}_2\text{CO}_2^- > \text{CH}_2\text{ClCO}_2^- > \text{CH}_3\text{CO}_2^-$ , which is consistent with a reaction initiated by CB electrons. We should expect the opposite order if the photo-Kolbe mechanism is working because electron density at the carboxyl group is decreasing with increasing number of chlorine atoms. In

this study, we did not detect  $C_2Cl_6$  from the fairly concentrated solution (6 mM) of trichloroacetate, even though it was formed during the photodegradation of  $CHCl_3$  and  $CCl_4$ .

In order to resolve this mechanistic dilemma, we propose the following photocatalytic mechanism of trichloroacetate degradation which is initiated by eq 21 and then followed by eqs 22 and 23:



A similar thermolytic decarboxylation mechanism (eq 24) of trichloroacetate is known.<sup>20</sup>



In agreement with our mechanism proposed above, Mao et al.<sup>13</sup> detected oxalate as a minor product from the photocatalytic degradation of trichloroacetate. The oxalate molecule can be formed from the dimerization of  $\bullet\text{CO}_2^-$  radicals. Since the carboxyl group of the trichloroacetate molecule has a very low electron density due to the presence of three electron-withdrawing substitutes, decarboxylation appears to result from self-rearrangement (eq 22) rather than from the direct photo-Kolbe reaction. Additional study of the trichloroacetate photodegradation on  $\text{TiO}_2$  is needed in order to verify the proposed mechanism.

## **Acknowledgments**

We thank Advanced research Projects Agency (ARPA) and the Office of Naval Research (ONR) {N0014-92-J-1901} for financial support. We also appreciate the help from Robert Rossi and Janet Kesselman in GC analysis.

## References

- (1) Hoffmann, M.R.; Martin, S.T.; Choi, W.; Bahnemann, D.W. *Chem. Rev.* **1995**, *95*, 69.
- (2) Serpone, N., Pelizzetti, E., Eds. *Photocatalysis - Fundamentals and Applications*; Wiley-Interscience: New York, 1989.
- (3) Ollis, D.F., Al-Ekabi, H., Eds, *Photocatalytic Purification and Treatment of Water and Air*; Elsevier: Amsterdam, 1993.
- (4) Mao, Y.; Schöneich, C.; Asmus, K.-D. *J. Phys. Chem.* **1992**, *96*, 8522.
- (5) Kormann, C.; Bahnemann, D.W.; Hoffmann, M.R. *Environ. Sci. Technol.* **1991**, *25*, 494.
- (6) Bahnemann, D.; Bockelmann, D.; Goslich, R. *Solar Energy Materials* **1991**, *24*, 564.
- (7) Köster, R.; Asmus, K.-D. *Z. Naturforsch.* **1971**, *26b*, 1108.
- (8) Mönig, J.; Bahnemann, D.; Asmus, K.-D. *Chem.-Biol. Interactions* **1983**, *45*, 15.
- (9) Mönig, J.; Asmus, K.-D. *J. Chem. Soc. Perkin Trans. II* **1984**, 2057.
- (10) Lal, M; Schöneich, C.; Mönig, J.; Asmus, K.-D. *Int. J. Radiat. Biol.* **1988**, *54*, 773.
- (11) Choi, W.; Hoffmann, M.R. *Environ. Sci. Technol.* **1995**, *29*, 1646.
- (12) Choi, W.; Hoffmann, M.R., *J. Phys. Chem.* **1996**, *100*, 2161.
- (13) Mao, Y.; Schöneich, C.; Asmus, K.-D. *J. Phys. Chem.* **1991**, *95*, 10080.
- (14) Chemseddine, A.; Boehm, H.P. *J. Mol. Catal.* **1990**, *60*, 295.
- (15) *Degussa Technical Bulletin Pigments #56*; Degussa: Hanau-Wolfgang, 1990.
- (16) Heller, H.G.; Langan, J.R. *J. Chem. Soc., Perkin Trans.* **1981**, *2*, 341.
- (17) Pruden, A.L.; Ollis, D.F. *Environ. Sci. Technol.* **1983**, *17*, 628.

- (18) Hsiao, C.-Y.; Lee, C.-L.; Ollis, D.F. *J. Catal.* **1983**, *82*, 418.
- (19) Robinson, E.A. *J. Chem. Soc.* **1961**, 1663.
- (20) March, J. *Advanced Organic Chemistry*, 3rd ed.; John Wiley & Sons: New York, 1985.
- (21) Pelizzetti, E.; Pramuro, E.; Minero, C.; Serpone, N.; Borgadello, E. In *Photocatalysis and Environment*; Schiavello, M., Ed.; NATO ASI Series; Kluwer Academic Publication: Dordrecht, Netherlands, 1988; p 527.
- (22) Al-Ekabi, H.; Serpone, N.; Pelizzetti, E.; Minero, C.; Fox, M.A.; Draper, R.B. *Langmuir*, **1989**, *5*, 250.
- (23) Mills, A.; Morris, S. *J. Photochem. Photobiol. A: Chem.* **1993**, *71*, 75.
- (24) Okamoto, K.-I.; Yamamoto, Y.; Tanaka, H.; Itaya, A. *Bull. Chem. Soc. Jpn.* **1985**, *58*, 2023.
- (25) The hydrolysis rate constant was taken from: Schwarzenbach, R.P.; Gschwend, P.M.; Imboden, D.M. *Environmental Organic Chemistry*; John Wiley & Sons: New York, 1993; p 368.
- (26) Bansal, K.M.; Henglein, A.; Sellers, R.M. *Ber. Bunsen-Ges. Phys. Chem.* **1974**, *78*, 569.
- (27) Lilie, V.J.; Beck, G.; Henglein, A. *Ber. Bunsen-Ges. Phys. Chem.* **1971**, *75*, 458.
- (28) Ross, A.B.; Neta, P. *Rate Constants for Reactions of Aliphatic Carbon-Centered Radicals in Aqueous Solution*; NSRDS-NBS 70; National Bureau of Standards: Washington, DC, 1982.
- (29) *CRC Handbook of Chemistry and Physics*, 74th Ed.; CRC Press: Boca Raton, Florida, 1993.
- (30) Ollis D.F.; Hsiao, C.-Y.; Budiman, L.; Lee, C.-L. *J. Catal.* **1984**, *88*, 89.

(31) The half-wave potential of trichloroacetate reduction is  $-0.49$  V (vs. NHE), which is comparable to  $\text{TiO}_2$  CB electron potential ( $-0.5$  V at pH 7); The half-wave potential was taken from: Meites, T.; Meites, L. *Anal. Chem.* **1955**, *27*, 1531.

**Table I.** Chloride Production ( $\mu\text{M}$ ) after 1-hr of Photolysis<sup>a</sup> of 6 mM Trichloroacetate Solution on  $\text{TiO}_2$  as a Function of pH.

pH	2.1	3.0	5.8	12.1
$\text{O}_2$ -saturated	870	700	520	400
$\text{N}_2$ -saturated	840	680	740	420

<sup>a</sup> Light illumination through an IR water filter and a UV-band pass filter onto a 35 mL quartz reactor with an intensity of  $1.4 \times 10^{-3}$  einstein  $\text{L}^{-1} \text{min}^{-1}$

**Table II.** Concentrations of Cl<sup>-</sup>, C<sub>2</sub>Cl<sub>6</sub>, and C<sub>2</sub>Cl<sub>4</sub> Produced after 1-hr Photolysis<sup>a</sup> of 1 mM CCl<sub>4</sub> in Air-Equilibrated TiO<sub>2</sub> Suspensions in the Presence of *tert*-Butanol (t-BuOH), 2-Propanol (2-PrOH), and Methanol as Electron Donors

	pH <sup>b</sup> 2.7				pH 5				pH12			
	Cl <sup>-</sup> (mM)	CHCl <sub>3</sub> (μM)	C <sub>2</sub> Cl <sub>6</sub> (μM)	C <sub>2</sub> Cl <sub>4</sub> (μM)	Cl <sup>-</sup> (mM)	CHCl <sub>3</sub> (μM)	C <sub>2</sub> Cl <sub>6</sub> (μM)	C <sub>2</sub> Cl <sub>4</sub> (μM)	Cl <sup>-</sup> (mM)	CHCl <sub>3</sub> (μM)	C <sub>2</sub> Cl <sub>6</sub> (μM)	C <sub>2</sub> Cl <sub>4</sub> (μM)
no alcohol	0.02	n.d. <sup>c</sup>	trace <sup>d</sup>	n.d.	0.03	n.d.	trace	n.d.	0.09	n.d.	trace	n.d.
0.1 M t-BuOH	0.22	n.d.	trace	n.d.	0.17	2.2	trace	n.d.	0.81	n.d.	trace	trace
0.1 M 2-PrOH	1.9	51.3	0.51	9.1	2.2	75.1	0.56	20.1	2.5	20.6	trace	7.5
0.1 M CH <sub>3</sub> OH	0.04	4.7	0.08	0.56	0.14	1.2	0.08	0.34	2.1	4.4	trace	9.9

<sup>a</sup> Light illumination through an IR water filter and a UV-band pass filter onto a 35 mL quartz reactor with an intensity of  $1.4 \times 10^{-3}$  einstein L<sup>-1</sup> min<sup>-1</sup>. <sup>b</sup> initial pH before irradiation. <sup>c</sup> not detected. <sup>d</sup> trace amount < 30 nM.

**Table III.** CO<sub>2</sub>, CO, and Cl<sup>-</sup> Generation after 2-hr of Photolysis<sup>a</sup> of CHCl<sub>3</sub> on TiO<sub>2</sub>.

pH/ saturated gas	N <sub>CO<sub>2</sub></sub> (μmol)	N <sub>CO</sub> (μmol)	N <sub>Cl<sup>-</sup></sub> (μmol)/3 <sup>c</sup>	N <sub>CO<sub>2</sub></sub> + N <sub>CO</sub> (μmol)
(12.2, 11.9) <sup>b</sup> / N <sub>2</sub>	3	149	187	152
(12.2, 11.6)/ O <sub>2</sub>	160	12	187	172
(12.2, 12.2)/ no light	3	9	17	12
(11.9, 11.6)/ N <sub>2</sub>	3	56	97	59
(11.9, 10.3)/ O <sub>2</sub>	162	3	163	165
(11.4, 10.9)/ N <sub>2</sub>	1	11	25	12
(11.4, 3.2)/ O <sub>2</sub>	49	n.d. <sup>d</sup>	90	49
(10.2, 8.6)/ N <sub>2</sub>	1	n.d.	4	1
(10.2, 2.7)/ O <sub>2</sub>	52	n.d.	60	52
(5.0, 4.1)/ N <sub>2</sub>	1	n.d.	2	1
(5.0, 2.7)/ O <sub>2</sub>	41	n.d.	47	41

<sup>a</sup> Light illumination through an IR water filter only onto a 100 mL pyrex reactor; [TiO<sub>2</sub>] = 0.5 g/L in the presence of near saturated CHCl<sub>3</sub> (0.5 mL/100 mL) in the reactor.

<sup>b</sup> The first and second numbers in the parenthesis are pH of the suspension before and after the photolysis, respectively. <sup>c</sup> The numbers of chloride ions are divided by 3 to make them equivalent to those of CO<sub>2</sub> and CO on *per* CHCl<sub>3</sub> molecule basis. <sup>d</sup> not detected within the sensitivity limit of this experiment

**Table IV.** CO<sub>2</sub>, CO, and Cl<sup>-</sup> Generation after 2-hr of Photolysis<sup>a</sup> of CCl<sub>4</sub> on TiO<sub>2</sub> with *tert*-Butanol (t-BuOH) or 2-Propanol (2-PrOH) Present as Electron Donors.

pH <sup>b</sup> / gas/ electron donor <sup>c</sup>	N <sub>CO<sub>2</sub></sub> (μmol)	N <sub>CO</sub> (μmol)	N <sub>Cl<sup>-</sup></sub> (μmol)/4 <sup>d</sup>
12.2/ N <sub>2</sub> / t-BuOH	4	4	25
12.2/ O <sub>2</sub> / t-BuOH	33	1	38
12.2/ N <sub>2</sub> / 2-PrOH	1	11	58
12.2/ O <sub>2</sub> / 2-PrOH	86	3	115
5.0/ N <sub>2</sub> / 2-PrOH	1	1	9
5.0/ O <sub>2</sub> / 2-PrOH	36	n.d.	48

<sup>a</sup> Light illumination through an IR water filter only onto a 100 mL pyrex reactor; [TiO<sub>2</sub>] = 0.5 g/L in the presence of excess liquid CCl<sub>4</sub> (0.5 mL) in the reactor. <sup>b</sup> Initial pH of the suspension before the light illumination. <sup>c</sup> The electron donor concentration for each experiment was 0.1 M. <sup>d</sup> The numbers of chloride ions are divided by 4 to make them equivalent to those of CO<sub>2</sub> and CO on *per* CCl<sub>4</sub> molecule basis.

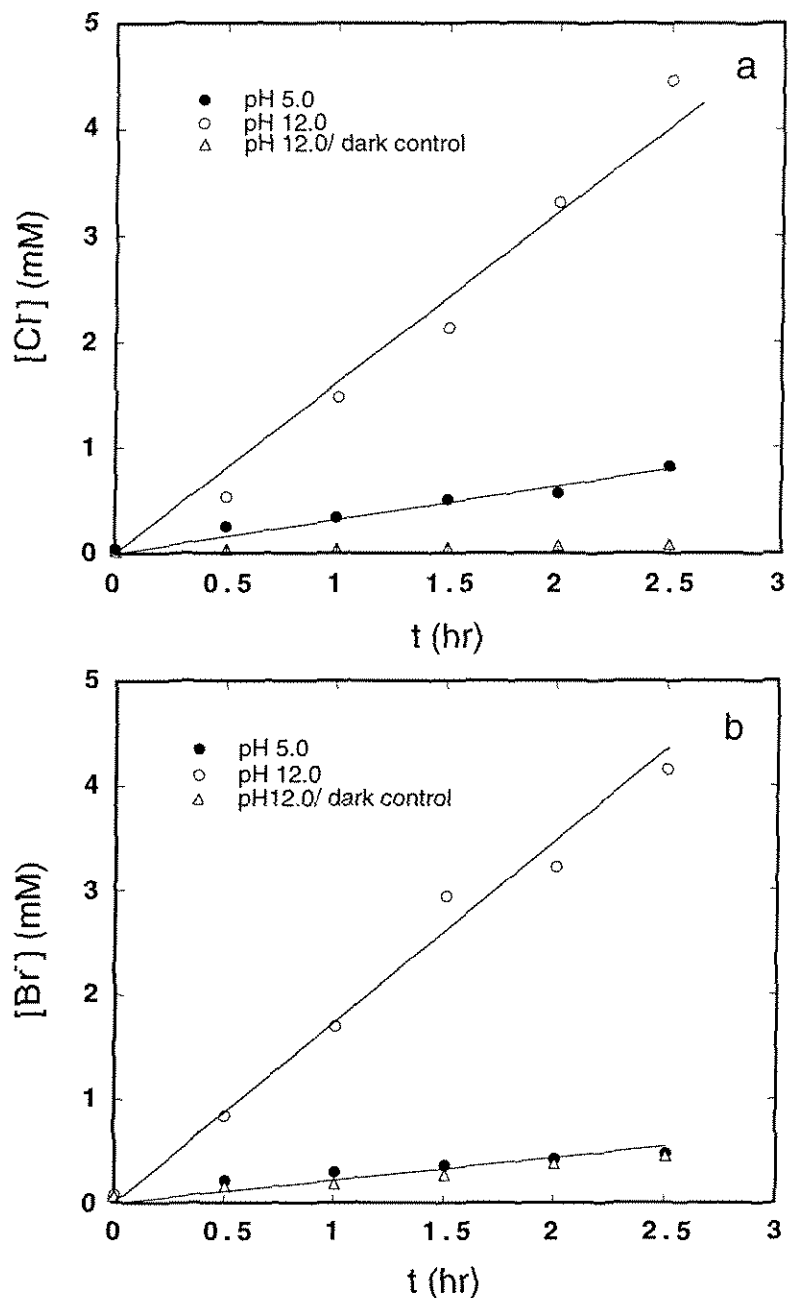


**Figure 1.** The production of halide ions from the photocatalytic decomposition of (a) 6 mM  $\text{CHCl}_3$  and (b) 6 mM  $\text{CHBr}_3$  solutions, which were saturated with  $\text{N}_2$  prior to the photolysis, in a sealed reactor at the initial pH 5 and 12 as a function of irradiation time. The halide generations from dark hydrolysis of the same substrates at pH 12 are shown as well. There was no hydrolysis at pH 5.

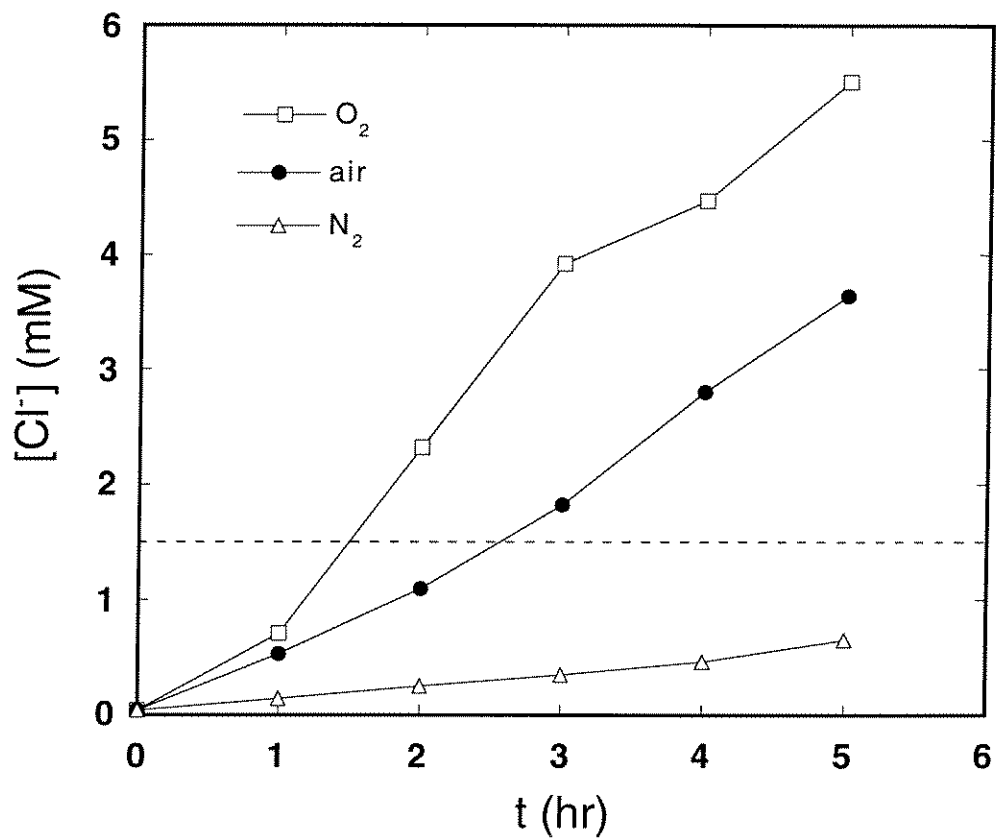


**Figure 2.** Chloride generation from the photolysis of 6 mM  $CHCl_3$  solutions ( $pH_i$  4.5) which were saturated with  $O_2$ , air, and  $N_2$ , respectively prior to irradiation. The dotted line represents the chloride level corresponding to the stoichiometric consumption of dissolved oxygen (0.25 mM) in an air-saturated solution.

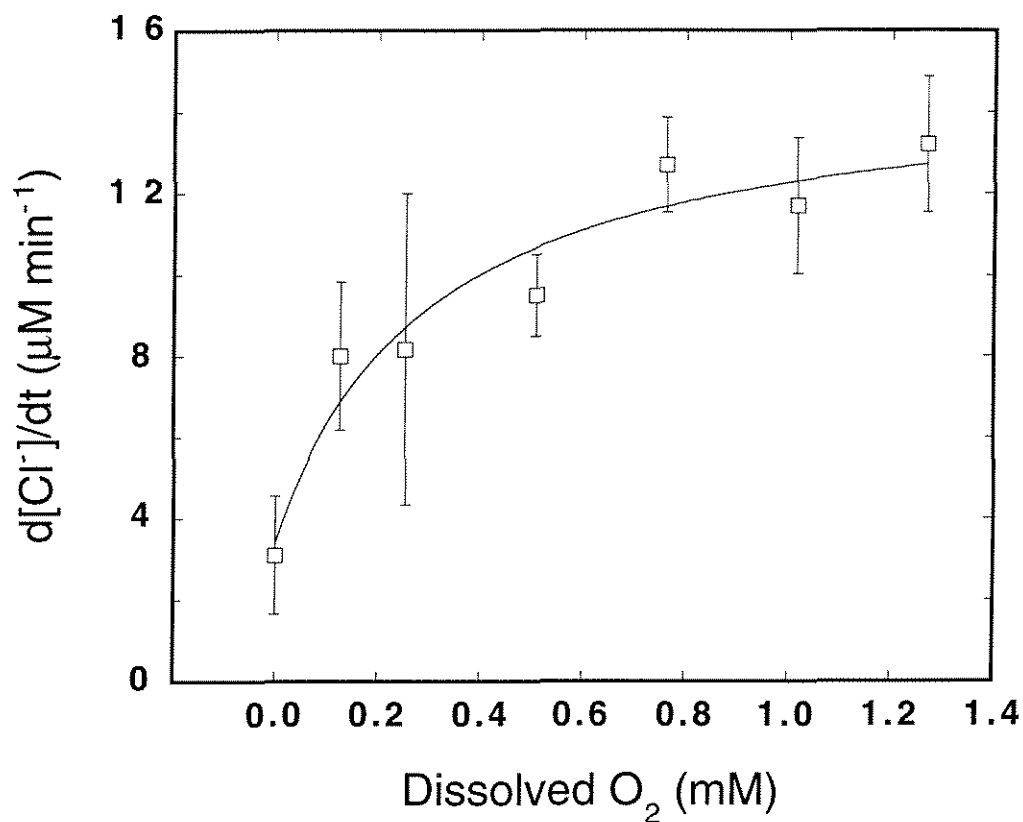


**Figure 3.** Dependence of the photocatalytic chloride generation rates in 6 mM  $\text{CHCl}_3$  solution on the dissolved oxygen concentration. The dechlorination rates were measured over an initial 1-hr photolysis period. The concentration of dissolved oxygen was varied by changing the ratio of the flow rates of  $\text{O}_2$  and  $\text{N}_2$  bubbling gases and calculated by assuming that the dissolved oxygen concentration in an  $\text{O}_2$ -saturated solution was 1.27 mM. The solid line is a fit to eq 12.

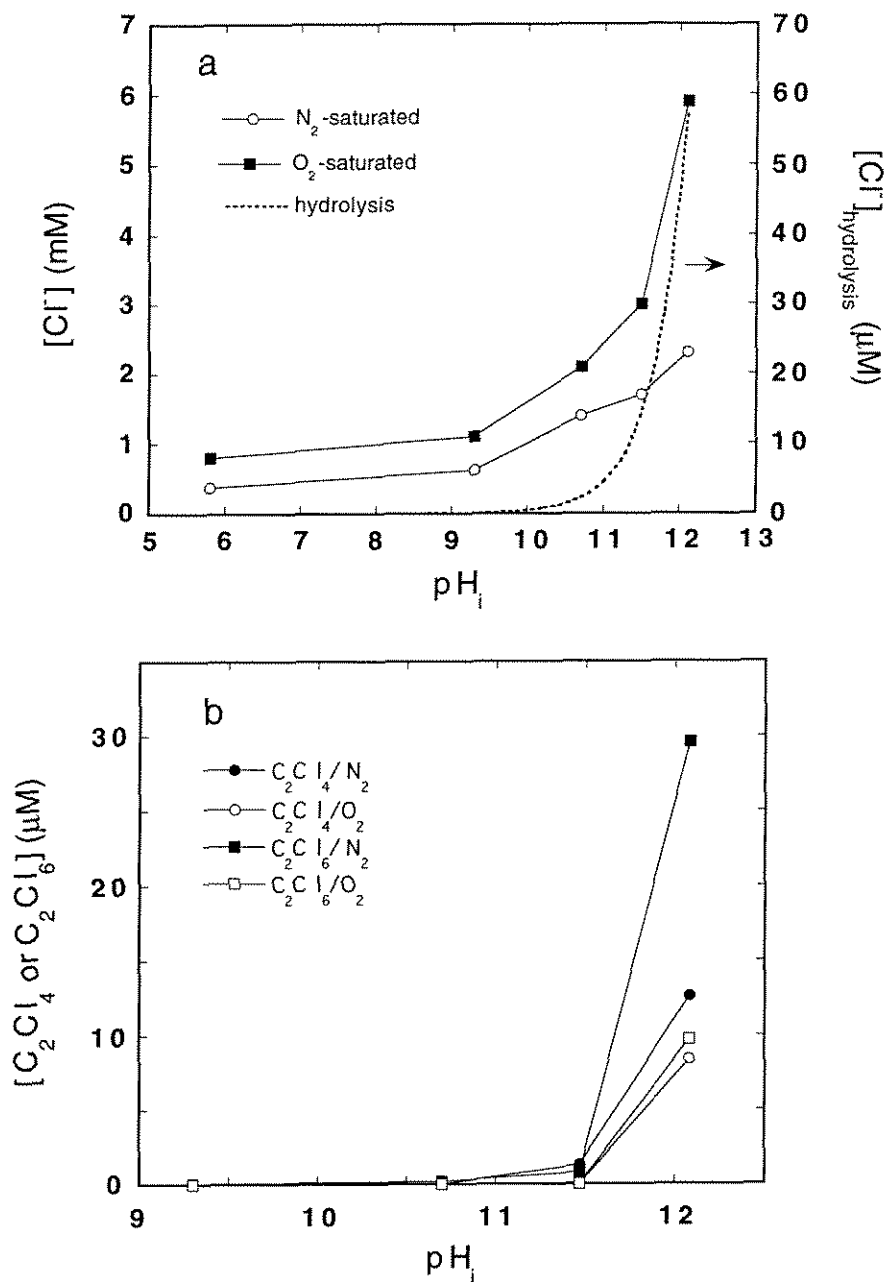


**Figure 4.** Effect of the initial pH of  $\text{TiO}_2$  suspension on the photocatalytic production of (a) chloride and (b)  $\text{C}_2\text{Cl}_4$  and  $\text{C}_2\text{Cl}_6$  in 6 mM  $\text{CHCl}_3$  solutions, which were saturated with  $\text{O}_2$  or  $\text{N}_2$  prior to irradiation. Concentrations were measured after 1 hr irradiation. The dotted line in (a) represents calculated pH-dependent chloride production after 1 hr dark hydrolysis.

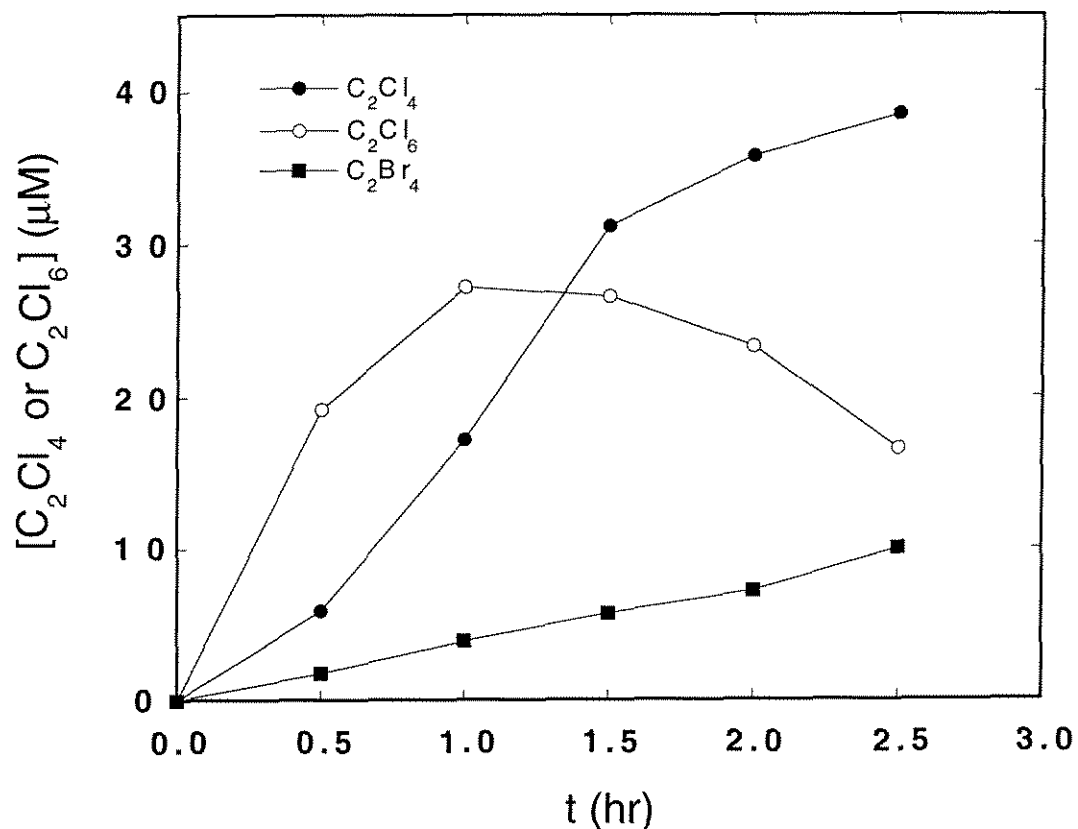


**Figure 5.** Production of dimerized halogenated intermediates ( $C_2Cl_4$  and  $C_2Cl_6$  from 6 mM  $CHCl_3$  solution and  $C_2Br_4$  from 6 mM  $CHBr_3$  solution) as a function of irradiation time. The concentration of  $C_2Br_4$  could not be quantified since its authentic sample was not available. The data were obtained from the same photolysis run of Figure 1. The  $TiO_2$  suspension was initially saturated with  $N_2$  and set to pH 12 before irradiation.

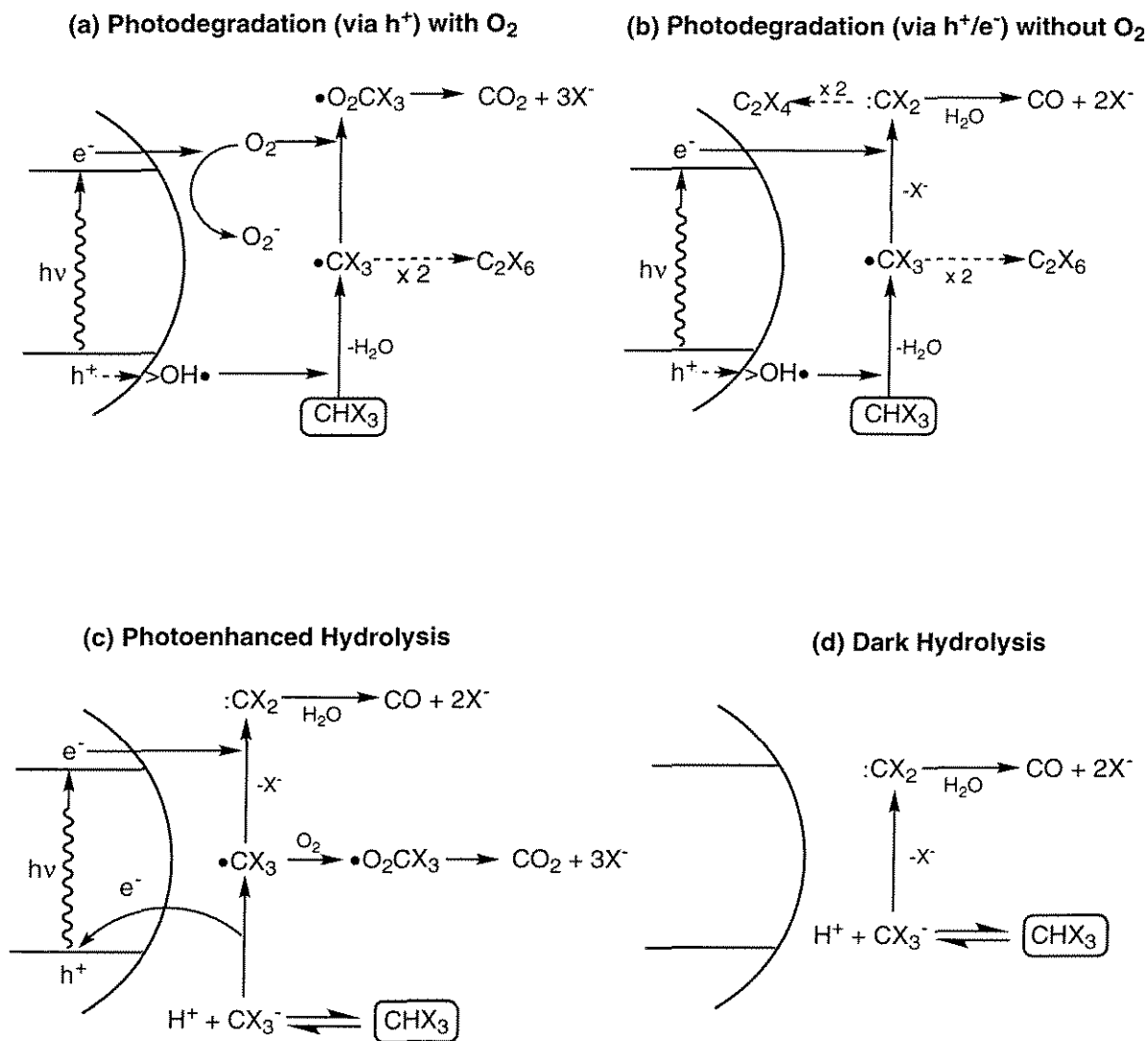


**Figure 6.** Three proposed photocatalytic mechanisms of  $CHX_3$  ( $X = Cl$  or  $Br$ ) degradation on  $TiO_2$  and a dark hydrolysis reaction are illustratively compared.

## **Chapter 6**

### Summary and Conclusions

The photoinduced redox reactions of chlorinated hydrocarbons on  $\text{TiO}_2$  colloids are investigated in this thesis. The chlorinated compounds used in the degradation studies are  $\text{CHCl}_3$  and  $\text{CCl}_4$ , each of which represents a photooxidizable and a photoreducible compound, respectively. Even though they are structurally simple, their degradation mechanisms turn out to be fairly complex. Quantum-sized (Q-sized)  $\text{TiO}_2$  colloids are synthesized by sol-gel method and used as photocatalysts in Chapter 2 while commercially available  $\text{TiO}_2$  (Degussa P25) is used in the studies of Chapters 3, 4, and 5.

The Q-sized  $\text{TiO}_2$  particle (diameter 20 ~ 40 Å) represents a unique situation where the whole particle is practically all surface and the band-gap increases to yield larger redox potentials.<sup>1</sup> The large specific surface area and increased redox overpotential may imply the higher quantum yield. However, the Q-sized  $\text{TiO}_2$  has been found to have lower quantum yields than bulk  $\text{TiO}_2$ .<sup>2</sup> Why the Q-sized  $\text{TiO}_2$  is less photochemically active still remains an open question. The metal-ion doping study of Q-sized  $\text{TiO}_2$ , which is presented in Chapter 2, was motivated to increase its low quantum yields.

Even though  $\text{TiO}_2$  is an excellent photocatalyst for the destruction of hazardous organic chemicals which are widely dispersed in the environment with dilute concentrations, it suffers from low photoefficiencies, particularly for the aqueous solution processes. The overall low efficiency in  $\text{TiO}_2$  photocatalysis results from the high recombination rate of photogenerated electron-hole pairs. By introducing a metal-ion redox energy level in the energy band gap one can expect to suppress the recombination by trapping some of charge carriers and to enhance interfacial charge transfer.

The effects of metal ion dopants in TiO<sub>2</sub> lattice on the photocatalytic degradation of CHCl<sub>3</sub> and CCl<sub>4</sub> are discussed in Chapter 2. The main underlying theme throughout this chapter is *how we enhance the quantum yield of the photocatalytic process*. The results of this study reveal how the role of dopants is related to the interfacial charge transfer. Due to the small size of a Q-sized particle, the trapped charge-carrier in the lattice can be easily transferred to the interfacial region. When the dopants are isolated from the surface, the effect of the dopant on the photoreactivity is detrimental. This means that a metal-ion dopant which has a redox energy level in the band gap can serve as a mediator of interfacial charge transfer in some cases or as a recombination center in the others.

From the results of this study, several requirements for a good dopant are suggested. First, the redox energy level of a metal-ion dopant should lie closely to the band edges. That is, the dopant should be a shallow trap in order to facilitate the detrapping of trapped charge-carriers. Colloids doped with Fe<sup>3+</sup> show the highest photoreactivity because it is a shallow trap. Second, the dopants should be distributed near the surface region. A homogeneous solid solution of dopants in the lattice will result in reduced quantum yields. Since the spatial distribution of dopants in the lattice strongly depends on the history of photocatalyst preparation, various TiO<sub>2</sub> samples doped with the same dopant and concentration could show a wide range of photoreactivities. Third, the dopant concentration should be in the optimal range. Too many dopants in the lattice induce enhanced recombination. Maximum solar energy absorption in the heavily doped TiO<sub>2</sub> is thus limited by the reduced photoreactivity.

In Chapters 3 and 4, the kinetics and mechanism of photoreductive CCl<sub>4</sub> degradation on TiO<sub>2</sub> are discussed. The main finding of this study is that CCl<sub>4</sub>

could be reduced by sequential two electron transfers with forming dichlorocarbene as an intermediate. As a result,  $\text{CCl}_4$  could be degraded in the anoxic environment on illuminated  $\text{TiO}_2$ . The study demonstrates how heterogeneous radical chemistry can be different from its homogeneous counterpart.<sup>3</sup> The radiolytic degradation of  $\text{CCl}_4$  in aqueous solution requires the presence of dissolved oxygen because the only known degradation pathway goes through the reaction of trichloromethyl radical with an oxygen molecule.<sup>4</sup> However, the heterogeneous photocatalytic degradation of  $\text{CCl}_4$  can follow an alternative pathway without the need of oxygen. On the other hand, the photocatalytic system needs added electron donors for efficient  $\text{CCl}_4$  degradation, which cannot be recommended for practical applications.

Dichlorocarbene formation, which is observed in the  $\text{CCl}_4/\text{TiO}_2/\text{UV}$  system, is also found in the  $\text{CHCl}_3/\text{TiO}_2/\text{UV}$  system (Chapter 5). This means that the chemistry of photogenerated trichloromethyl radical on  $\text{TiO}_2$  follows a similar pathway regardless of whether it originates from a reaction with a hydroxyl radical ( $\text{CHCl}_3$ ) or from a reaction with a CB electron ( $\text{CCl}_4$ ). However, the reaction of trichloromethyl radical in the  $\text{CCl}_4$  system is strongly influenced by the presence of electron donors. This fact is related to general issues of photodegradation in multi-components system. Most of laboratory kinetics studies of photodegradation have been performed for a single compound system. Since real polluted water contains a large number of chemical species, mutual interactions between different organic and inorganic substances during photodegradation should be investigated.

Even though a wide variety of organic compounds have been demonstrated to be completely mineralized by  $\text{TiO}_2$  photocatalysis,<sup>5</sup> our understanding of complex photochemical mechanism is often speculative and

largely inconclusive. The complexity in mechanism mainly arises from the presence of photoactive solid surface. Therefore, it is vitally important to understand the interfacial interactions between the photocatalyst surface and organic substrates. Many critical questions remain unanswered. What portion of photodegradation reactions leading all the way to complete mineralization occur actually on the surface? Do intermediate radicals remain on surface until they are completely destroyed? Then, how does the photocatalyst surface affect the reaction pathways of radicals?<sup>6</sup> What factor determines whether the VB hole transfer is direct or indirect?<sup>7</sup> It may depend on surface-substrate interactions as well as on the chemical structure of substrate. On the other hand, how does the electrical double layer affect the interfacial interactions and charge transfer? Is the surface-substrate interaction perturbed under photoillumination?<sup>5</sup> If so, what is its implication to the photodegradation kinetics? Quantitative relationship between the surface-substrate interaction and the photodegradation kinetics needs to be established.<sup>8</sup> Future research should be focused on understanding the novel interactions between the photoilluminated surface and substrates.

Another important aspect of future photocatalytic research lies in the science of photocatalyst preparation. Current technology of improving photocatalyst efficiency largely depends on empirical approaches. Although Degussa P25 TiO<sub>2</sub> is widely used in photocatalytic research due to its relatively higher photoactivity than other commercial TiO<sub>2</sub> samples, no unifying explanation for the higher photoactivity of Degussa TiO<sub>2</sub> exists. There is little understanding regarding how the history of photocatalyst preparation is related to its photoactivity.<sup>9</sup> Too many parameters seem to be involved in determining the photoactivity of TiO<sub>2</sub> samples such as crystallinity, surface area, particle size and morphology, characteristics of defect sites, and surface hydroxylation. Once the

effect of each parameter on photoactivity is understood, the synthesis of photocatalyst could be engineered to maximize its photoactivity.

## References

- (1) Grätzel, M. *Nature* **1989**, *338*, 540.
- (2) Martin, S.T.; Herrmann, H.; Choi, W.; Hoffmann, M.R. *J. Chem. Soc. Faraday Trans.* **1994**, *90*, 3315.
- (3) Mao, Y.; Schöneich, C.; Asmus, K.-D. *J. Phys. Chem.* **1992**, *96*, 8522.
- (4) Mönig, J.; Bahnemann, D.; Asmus, K.-D. *Chem.-Biol. Interactions* **1983**, *45*, 15.
- (5) Hoffmann, M.R.; Martin, S.T.; Choi, W.; Bahnemann, D.W. *Chem. Rev.* **1995**, *95*, 69.
- (6) Chapter 5 in this thesis.
- (7) (a) Cunningham, J.; Srijaranai, S. *J. Photochem. Photobiol. A: Chem.* **1988**, *43*, 329. (b) Stafford, U.; Gray, K.A.; Kamat, P.V. *J. Phys. Chem.* **1994**, *98*, 6343.
- (8) Cunningham, J.; Al-Sayyed, G. *J. Chem. Soc. Faraday Trans.* **1990**, *86*, 3935.
- (9) Sclafani, A.; Pamisamo, L.; Schiavello, M. *J. Phys. Chem.* **1990**, *94*, 829.